SAMSO-TR-NO.-76-38

(12)

FLEET SATELLITE COMMUNICATIONS SYSTEM PROJECT

COMMUNICATIONS CRITICAL DESIGN REVIEW PACKAGE (U) APPENDIX A

PART 1. INTERMODULATION PHENOMENOLOGY INVESTIGATION

PART 2. INTERMODULATION CANCELLATION STUDY

DOC. NO. 24200-540-006-01

22 November 1974

Prepared for

DEPARTMENT OF THE AIR FORCE
Headquarters Space and Missile Systems Organization
Contract No. F04701-73-C-0011

APPROVED FOR PUBLIC RELEASE;DISTRIBUTION UNLIMITED.

TRW
SYSTEMS GROUP

ONE SPACE PARK • REDONDO BEACH, CALIFORNIA 90278

DISCLAIMER NOTICE

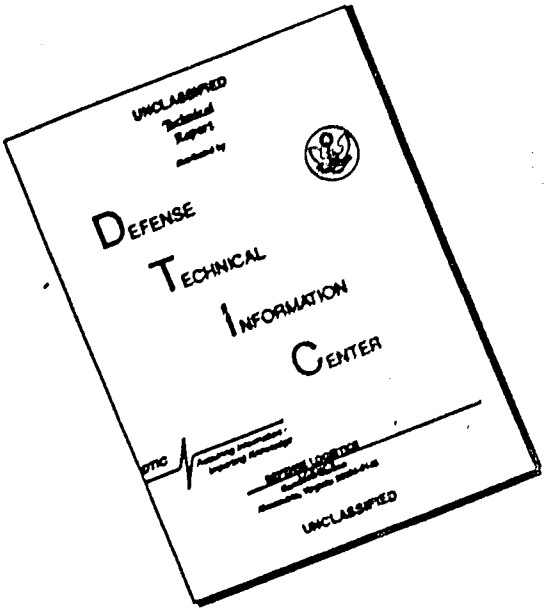

THIS DOCUMENT IS BEST QUALITY AVAILABLE. THE COPY FURNISHED TO DTIC CONTAINED A SIGNIFICANT NUMBER OF PAGES WHICH DO NOT REPRODUCE LEGIBLY.

This final report was submitted by TRW Systems Group, One Space Park, Redondo Beach, California 90278, under Contract F04701-73-C-0011 with the Space and Missile Systems Organization, Deputy for Space Communications Systems, P. O. Box 92960, Worldway Postal Center, Los Angeles, California 90009. Major Michael E. McDonald, Chief, Subsystem Branch, FLTSATCOM System Program Office (SKF), was the Project Engineer.

This report has been reviewed by the Information Office and is releasable to the National Technical Information Service (NTIS). At NTIS it will be made available to the general public, including foreign nationals.

This technical report has been reviewed and is approved for publication.

Michael E McDonald

MICHAEL E. McDONALD, MAJ, USAF
Chief, Subsystem Branch
FLTSATCOM System Program Office
Deputy for Space Communications Systems

GEORGE E. BRETON, COL, USAF
Director of Engineering
FLTSATCOM System Program Office
Deputy for Space Communications Systems

FOR THE COMMANDER

Edwin A. Coy

EDWIN A. COY
Brigadier General, USAF
Deputy for Space Communications Systems

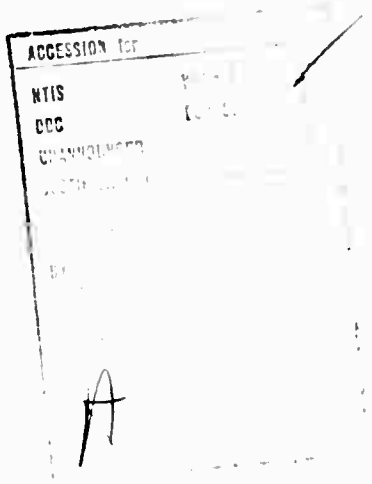

SECURITY CLASSIFICATION OF THIS PAGE (When Data Entered)

REPORT DOCUMENTATION PAGE

READ INSTRUCTIONS BEFORE COMPLETING FORM

1 REPORT NUMBER: SAMSO-TR-76-38	2 GOVT ACCESSION NO
3 RECIPIENT'S CATALOG NUMBER	
4 TITLE (and Subtitle): Communications Critical Design Review Package, Appendix A-2 1, Intermodulation Phenomenology Investigation. 2, Intermodulation Cancellation Study.	5 TYPE OF REPORT & PERIOD COVERED: Final Report. May-Nov 1974
	6 PERFORMING ORG. REPORT NUMBER: 24200-540-006-01
7 AUTHOR(s): D. E. Royal, S. H. Cushner	8 CONTRACT OR GRANT NUMBER(s): F04701-73-C-0011
9 PERFORMING ORGANIZATION NAME AND ADDRESS: TRW System Group, One Space Park, Redondo Beach CA 90278	10 PROGRAM ELEMENT, PROJECT, TASK AREA & WORK UNIT NUMBERS
11 CONTROLLING OFFICE NAME AND ADDRESS: SAMSO/SK, PO BOX 92960, Worldway Postal Center, Los Angeles CA 90009	12 REPORT DATE: 22 Nov 1974; 13 NUMBER OF PAGES: 183
14 MONITORING AGENCY NAME & ADDRESS (if different from Controlling Office)	15 SECURITY CLASS. (of this report): UNCLASSIFIED; 15a DECLASSIFICATION/DOWNGRADING SCHEDULE

16 DISTRIBUTION STATEMENT (of this Report)

Approved for public release; distribution unlimited.

17 DISTRIBUTION STATEMENT (of the abstract entered in Block 20, if different from Report)

18 SUPPLEMENTARY NOTES

19 KEY WORDS (Continue on reverse side if necessary and identify by block number)

Intermodulation, Intermodulation Phenomenology, Intermodulation Cancellation, Solder joints, Copper plating, Nickel plating, Receive helix, Antenna array, Antenna structure, IM product suppression, Antenna helix, Intermodulation floor levels, Intermodulation generators, Computer model of intermodulation propagation.

20 ABSTRACT (Continue on reverse side if necessary and identify by block number)

The Intermodulation (IM) Phenomenology Investigation was instigated to obtain an understanding of the IM generating phenomena involved in FLTSATCOM UHF Communications hardware, and thus to determine materials and processes that would reduce the IMs to acceptable levels. The two IM generating phenomena which were identified as being particularly troublesome to FLTSATCOM were untrimmed soft solder joints and the use of electroless nickel as a preparatory coating for plating copper on aluminum. Guidelines

OVER

DD FORM 1 JAN 73 1473 EDITION OF 1 NOV 65 IS OBSOLETE

SECURITY CLASSIFICATION OF THIS PAGE (When Data Entered)

Cont Blk 19: Pressure joints, Intermodulation level, Effect of number of carriers on intermodulation level, Intermodulation reduction guidelines, Coaxial connectors, Active and Passive Suppression of intermodulation.

Cont Blk 20:

for IM reduction are given.

In the Intermodulation Cancellation Study, 3/8 scale measurements were made. Both active and passive methods of suppression were investigated which reduced IMs but none of the systems investigated were directly applicable to FLTSATCOM.

PART 1

INTERMODULATION (IM) PHENOMENOLOGY INVESTIGATION

FOREWORD

Part 1 of this report (Intermodulation Phenomenology) was edited by S.H. Cushner and contains contributions by:

G.L. Clark
S.H. Cushner
A.V. Haeff
R.E. Harrison
L.O. Heflinger
P. Molmud
R.A. Smith
J.Z. Wilcox

CONTENTS

CONTENTS (Continued)

SUMMARY

This investigation was undertaken to support the FLTSATCOM (FSC) UHF hardware test program and to develop materials and process guidelines for the flight hardware development. The phenomenology program consisted of both an experimental and theoretical evaluation of IM producing effects present in the FSC system.

An initial step of collection of an IM data bank had been taken, but upon examination only very little information of direct use was found. The disparities were either in terms of vastly different frequencies or very different environments. For example, ship based systems with the IM sources associated with materials and structures not necessarily part of the affected transmitter/receiver system, or ground based systems.

The theoretical work had as its principal goal the establishment of a floor for IM levels in UHF components and a secondary goal of support for the experimental program. The latter program obtained data on the production of IM's in several cases of interest to FSC. The overall program guideline was to obtain sound results in a few selected areas rather than to do a broad survey.

The bulk of the experimental work was done on a common junction test fixture, which provided a single test volume within which potential IM generating structures and materials could be placed and then current-voltage transfer characteristics and power dependence measured. The noise level of the associated IM receiver was about -140 dBm. Based upon some guidance obtained from the data bank and those materials and processes which the FSC program had identified as suspicious, several effects were selected for study. These are shown in Table 1. Some of IM levels measured from several of the effects are also given in Table 1. Table 2 gives some estimates of IM levels determined to be "floor" in several components.

The principal conclusions of this report are a set of guidelines for materials and processes derived from the experiments on IM phenomena performed. These are given in digest form in Table 3.

Although this investigation was successful in revealing some IM phenomena of system level importance, and in showing some remedies, there remain considerable identified, knowledge gaps. These are summarized in terms of requirements for further work in Table 4.

Table 1. Principal Effects Studied Experimentally

• JUNCTION MECHANISMS	Experimentally determined that nonlinearity disappears when contact pressure increases. "Poor" contacts are easier to avoid with coaxial components than with waveguide components. These junction effects are large. In this investigation their levels suggested that other sources be examined (highly variable levels).
• MAGNETIC ARTIFACTS	It is well known that ferro-or-ferrimagnetic materials are good IM generators. Their use must be avoided or they must be used in low power density and/or poorly coupled areas. Their avoidance however is not easy. The use of tools containing iron in the drawing of tubing or in the machining of components apparently leaves magnetic inclusions. Nickel and iron have been found in all portions of the coaxial cable used in FSC. Also very small particles of magnetic "dirt" can easily be picked up on surfaces. (-140 dBm to -115 dBm for one meter of coaxial cable)
• SOFT SOLDER JOINTS	We have not uniquely identified the reason these joints generate IM's. The strongest likelihood is that portions of such a joint constitute a poor junction with the substrate metal. In this case it is difficult to increase the contact pressure. (< -140 dBm)

Table 1. Principal Effects Studied Experimentally (Continued)

• ELECTROLESS NICKEL PLATING	Nickel is a ferromagnetic material and so would be expected to produce IM's. However, the layer is overcoated with copper and to an extent is shielded. The shielding is incomplete. There are also some uncertainties concerning the IM behavior of the nickel in this role, in particular as regards the effect of temperature and strain. (< -140 dBm when covered by 0.0002 inches of copper)

Table 2. IM Floor Estimates

IM Floor Mechanism	Nominal IM Level for FSC f_1 = 240 MHz, f_2 = 270 MHz $(2f_2 - f_1)$, 30 Watts Each	Comments
Joule loss induced electrical conductivity modulation in coax walls	-170 dBm	Valid for length ℓ less than 50 meters P_1, P_2 are the powers at f_1, f_2. IM level given for ℓ = 5 meters and 0.390 coax.
Field induced electro-striction in solid dielectrical coax	-176 dBm	0.390 coax does not employ a solid dielectric. This mechanism in that coax would be drastically lower.
Non-linear term in the Lorentz force on conduction electrons	-190 dBm	

NOTE: In a copper component with a moderate Q; i.e., 500 the currents and consequently the IM levels will be greater. For example, for the Joule heating modulation, and a Q = 500 the IM level would be about -145 dBm, all other parameters being the same as above.

Table 3. Conclusion Digest

- Magnetic materials of nondeliberate origin in materials and processes appear to be significant IM generators.
- Soft solder joints are uncertain IM sources. Their effects are not understood.
- Electroless nickel plating on aluminum as a preparatory layer for a copper coat is acceptable so long as the copper coating exceeds 0.0002 mil in thickness.
- IM "floor" levels are low, but may in some cases be close to operating levels.

Table 4. Requirements for Further Work

- Diagnostics of IM sources by observed behavior (signature)
- Clarification of the role of magnetic impurities and of solder joints
- Extension of phenomenology efforts to include stripline components, thermal wrap, and other surface plating/painting materials
- Study of "good" pressure contacts to determine low level IM problems.

1. INTRODUCTION

This Appendix presents the results of a portion of the work performed under an Intermodulation Phenomenology Investigation within the FLTSATCOM (FSC) program. The work reported here was done in support of the hardware, and process and material evaluation efforts within the FSC program. The investigation consisted of two principal efforts. The first, an experimental effort to study a few specific IM generating phenomena in a controlled manner. This experimental effort was supported by materials analysis using both visible light metallography and microscopy, and a scanning electron microprobe. The second was a theoretical effort to obtain estimates of IM producing phenomena which might be irreducible limits in various components. In addition, the theoretical effort provided support to the experimental effort. This report presents in the following sections the technical approach (Section 2) used in the experimental portion, and gives in digest form the models and principal results obtained from the theoretical portion. The detailed theoretical treatments are collected in a series of Addenda to this Appendix.

The remaining portion of the work performed in this task was the investigation of methods for cancelling transmitter generated intermodulation (IM) products by subtraction at the receiver output. These efforts are reported separately in Part 2 of this Appendix, "Intermodulation Cancellation Study."

The overlapping of receive bands with transmitter generated IM lies at the root of the problem. Because of this, reduction of the strength of IM is essential. The source of the IMs in FSC as with some other programs is in passive components. In broad terms, materials and processes used in fabrication of the UHF equipment can exhibit a number of physical phenomena which respond nonlinearly to electric fields and to currents. It is this nonlinear behavior which produces the IM.

1.1 STATEMENT OF THE PROBLEM

The central problem for this task was to obtain an understanding of the IM generating phenomena involved in the FSC hardware, and on this basis determine materials and processes that will reduce the IM's to acceptable

levels. The general framework of the generation and propagation of such IM is shown in Figure 1. On this basis it can be seen that the IM level which is acceptable in a given system element varies, depending upon how much isolation (propagation loss) exists between the producing element and the receive antenna, and the efficiency with which the IM is produced.

The initial experimental efforts were done on junctions. It was found that the IM levels produced were large compared to these found in FSC hardware. Further, that the remedy for junction produced IM's was to increase the forces on the elements comprising the junction.

Two IM generating phenomena which were identified as being particularly troublesome in FSC hardware were soft solder joints; and, the use of electroless nickel as a preparatory coating for plating copper on aluminum. It is desirable to find ways to allow greater use of these practices, since their avoidance represents a burden to the system design.

1.2 SCOPE OF EFFORT AND PROGRAM GOALS

Shortly after the initial observation of the IM problem many guidelines were established based upon earlier work. These guidelines were rather general, and were implemented rapidly into fabrication work in process. An outline of these is shown in Table 5.

Table 5 is a brief summary of materials and processes which have been evaluated as risky so far as IM production is concerned. The basis for this conclusion is a very conservative one; i.e., materials and processes have been avoided if there was any suspicion about their use. The items in this tabulation can of course be used so long as they are illuminated with sufficiently low power density and/or their IM's are not strongly coupled into the receive antenna.

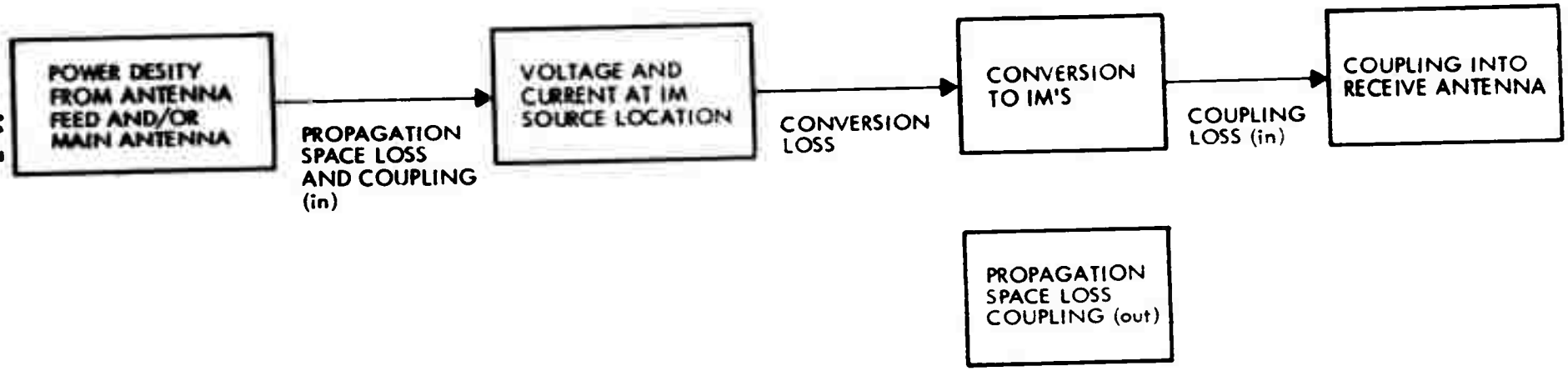

KNOWLEDGE OF THE VALUES OF THE COUPLING AND LOSS FACTORS ALLOWS DETERMINATION OF THE REQUIREMENT FOR THE LEVEL OF AN IM ASSOCIATED WITH A GIVEN LOCATION AND MECHANISM

Figure 1. Generation, Propagation, and Coupling Relationship of IM's

Table 5. Initially Established Material and Process Guidelines

Materials or Process	Metals	Non Metals and Combinations
Surface finishes (grinding, polishing)	All ferro-magnetic metals	BN, duroid, Al-Kapton, micro-wave absorber, graphite, Q-Clad, Al-Mylar, carbon metallized films and conduc-tive glass, ferrites
Platings		Anodized aluminum
Paints		Leafing aluminum paint and other metal containing paints
Bonding – pressure, adhesives, soldering, brazing, welding		"Light" pressure contacts, metal loaded epoxies, soft solder
Surface artifacts		Metal chips, solder and con-ductive epoxy blobs

The phenomenology effort was established shortly following this, and comprised the following tasks:

TASK DESCRIPTION

1. IM Phenomenology Experimental Effort

   - Demonstrate production of IM products in deliberately fabri-cated non-linear junctions and materials.
   - Determine the importance of IM producing mechanism relative to FSC hardware practices.
   - Determine means of characterizing the source strength of the important mechanisms.
   - Recommended materials, fabrication techniques, and practices that will minimize IM generation in passive FLTSATCOM components.

2. IM Phenomenology Theoretical Effort

   - Provide support of experimental program.
   - Establish a "floor" for IM production in critical components.

3. IM Modeling Support

- Develop computer model of IM propagation in coaxial components.

The scope of the program was limited to those IM producing phenomena which directly affected FSC in terms of the established direction of the hardware effort. A number of techniques, e.g., stripline transmission lines and components, had been determined to be bad from an IM standpoint, and so were eliminated from the design. The phenomenology investigation did not specifically include such phenomena in stripline, as shown in the task statement above. The problem of establishing a lower limit (floor) to IM production in passive elements was specifically addressed in a theoretical approach.

As part of the work to reduce IM levels, tasks were also initiated to determine if IM's could be cancelled by subtraction of a sample signal containing IM's and not received signal from the received output. Both active and passive cancellation schemes received attention. In addition, a new receive antenna consisting of 4 helical elements was briefly evaluated. This latter configuration can satisfy the requirements of the FSC receive antenna, and in addition has intermod advantages for implementing an IM cancellation scheme. This work on IM cancellation is reported separately.

The following sections of this Appendix describe the technical approach (Section 2) to the investigation for both the experimental and theoretical efforts. In the former, the design and fabrication considerations for the testing apparatus is given. The experimental procedures followed in its calibration relative to the Process Test Fixture used in FSC hardware development and in the investigation of the IM phenomenology are presented.

Section 3 gives the conclusions reached from the investigation, and in Section 4 the requirements for future work in the generation of IM's in passive components.

A series of addenda contain the detailed analysis of the possible IM floor phenomena and some other analytical work performed in support of the FSC program.

2. TECHNICAL APPROACH

2.1 EXPERIMENTAL EFFORT

Experimental effort instrumentation requirements are as follows:

- Spatially localize the IM generation region
- Sufficient sensitivity so that IM levels generated by individual sources can be measured
- Build separate apparatus so that measurements could be made by different methods and without interference to program hardware development.

This section presents the experimental and theoretical aspects of the IM investigation. In 2.1 the design considerations and operating parameters of the test apparatus are given. Following this the IM phenomena studied and principal results obtained are stated. The format for the bulk of this section is that of annotated summary charts. The results include a few items which could not be fully studied, but which appear to be relatable to observations made in some of the hardware tests.

APPARATUS DESIGN CONCEPT

- HIGH-Q RESONANT LINES TO PRODUCE A SINGLE LOCALIZED REGION HAVING LARGE RF CURRENTS (COMPARABLE CURRENTS DO NOT EXIST AT ANY OTHER POINT IN THE APPARATUS)
- TO LOCALIZE IM GENERATION RESONANT LINES ARE SEPARATED EXCEPT FOR A 2 CM COMMON PATH IN THE HIGH CURRENT REGION
- IN OUTCOUPLING AND DETECTION CIRCUIT COUPLED ONLY TO THE COMMON PATH
- PRIMARY FREQUENCIES DECOUPLED FROM THE DETECTION CIRCUIT
- LOW-LEVEL IM SIGNALS RECOVERED FROM NOISE BY SYNCHRONOUS DETECTION
- THE RESULTS OBTAINED WITH THIS APPARATUS ARE COMPARABLE TO THE LEVELS MEASURED IN UNMODULATED CARRIER TESTS RATHER THAN THOSE MEASURED IN NOISE LOADED CHANNEL TESTS

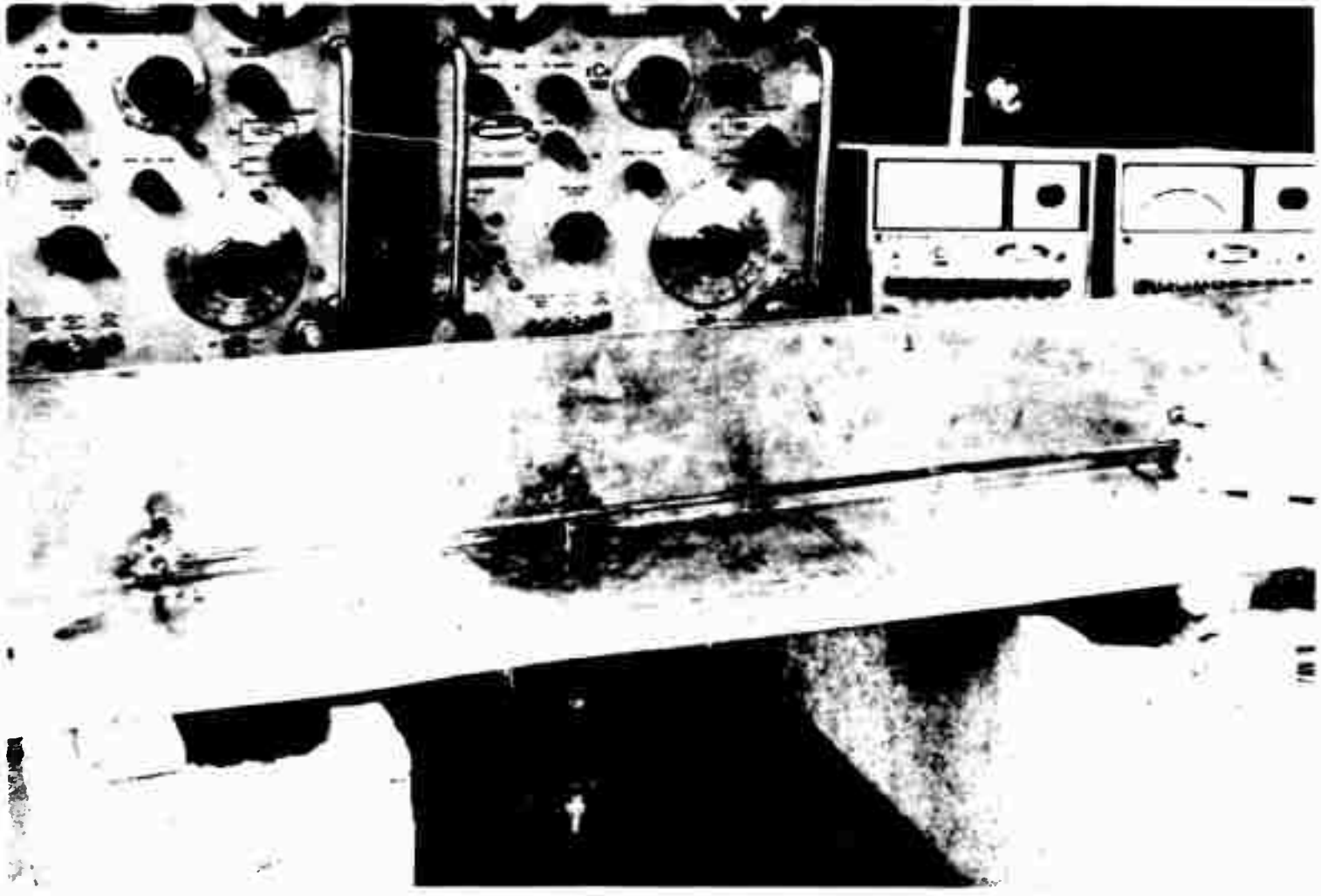

OVERALL VIEW OF RESONANT STRUCTURE WITH COVER REMOVED

Figure 2. Double-Resonance Intermodulation Measurement Apparatus

CLOSE-UP OF INTERACTION REGION

Figure 2. Double-Resonance Intermodulation Measurement Apparatus (Continued)

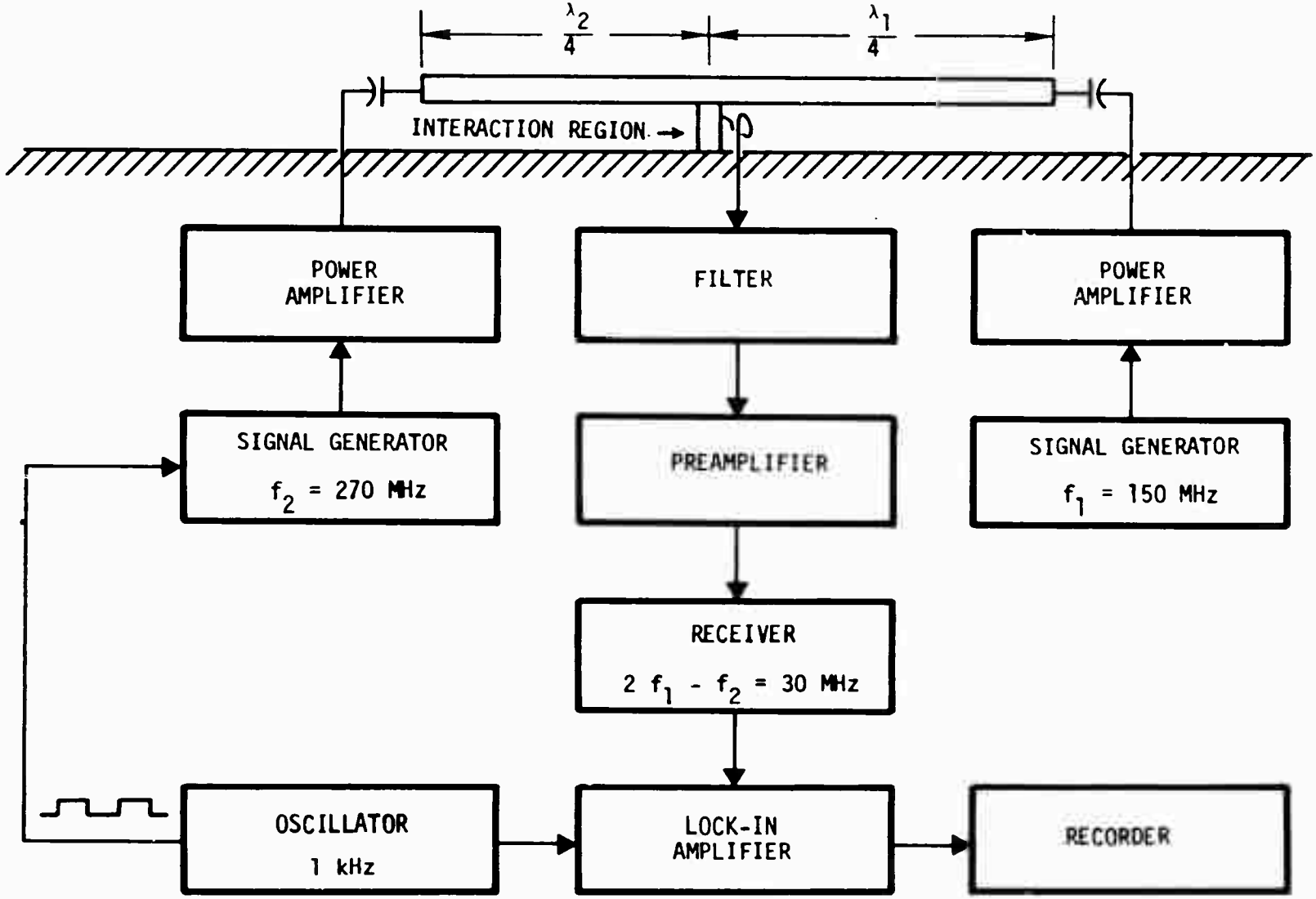

Figure 3. Double-Resonance Apparatus Configuration

DOUBLE-RESONANCE APPARATUS

PERFORMANCE PARAMETERS

TRANSMITTER FREQUENCIES

f_1 = 150 MHz

f_2 = 270 MHz

B FIELD IN TEST REGION

0 TO 8.5 GAUSS AT 270 MHz
0 TO 15 GAUSS AT 150 MHz

INTERMODULATION FREQUENCY

$2f_1 - f_2$ = 30 MHz

RECEIVER SENSITIVITY

-140 dBm (1 SECOND INTEGRATING TIME)

TEST REGION DIAMETER

1 mm (MINIMUM)

NATURE OF TRANSMITTER SIGNALS

CW AND 1 KHz SQUAREWAVE PULSE MODULATION
FOR LOCK IN DETECTION

FACTORS GOVERNING DETECTABILITY OF IM SOURCES

THE DETECTABILITY OF IM SOURCES IN ANY APPARATUS OR SYSTEM IS A FUNCTION, NOT ONLY OF THE SENSITIVITY OF THE RECEIVER, BUT OF THE TYPE OF SOURCE, THE FIELD EXCITING IT, AND THE COUPLING BETWEEN THE SOURCE AND THE RECEIVER. WHEN MORE THAN ONE SOURCE IS INVOLVED, EACH SOURCE MAY HAVE DIFFERENT CHARACTERISTICS, EXCITING FIELDS, AND COUPLINGS TO THE RECEIVER. IN SUMMING THE CONTRIBUTION FROM MULTIPLE SOURCES, THE RELATIVE PHASES MUST BE TAKEN INTO ACCOUNT.

THE DOUBLE-RESONANCE APPARATUS WAS DESIGNED TO MAXIMIZE THE EXCITING FIELD AT THE IM SOURCE AND THE COUPLING OF THE IM SIGNAL TO THE RECEIVER. THE ACTUAL RECEIVER SENSITIVITY (-140 dBm) WAS NOT AS GREAT AS THE SENSITIVITY OF THE RECEIVERS USED FOR IM MEASUREMENTS ON THE FLTSATCOM SYSTEM, BUT THE HIGH FIELD INTENSITIES ATTAINABLE AND GOOD COUPLING MORE THAN MADE UP FOR THIS LACK.

COMPARISON OF MEASUREMENT SYSTEM SENSITIVITIES

A DIRECT COMPARISON OF THE SENSITIVITIES OF THE DOUBLE-RESONANCE APPARATUS AND THE COAXIAL PROCESS TEST FIXTURE WAS MADE BY ATTACHING TINY IRON SPHERES TO THE 3/8"-DIAMETER CENTER CONDUCTOR OF THE COAXIAL TEST FIXTURE AND ALSO MEASURING THESE SAME SPHERES IN THE DOUBLE-RESONANCE APPARATUS.

A SINGLE IRON SPHERE 500 MICROMETERS IN DIAMETER GAVE A -95 dBm SIGNAL IN THE DOUBLE-RESONANCE APPARATUS WHEN PLACED IN A WEAK FIELD POSITION. IN A STRONG FIELD POSITION, THIS PARTICLE GAVE A -55 dBm SIGNAL. IN THE COAXIAL TEST FIXTURE, THIS SAME PARTICLE WAS NOT OBSERVABLE ABOVE THE NOISE.

A FURTHER TEST WAS CARRIED OUT IN THE COAXIAL TEST FIXTURE WITH 20 IRON SPHERES ATTACHED TO THE CENTER CONDUCTOR. THE OBSERVED IM LEVEL WAS -108 dB, ONLY 24 dB ABOVE THE SYSTEM NOISE LEVEL. THE RELATIVELY LOW SENSITIVITY OF THE COAXIAL TEST APPARATUS CAN BE SHOWN, BY THE SCALING LAWS PRESENTED LATER, TO BE ACCOUNTED FOR BY THE LARGE RADIUS OF THE CENTER CONDUCTOR AND THE ABSENCE OF HIGH Q RESONANCE.

THE GOOD QUANTATIVE AGREEMENT BETWEEN THE TWO MEASUREMENT SYSTEMS, OBTAINED VIA THE SCALING LAWS PRESENTED LATER, INDICATES THAT THE IM BEHAVIOR OBSERVED AT 30 MHz IN THE DOUBLE-RESONANCE APPARATUS IS NOT DIFFERENT FROM THE BEHAVIOR AT THE 300 MHz IM FREQUENCY OF THE FLTSATCOM SYSTEM.

POTENTIAL SOURCES OF INTERMODULATION INVESTIGATED EXPERIMENTALLY

*MAGNETIC PARTICLES

*PRESSURE CONTACTS

*SOLDER JOINTS

GRAPHITE FIBERS

THERMAL RESISTANCE MODULATION

*NICKEL PLATING

---

* DENOTES PRINCIPAL SUBJECTS

SECTION 2.1.1

MAGNETIC MATERIALS OF NONDELIBERATE ORIGIN

MAGNETIC PARTICLES

- IT WAS INITIALLY ASSUMED THAT, SINCE MAGNETIC MATERIALS WERE KNOWN TO BE NONLINEAR, SUCH MATERIALS WOULD NOT BE USED IN THE SYSTEM AND THAT CONSEQUENTLY, IT WOULD NOT BE NECESSARY TO INVESTIGATE THEM. HOWEVER, IN ATTEMPTING TO ACHIEVE A LOW BACKGROUND LEVEL OF INTERMODULATION, IT WAS DISCOVERED THAT THE BACKGROUND IM LEVEL WAS CAUSED BY MINUTE UNSUSPECTED MAGNETIC PARTICLES IN THE INTERACTION REGION. THEIR EXISTENCE WAS PROVED BY A LARGE DECREASE IN THE IM LEVEL WHEN A PERMANENT MAGNET WAS HELD NEAR THE REGION. THESE PARTICLES WERE INDIVIDUALLY FOUND UNDER MAGNIFICATION AND REMOVED. WITH THE REMOVAL OF EACH PARTICLE, THE BACKGROUND LEVEL DECREASED, UNTIL A RESIDUAL LEVEL OF 0.02 MICROVOLTS (-141 dBm) WAS REACHED. APPLICATION OF A PERMANENT MAGNET CAUSED THIS RESIDUAL LEVEL TO DISAPPEAR, INDICATING THE CONTINUED PRESENCE OF UNDISCOVERED MINUTE MAGNETIC PARTICLES. FREQUENT REMOVAL OF NEW MAGNETIC PARTICLES WAS REQUIRED TO RESTORE LOW BACKGROUND LEVELS.

- THE MAGNETIC PARTICLES CAUSING THE BACKGROUND IM WERE FOUND TO BE FAR BELOW THE DETECTION THRESHOLD OF A LABORATORY FLUX-GATE MAGNETOMETER HAVING 300 TIMES THE SENSITIVITY OF THE EQUIPMENT ROUTINELY USED TO EXCLUDE MAGNETIC MATERIALS FROM SPACECRAFT.

- SAMPLES OF THE COAXIAL LINE PLANNED FOR USE IN THE FLTSATCOM SYSTEM WERE SHOWN BY MICROPROBE ANALYSIS TO CONTAIN IRON PARTICLES ON BOTH INNER SURFACES. SCRAPINGS FROM THE SURFACES GAVE LARGE IM SIGNALS WHEN PLACED IN THE INTERACTION REGION.

GENERAL OBSERVATION OF INTERMODULATION USING MAGNETIC TEST SAMPLES

- SMALL MAGNETIC PARTICLES DO NOT FOLLOW THE EXPECTED $I_1^2 I_2$ DEPENDENCE. THIS LAW IS ALSO NOT OBEYED IN THE FLTSATCOM SYSTEM AT LOW IM LEVELS.

- IN SOME CASES, PARTICULARLY AT LOW LEVELS, THE IM IS OBSERVED TO REACH A MAXIMUM AND THEN DECREASE WITH AN INCREASE IN ONE OF THE DRIVE CURRENTS. SIMILAR BEHAVIOR HAS BEEN OBSERVED IN THE FLTSATCOM SYSTEM. THIS EFFECT IS CONSISTENT WITH THE OBSERVED REDUCTION IN IM WHEN ADDITIONAL TRANSMITTERS ARE ENERGIZED. (SEE ADDENDUM 7.) SEE FIGURE 4.

- THE ANOMALOUS BEHAVIOR OF SMALL MAGNETIC PARTICLES WAS OBSERVED AT MAGNETIC FIELDS OF ONLY A FEW OERSTEDS, FAR BELOW THOSE REQUIRED TO DRIVE MACROSCOPIC MAGNETIC SAMPLES INTO SATURATION. THESE LOW FIELD INTENSITIES ARE COMPARABLE TO THOSE PRESENT IN THE FLTSATCOM SYSTEM.

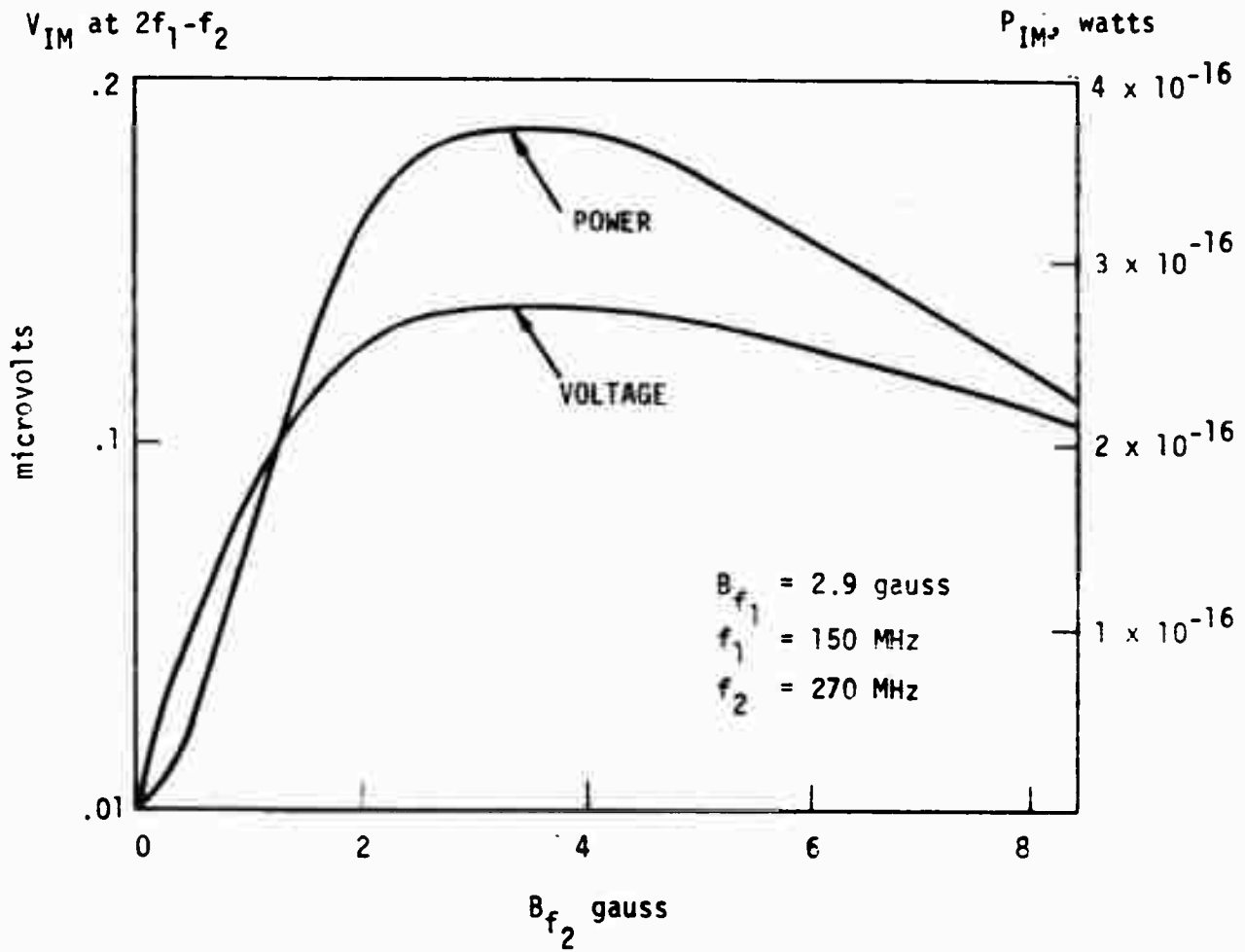

Figure 4. IM Voltage and Power for 1 Micrometer Iron Particles Showing a Maximum

The isometric plots shown in this section show clearly the departure of IM production from an ($i_{f_1}^2$ i_{f_2}) dependence (two carrier third order IM) particularly at low drive currents (or corresponding magnetic flux density levels). They suggest that at higher drive (see Figure 5) levels the behavior approaches the ($i_{f_1}^2$ i_2) variety. The ideal ($i_{f_1}^2$ i_{f_2}) behavior is shown in Figure 6.

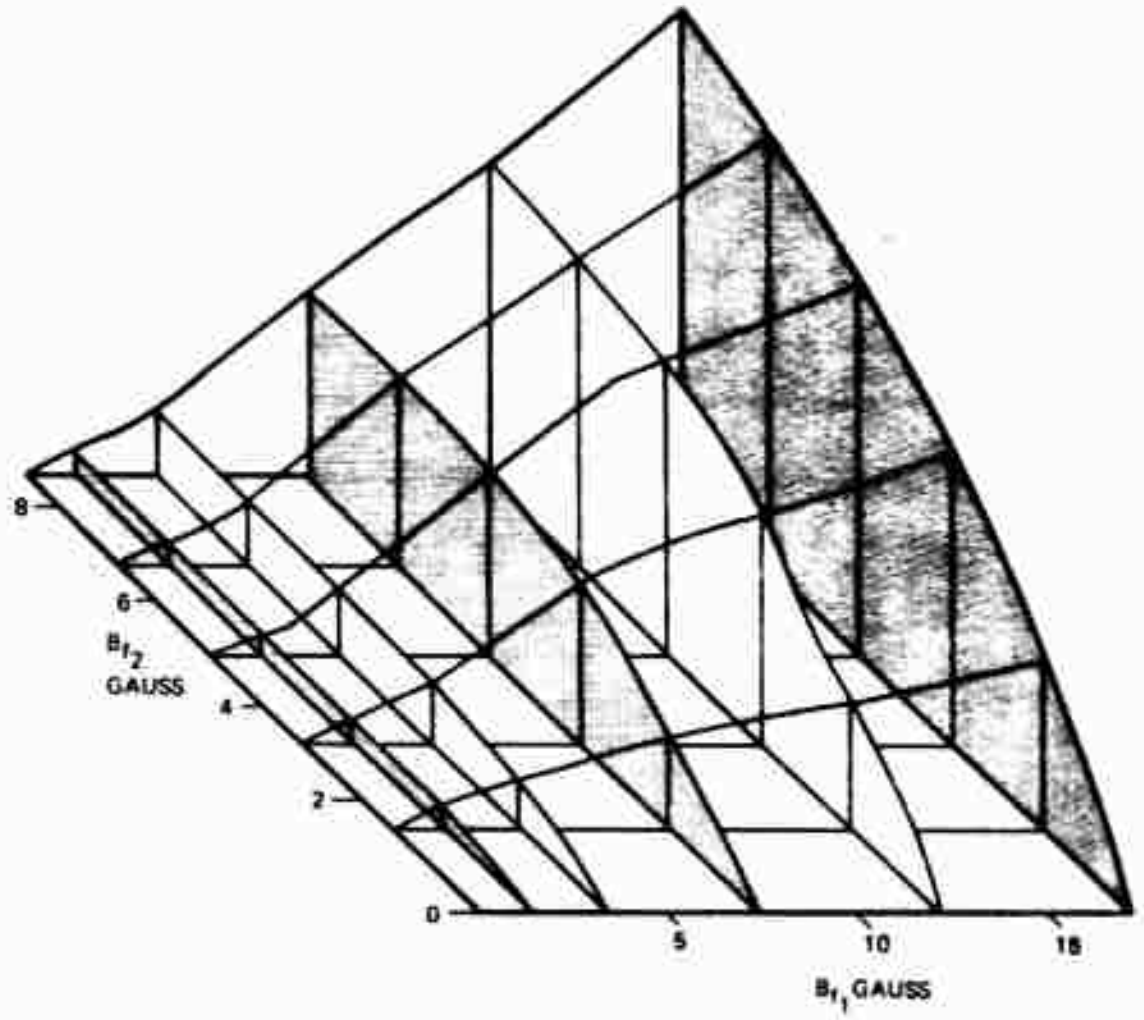

Figure 5. Observed Behavior of 3rd Order IM Voltage $V_{2f_1-f_2}$, as a Function of Magnetic Field from Transmitters. The Particles Used Here Are About 1 μm Diameter (Iron).

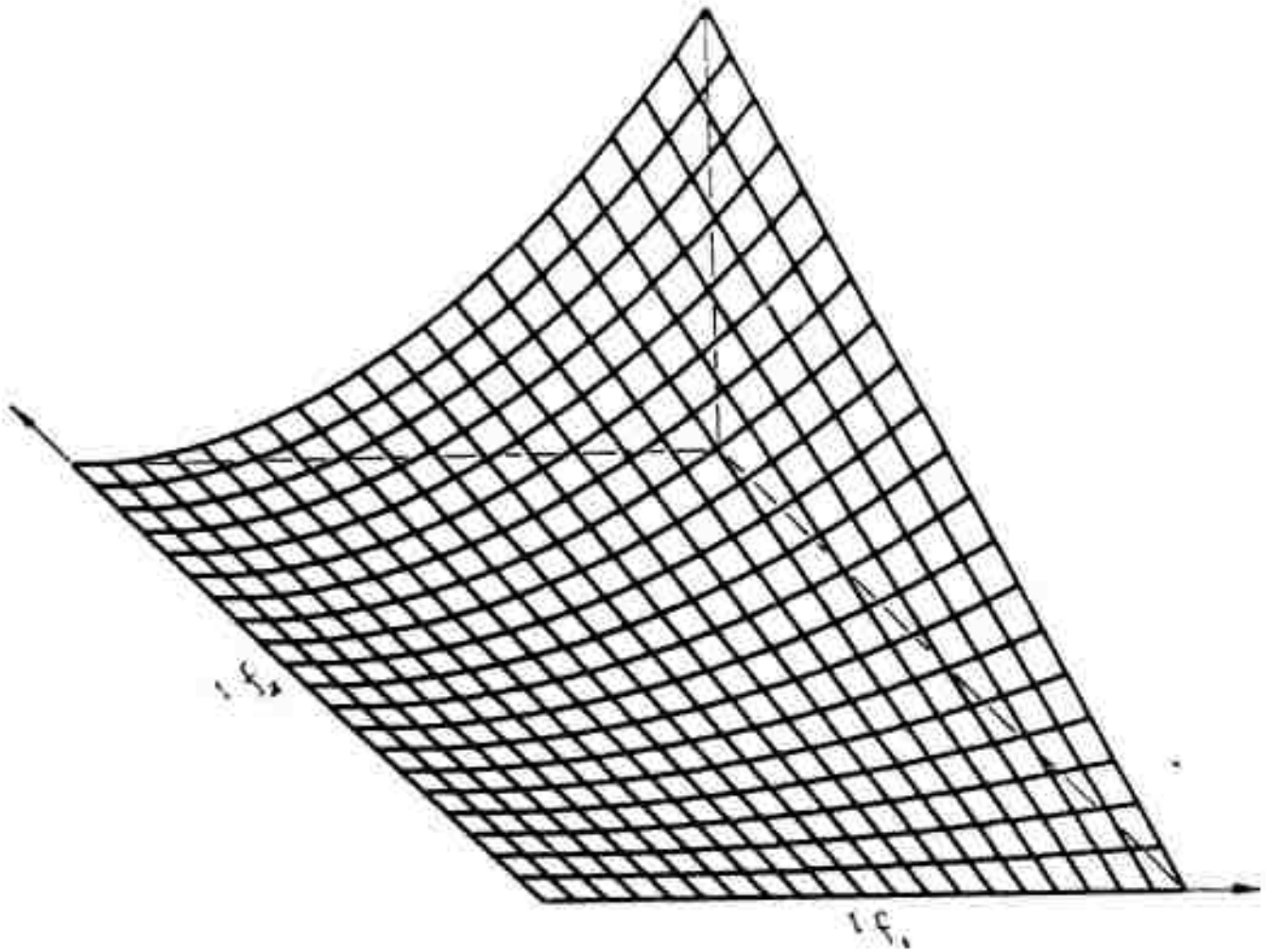

NOTE: The currents, I_{f_1} and I_{f_2} shown on this plot are proportional to magnetic flux densities, B. The latter variable is used on the preceding figure.

Figure 6. IMs from a Source, V_{IM}, Proportional to $I_1^2 I_2$ (Ideal)

SPECULATIONS ON MECHANISM OF MAGNETIC PARTICLE INTEPMODULATION

- THE CLASSICAL MACROSCOPIC MAGNETIZATION CURVE OF A MAGNETIC MATERIAL DOES NOT EXPLAIN THE OBSERVED ANOMALOUS CURRENT DEPENDENCE OF MAGNETIC PARTICLES AT LOW LEVELS.

- SUDDEN CHANGES IN THE STATE OF MAGNETIC DOMAINS IN RESPONSE TO LOW INTENSITY FIELDS MAY PROVIDE A SOURCE OF NON-LINEARITY FOR THE GENERATION OF INTERMODULATION. THESE CHANGES ARE CHARACTERIZED AS A SWITCHING BETWEEN TWO EXTREME STATES.

    - ALL ESSENTIAL FEATURES OF THE INTERMODULATION OBSERVATIONS ON MAGNETIC PARTICLES HAVE BEEN DUPLICATED BOTH EXPERIMENTALLY (AT AUDIO FREQUENCIES) AND ANALYTICALLY* ON THE BASIS OF A TWO-STATE SWITCHING MODEL OF A MAGNETIC DOMAIN. IN PARTICULAR, THE PRESENCE OF MAXIMA AND THE REDUCTION OF IM UPON ADDITION OF TRANSMITTERS ARE RE-CREATED BY THE MODEL. THESE FEATURES HAVE BEEN SHOWN EXPERIMENTALLY TO BE INDEPENDENT TO THE PRESENCE OR ABSENCE OF HYSTERESIS IN THE SWITCHING ACTION. THE "THIRD-TRANSMITTER DEPRESSION" EFFECT HAS ALSO BEEN SHOWN EXPERIMENTALLY AND ANALYTICALLY TO BE INDEPENDENT OF THE FREQUENCY OF THE THIRD TRANSMITTER. THE ISOMETRIC PLOT IS SHOWN IN FIGURE 7.

---

* THE MATHEMATICAL TECHNIQUE IS DESCRIBED IN CHAPTER 13 OF W. B. DAVENPORT AND W. L. ROOT, RANDOM SIGNALS AND NOISE, MCGRAW HILL, 1958, PP. 277-311.

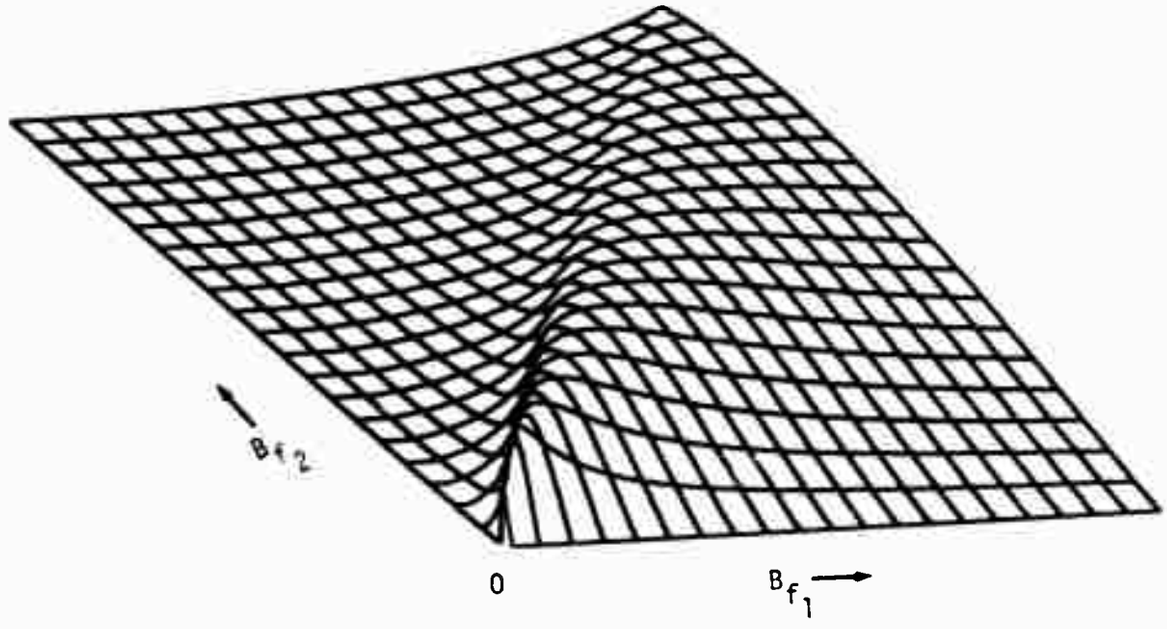

Figure 7. IM Voltage $V_{2f_1-f_2}$ from a Two State (Hard Limiter) Nonlinearity (Theoretical and Audio Frequency Analog Model)

SCALING RELATIONS

ALTHOUGH MEASUREMENTS WERE MADE IN THE DOUBLE-RESONANCE TEST APPARATUS OVER THE ENTIRE RANGE OF CURRENTS AND FIELDS PRESENT IN THE FLTSATCOM SYSTEM, THE SMALL SIZE OF SOME OF THE MAGNETIC SAMPLES MADE IT NECESSARY TO USE HIGHER FIELDS. SCALING RELATIONS WERE THEN REQUIRED TO RELATE THESE MEASUREMENTS TO THE SYSTEM.

THE FOLLOWING SCALING LAWS INCLUDE ONE UNKNOWN FUNCTION, $f(B_1,B_2)$, WHICH HAS BEEN EMPIRICALLY DETERMINED IN A FEW CASES. MOST THEORETICAL TREATMENTS OF IM PREDICT THAT THIS FUNCTION IS PROPORTIONAL TO $I_1^2 I_2$. THIS KIND OF BEHAVIOR HAS BEEN OBSERVED IN A FEW CASES, PARTICULARLY AT HIGH INTERMODULATION LEVELS, BUT LARGE DEPARTURES FROM THIS LAW ARE MORE FREQUENTLY OBSERVED, PARTICULARLY AT LOW LEVELS.

EQUATIONS AND DEFINITIONS:

$$P_{IM} = \frac{V_{IM}^2}{50}$$

$$V_{IM} = \sum_{1}^{N} \omega M_i I_{IMi}$$

$$I_{IMi} = f(B_{1i} B_{2i})$$

$$B_{ji} = \frac{\mu_o I_j}{2\pi r_i}$$

$$M_i \approx \frac{\mu_o A_i}{2\pi r_i}$$

P_{IM} = $2f_1 - f_2$ intermodulation power

V_{IM} = intermodulation voltage at receiver

ω = intermodulation frequency

M_i = mutual inductance between ith particle and circuit

I_{IMi} = current in ith particle at $2f_1 - f_2$

B_{ji} = flux density in coaxial line at f_j and radius r_i

r = radius from axis of coaxial line

A = cross-sectional area of particle

SCALING WITH NUMBER OF PARTICLES

- THEORY PREDICTS IM POWER PROPORTIONAL TO THE SQUARE OF THE NUMBER OF PARTICLES.

- TESTS IN DOUBLE-RESONANCE IM APPARATUS SHOWED FOUR TIMES THE IM POWER WITH TWO 100 MICROMETER IRON SPHERES AS WAS MEASURED WITH ONLY ONE.

- TESTS IN COAXIAL LINE APPARATUS SHOWED 24 DB OF IM ABOVE POLISHED COPPER REFERENCE ROD WITH 20 IRON SPHERES IN THE HIGH MAGNETIC FIELD REGION AND ONLY NOISE LEVEL IM WITH ONE SPHERE. IF THE IM POWER SCALES WITH THE SQUARE OF THE NUMBER OF PARTICLES, THE POWER LEVEL WITH ONE IRON SPHERE SHOULD HAVE BEEN 2 DB BELOW THE REFERENCE LEVEL AND UNOBSERVABLE. IF THE IM POWER WERE TO BE LINEAR WITH THE NUMBER OF PARTICLES, THE LEVEL WITH ONE SPHERE SHOULD HAVE BEEN 11 DB ABOVE THE REFERENCE, AN EASILY DETECTABLE LEVEL OF IM. THIS EXPERIMENT IS CONSISTENT WITH A SQUARE LAW RELATION AND INCONSISTENT WITH A LINEAR DEPENDENCE.

ESTIMATE OF INTERMODULATION LEVEL DUE TO MINUTE IRON PARTICLES FOUND IN COAXIAL LINE

PROCEDURE: THE OUTER SURFACE OF THE INNER CONDUCTOR OF THE "390 DIAMETER" COAXIAL LINE WAS SCANNED BY A MICROPROBE AND FOUND TO HAVE MANY SMALL IRON PARTICLES ON ITS SURFACE.*

THE SURFACE OF THE CONDUCTOR WAS SCRAPED OFF WITH A DIAMOND STYLUS AND THE SCRAPINGS WERE MEASURED IN THE DOUBLE-RESONANCE IM MEASUREMENT APPARATUS.

THE SCRAPINGS CREATED A MEASURABLE LEVEL OF IM. IT WAS SHOWN TO BE OF MAGNETIC ORIGIN BY APPLYING A STEADY MAGNETIC FIELD TO THE INTERACTION REGION AND OBSERVING A SUBSTANTIAL DECREASE IN IM LEVEL. THE IM OBSERVED WAS .04 MICROVOLTS ACROSS 50 OHMS WITH MAGNETIC FIELDS OF 10 and 7.6 GAUSS AT f_1 AND f_2, RESPECTIVELY.

THE IM LEVEL WAS THEN SCALED TO 1 METER OF COAXIAL LINE AT RF MAGNETIC FIELDS REPRESENTATIVE OF THE FLTSATCOM SYSTEM, .9 GAUSS, USING THE SCALING RELATIONS PRESENTED ABOVE.

RESULTS:

- UNDER THE ASSUMPTION THAT IM's SCALE ACCORDING TO $I_1^2 I_2$, A 1 METER LENGTH OF COAXIAL LINE IN THE SYSTEM SHOULD PRODUCE AN IM LEVEL OF - 140 DBM.
- IF THE IM SCALES IN THE MANNER OBSERVED FOR THE 1-MICROMETER PARTICLES INVESTIGATED (SEE CHART A-2), THEN THE EXPECTED LEVEL FOR 1 METER OF COAXIAL LINE WOULD BE - 112 DBM.

---

* THE FOLLOWING PAGE SUMMARIZES THE SUPPORTING MATERIALS ANALYSIS.

SUPPORTING MATERIALS ANALYSIS

0.390 COAXIAL CABLE INCLUSIONS (NICKEL AND IRON)			COMMENT
OUTER CONDUCTOR (COPPER)	OUTSIDE	≥ 30 PER CM^2	SHARP GROOVES VISIBLE ON INSIDE OF OUTER CONDUCTOR AT 160X.
	INSIDE	≥ 30 PER CM^2	
INNER CONDUCTOR (SILVER PLATED COPPER)	OUTSIDE	≥ 6 PER CM^2	
	INSIDE	0	

COTTON TIPPED SWABS (COAXIAL CONNECTOR CLEANING)

USED SWABS	IRON PARTICLES
	TIN, LEAD (SOLDER PROPORTIONS) ZINC SILVER
UNUSED SWABS	CARBON, CHLORINE, POTASSIUM, NICKEL (TRACE)

SECTION 2.1.2

IM GENERATION AT POOR (LOW CONTACT PRESSURE) CONTACTS

PRESSURE CONTACT INTERMODULATION

- POOR CONTACTS BETWEEN PIECES OF METAL CREATED THE LARGEST IM SIGNALS OBSERVED. METAL OBJECTS LYING ON THE WORKBENCH A FEW FEET AWAY COULD CREATE STRONG IM IF THEY WERE LIGHTLY TOUCHING EACH OTHER.

- BRAIDED WIRE SHIELDING, USED AS AN OUTER CONDUCTOR IN FLEXIBLE COAXIAL CABLE, WAS FOUND TO GENERATE STRONG IM, UNDOUBTEDLY DUE TO THE POOR CONTACTS BETWEEN THE METAL STRANDS.

- COAXIAL CONNECTORS WERE TESTED BY USING THE TWO MATING PARTS OF THE CENTER CONDUCTOR TO FUNCTION AS THE COMMON PATH OF THE DOUBLE-RESONANCE IM APPARATUS. A TYPE N CONNECTOR AND A TYPE TNC CONNECTOR WERE TESTED.

    - TYPE N (SILVER-PLATED) - THIS CONTACT WAS EXTREMELY ERRATIC. THE IM VOLTAGE DRIFTED UP AND DOWN OVER A PERIOD OF MINUTES AND CHANGED BY A FACTOR OF UP TO 100 FROM ONE MATING OF THE CONTACTS TO THE NEXT.

    - TYPE TNC (GOLD-PLATED) - THIS CONTACT WAS MUCH BETTER THAN THE TYPE N. THE IM LEVEL WAS MUCH LOWER AND LESS ERRATIC.

SECTION 2.1.3

IM GENERATION AT SOFT SOLDERED JOINTS

SOFT SOLDER JOINT INTERMODULATION

- NO INTERMODULATION WAS OBSERVED THAT COULD BE ATTRIBUTED TO A WELL-MADE SOFT SOLDER JOINT.

- SEVERAL ATTEMPTS WERE MADE TO CREATE BAD SOLDER JOINTS THAT WOULD GENERATE IM. ONLY A VERY WEAK SOURCE COULD BE MADE, AND IT WAS OBVIOUSLY A COLD JOINT AND WOULD HAVE FAILED ANY INSPECTION.

- ONE SOLDER JOINT THAT PRODUCED IM WAS MADE BY ACCIDENT. THE WIRE THAT COUPLES OUT THE IM VOLTAGE, VISIBLE IN FIG. 2, WAS AT ONE TIME POORLY SOLDERED TO THE COMMON PATH POST. INSPECTION UNDER MAGNIFICATION REVEALED THE CRYSTALLIZED APPEARANCE OF A COLD SOLDER JOINT. APPLICATION OF HEAT TO THE JUNCTION ELIMINATED ANY FURTHER IM FROM THIS SOURCE.

- A 1-INCH BAND OF SOFT SOLDER WAS APPLIED IN THE CENTER OF A COPPER ROD MADE TO FIT THE COAXIAL TEST APPARATUS. THE TEST RESULT SHOWED NO SIGNIFICANT IM OVER THE BACKGROUND LEVEL.

- THE DISCREPANCY BETWEEN THE ABOVE RESULTS AND THE EXPERIENCE WITH THE SYSTEM TESTS IS UNRESOLVED. A SPECULATIVE CONJECTURE IS THAT SOME SOLDER MAY CONTAIN IRON PARTICLES WHICH UPON FLOATING TO THE SURFACE MIGHT CREATE IMs.

SECTION 2.1.4

IM GENERATION BY ELECTROLESS NICKEL PLATING

ELECTRO-LESS NICKEL PLATE INTERMODULATION

TWO ALUMINUM RODS WERE PLATED WITH ELECTRO-LESS NICKEL AND TESTED IN THE COAXIAL TEST APPARATUS. A FINE COPPER WIRE WAS PLATED AT THE SAME TIME AND TESTED IN THE DOUBLE-RESONANCE APPARATUS.

- THE IM OBSERVED IN THE COAXIAL TEST APPARATUS WAS NOT SIGNIFICANTLY ABOVE NOISE LEVEL. A 1/4-INCH PIECE OF THE PLATED WIRE, HOWEVER, GAVE A 100 MICROVOLT SIGNAL WHEN PLACED IN THE GAP OF THE DOUBLE-RESONANCE APPARATUS. THE DISCREPANCY WAS FOUND TO BE DUE TO A VERY LARGE DIFFERENCE IN SENSITIVITY OF THE TWO SYSTEMS.

- THE TWO PLATED ALUMINUM RODS WERE HEAT-TREATED AT 300°C FOR 15 MINUTES. THEN ONE OF THE RODS WAS ELECTROPLATED WITH 0.0002 INCH OF COPPER. THE UNOVERCOATED ROD GENERATED IM 20 dB ABOVE THE BACKGROUND LEVEL. THE COPPER-PLATED ROD DID NOT SHOW SIGNIFICANT IM OVER THE POLISHED COPPER ROD BASELINE.

SECTION 2.1.5

IM GENERATION BY THERMAL MODULATION OF RESISTANCE

IM GENERATION BY THIN GRAPHITE FIBERS

THERMAL MODULATION OF RESISTANCE INTERMODULATION

- THERE IS NO DOUBT THAT IM CAN BE GENERATED BY CHANGES IN RESISTANCE OF A CONDUCTOR IN RESPONSE TO CONDUCTED CURRENTS. THE EFFECT HAS BEEN OBSERVED AT LOW FREQUENCIES AS WELL AS BEING SHOWN THEORETICALLY TO EXIST AT RADIO FREQUENCIES.

- ATTEMPTS TO OBSERVE THERMAL IM IN A GOOD CONDUCTOR AT RADIO FREQUENCIES HAVE NOT BEEN SUCCESSFUL.

- THEORETICAL ESTIMATES OF IM LEVELS THAT SHOULD BE GENERATED AT RADIO FREQUENCIES INDICATE THAT THEY ARE TOO LOW TO BE SIGNIFICANT.

GRAPHITE FIBER INTERMODULATION

- A SMALL BUNDLE OF GRAPHITE FIBERS WAS PLACED IN THE GAP OF THE COMMON JUNCTION (SEE FIG. 2). THE VOLTAGE ACROSS THE GAP IS ONLY A FEW VOLTS. MODERATE INTENSITY IM WAS OBSERVED.

- WHEN THE FIBERS WERE PLACED IN THE HIGH FIELD REGIONS AT THE ENDS OF THE HORIZONTAL BAR (SEE FIG. 2), THE FIBERS WERE PICKED UP BY THE FIELD AND DRAWN TO THE BAR, WITH A DRAMATIC INCREASE IN IM LEVEL. THEY STOOD ON END ON THE HORIZONTAL BAR, SOMETIMES MOVING SIDEWAYS INTO HIGHER FIELD REGIONS AND OFTEN IGNITING IN BRILLIANT ARCS, ACCOMPANIED BY STRONG BURSTS OF IM.

- BEFORE THE BACKGROUND LEVEL OF IM COULD BE RESTORED TO ITS PREVIOUS VALUE, THE WHOLE APPARATUS HAD TO BE CLEANED AND EVERY GRAPHITE FIBER REMOVED.

2.2 THEORETICAL INVESTIGATIONS

The theoretical effort in this investigation consisted of 1) establishment of IM floor levels in various UHF components, and 2) the theoretical evaluation of physical effects whose nonlinear behavior could produce IM's (support to the experimental program).

Many of the estimates of lower limits (floor levels) for IM production given here have been made using the basic coaxial transmission line geometry. This reduces computational difficulties without sacrificing the generality of the results. However, we have shown that even very low level IM phenomena in coaxial cable can attain observable values in components (filters, multicoupler etc.) which, to some extent, are tuned. The degree of enhancement depends upon the Q of the component and the order of the IM product. (See Addendum 6.) The following paragraphs contain short summaries of the IM floor mechanisms which have been evaluated. Table 2-1 gives the major numerical results.

2.2.1 IM Floor Estimates

2.2.1.1 Deviations from Ohms Law

A 1 percent deviation from ohms law, varying as the square of the electric field, is to be expected[1] in metals, at a field level of 5 esu (1500 v/cm) in the metal. In the coax UT 141 field levels of $\sim 3 \times 10^{-5}$ esu (9×10^{-3} v/cm) are expected in the Cu walls leading to deviations from ohms law of 4×10^{-13}. The fluctuations in conductivity due to thermal heating of the Cu will be two orders of magnitude greater, completely dominating Guth's prediction. Thus, no further notice of such effects is taken.

2.2.1.2 Joule Heating of Coax Walls (Addendum 1)

A TEM mode propagating in a coax will lose energy to the walls by Joule heating. The coax walls as a consequence of this heating will have their conductivity varying with double the TEM frequency. When two signals of different frequency propagate simultaneously, then the wall conductivity

---

[1] E. Guth and J. Mayerhofer, "On the Deviation From Ohm's Law at High Current Density," Phys. Rev., Vol. 57, 1940, p. 908.

Table 2-1. Major Numerical Results

IM Floor Mechanism	Nominal IM Level for FSC f_1 = 240 MHz, f_2 = 270 MHz $(2f_2 - f_1)$ 30 Watts Each	Comments
Joule loss induced electrical conductivity modulation in coax walls	-170 dBm	Valid for length ℓ less than 50 meters P_1, P_2 are the powers at f_1, f_2. IM level given for ℓ = 5 meters and 0.390 coax
Field induced electro-striction in solid dielectric coax	-176 dBm	0.390 coax does not employ a solid dielectric. This mechanism in that coax would be drastically lower
Nonlinear term in the Lorentz force on conduction electrons	-190 dBm	

NOTE: In a component with a moderate Q; ≈ 500 the currents and consequently the IM levels will be greater. For example for the Joule heating modulation, and a Q = 500 the predicted IM level would be about -145 dBm, all other parameters being the same as above.

will also display sum and difference frequency conductivity modulations. These signals propagating along these conducting surfaces with time dependent properties will generate third and higher order harmonies. In an analysis, we computed the third order (300 mc) power generated in coax* UT 250 with 240 MHz and 270 MHz propagating simultaneously. The IM power for distances short compared to the attenuation length (50 meters) (UT 250) is given by

$$P = 5.5 \times 10^{-25} P_1^2 P_2 Z^2$$

where Z is the coax length in meters and P_1 and P_2 are the power in the individual frequencies, 240 MHz and 270 MHz. When $P_1 = P_2 = 30$ watts, then the IM power peaks at 8×10^{-18} watts for 50 meters of cable. The IM power generated in any cable other things being equal will vary as a^{-6} where a is the radius of the inner conductor.

This thermal mechanism was also evaluated for a small whisker in a component. The analysis is given in Addendum 5 where it is shown that the resulting IM levels are negligibly small.

2.2.1.3 IM Production Due to Electrostriction of Dielectric Coax (Addendum 2)

In general, a dielectric subjected to a varying electric field will experience time dependent slight changes in density. Accompanying these density changes will be dielectric susceptibility changes and therefore, a time dependency to the dielectric constant. This time dependency of the dielectric constant will be a source of IM production in coaxes. An investigation of this effect shows that the IM power varies inversely as the bulk modulus squared. The bulk modulus for Teflon is unavailable. However, using the available data of Young's modulus which is probably too low for bulk modulus, we obtain IM power levels in coaxes which are lower by a factor of 4 than is produced by Joule heating.

*Table 2-2 gives the salient properties of the various kinds of coaxial cable referred to here.

Table 2-2. FLTSATCOM Cable Data

UT 141	Outer Conductor: Copper, O.D. = 0.141 in Dielectric: FEP Teflon, O.D. = 0.119 in (solid) Center Conductor: Silver-plated Copper, O.D. = 0.0359 in
UT 250	Outer Conductor: O.D. = 0.250 in Dielectric: TFE Teflon, O.D. = 0.214 in (solid) Center Conductor: O.D. = 0.064 in
390 Diameter Cable	Outer Conductor: O.D. = 0.392 in Insulator: Teflon, 5-splined, approximately 0.330 in Center Conductor: O.D. = 0.136 in

2.2.1.4 IM Due to the Nonlinear Character of the Lorentz Force (Addendum 3)

The conduction electrons in the metal walls of the coax will obey the equation of motion:

$$\frac{d\vec{v}}{dt} + \nu\vec{v} = \frac{e}{m}\left(\vec{E} - 4\pi\vec{P} + \frac{\vec{v}}{c} \times \vec{H}\right)$$

where $\vec{v}$ is the electric drift velocity, ν the collision frequency, $\vec{E}$ and $\vec{H}$ the local fields and $\vec{P}$ the polarization. The last term is nonlinear and is usually ignored in the theory of conductivity. However, its presence can be expected to result in IM products. An analysis of IM generation just due to this nonlinear term in the metal of coaxes shows that the IM power is two orders of magnitude lower than that produced by Joule heating.

2.2.1.5 IM Production Due to Field Emission

Another nonlinear process is field emission from sharp projections or burrs on the walls of the coax. The process is nonlinear because the emitted electron current density depends exponentially[2] on the electric field strength at the projection. However, the process is not attractive

[2] R.H. Good Jr. and E.W. Müller, "Field Emission," in Handbuch der Physik Vol. xxl, 1956, p. 188.

because of the extremely large fields and the low work function required to produce any appreciable current. For example, assume that the full 45 volts which may occur across the coax, discussed before, were applied to a projection of 10^{-5} cm in altitude and with an unrealistically low work function of 2 ev (corresponding to an activated cathode). Using Equation (5.19) of Reference [2] (Fowler-Nordheim theory) we find that the current density emitted under this field of 4.5×10^{6} volts/cm is only 1.9×10^{-9} amps/cm^2. The current density in the coax metal at IM frequencies, driven by the two impressed frequencies, on the other hand, is 46×10^{-9} amp/cm^2. It is hard to see how field emission can compete with the other mechanisms for IM production since we cannot usually expect such low work functions and such large fields at these projections.

The high field emission phenomenon has been theoretically evaluated both by TRW and independently by Dr. Vincent Folen (NRL) (private communication) and found to be negligibly small.

2.2.1.6 IM Generation in Resonant Cavities (Addendum 6)

In Addendum 2 it is pointed out that IM generation, by Joule heating, varied as the sixth power of the impressed fields propagating through the coax. Therefore, any condition, such as resonance, which increases field strength sharply should increase IM power. An analysis was made of IM generation in a coax employed as a resonant cavity. The coax of length, 5 meters, was resonant not only to the impressed frequencies, 270 MHz and 240 MHz, but also to the IM frequency 300 MHz. Due to this resonance, the IM power propagating in the cavity is augmented by six orders of magnitude over that produced in the conventional coax. Thus, in coax UT 141 with impressed powers of 30 watts, each at 270 MHz and 240 MHz, the power in the IM frequency of 300 MHz is 2×10^{-11} watts (traveling to right at 5 meters length of resonant cavity).

2.2.1.7 IM Generation by Tunneling

Metals in contact are very often separated by thin films of oxide. These films serve as a barrier for electron conduction between the two metals. However, electrons, under the influence of an electric field can tunnel through this barrier. Since the probability of tunneling is dependent exponentially on the strength of the electric field, the current in a circuit limited by such tunneling phenomena is highly nonlinear and is a

potential source of IM products. Calculations have not been performed on this phenomenon, mainly because it is not an irreducible mechanism. That is, simple techniques, such as increasing contact pressure or gold plating surfaces to be placed in contact markedly reduces IM production by this mechanism.

In addition to the IM floor estimates, several other theoretical problems were addressed in this investigation. These are described on the following paragraphs, with more detailed treatments given in the referenced addenda.

2.2.2 Computer Model

In order to evaluate the system effects of IM generation their source strengths must be known as well as how they propagate. These considerations led to formulation of a powerful computer model capable of accepting theoretical or experimentally generated values of IM source strengths and field or power dependences.

The results of this effort allow handling of the problem of the propagation of localized IM producing sources within a given component. It can handle multiple sources and account for relative (and time variable) phase changes between them. It also provides the electric or magnetic field intensities at stated positions within components. This model was to be furnished with experimental values of IM "source strength" and was to be used to obtain resultant IM values at the output port of the component. Additional details are contained in Addendum 4. The model was not completed to the required level to allow its use during this program.

2.2.3 IM Quieting Due to Out of Product Frequencies

An important observation made during hardware testing was the decrease in the level of a given IM, i.e., $(2f_1 - f_2)$ when one or more additional transmitters were turned on. When these new frequencies did not themselves contribute to the $(2f_1 - f_2)$ term, the level of this term decreased. Other new IM's occurred elsewhere. This problem was addressed analytically assuming that the transmitters were noise loaded. The analysis predicts a decrease in level for a specified form of nonlinearity. The details of the analysis are contained in Addendum 7, where intermodulation is analyzed due to a small discontinuous deviation from linearity for the case of

narrow-band Gaussian noise signal sources in combination. It is found that the presence of out-of-band channel signals reduces intermodulation products falling in a narrow-band receiver channel. This reduction was found to be inversely proportional to the number of equally intense (out-of-band) signals with that number raised to a power equal to the order of the intermodulation products that happen to fall in the receive band.

3. CONCLUSIONS AND GUIDELINES

A number of material and process type guidelines have evolved from this investigation. Many of them relate to magnetic materials. The undesirability of magnetic materials from an IM viewpoint is not new, however, the relative difficulty of avoiding their inclusion in, or pick up by, materials as a result of many processes needs to be emphasized.

The determination that copper walled semi-rigid coaxial cable contains nickel and iron inclusions implies that portions of the transmit antenna feed may also contain such inclusions. These elements may carry the drive current on outside surfaces where not only ferromagnetic inclusions are possible, but accrual of ferromagnetic contamination is rather likely.

Tests made on samples removed from inner and outer surfaces of both the inner and outer conductors of 0.390 coaxial line were made. These showed that samples taken from the surfaces of these conductors produced IMs while samples taken from within the volume of the copper did not produce IMs. This observation supported the electron microprobe results that the nickel and iron inclusions found in the material of the coax walls were found at the surface and not from the deeper lying layers.

These considerations are also important for other components (filters, multicoupler) that are machined. Both copper (test hardware) and aluminum (flight hardware) are soft and would be likely to pick up inclusions from the working tools. It is possible although unlikely that such materials which have not been drawn or previously machined would contain ferromagnetic impurities.

CONCLUSIONS AND GUIDELINES

- OF THE MANY POTENTIAL SOURCES OF IM THAT ARE KNOWN, SMALL MAGNETIC PARTICLES MAY BE THE MOST TROUBLESOME, FOR THE FOLLOWING REASONS:
  - ONLY VERY LOW FIELD INTENSITIES ARE REQUIRED TO PRODUCE NONLINEAR EFFECTS, IN CONTRAST TO OTHER MECHANISMS SUCH AS SEMICONDUCTOR FUNCTIONS, FIELD EMISSION, GLOW DISCHARGES, AND THERMAL RESISTANCE MODULATION.
  - EXTREMELY SMALL QUANTITIES OF MAGNETIC MATERIAL ARE REQUIRED TO GENERATE OBJECTIONABLE LEVELS OF IM. THESE LEVELS OF CONTAMINATION MAY OCCUR DUE TO AIRBORNE MAGNETIC DUST, DUE TO HANDLING OR TOOL WEAR DURING FABRICATION, OR THEY MAY BE ALREADY PRESENT IN THE STOCK FROM WHICH COMPONENTS ARE MADE.
  - THE SMALL QUANTITIES OF MAGNETIC MATERIAL PRESENT IN COMPONENTS OF A SYSTEM MAY BE UNDETECTABLE BY STANDARD MAGNETIC SCREENING DEVICES, OR EVEN SENSITIVE FLUX-GATE MAGNETOMETERS.

- MAGNETIC PARTICLES ARE BELIEVED TO BE A POSSIBLE SOURCE OF THE IM GENERATION OBSERVED IN THE FLTSATCOM SYSTEM.
  - MAGNETIC PARTICLES HAVE BEEN OBSERVED IN THE COAXIAL LINE PROCURED FOR THE SYSTEM, POSITIVELY IDENTIFIED, AND THEIR IM GENERATION MEASURED.
  - THE DEPARTURE FROM $I_1^2 I_2$ SCALING OBSERVED IN THE FLTSATCOM SYSTEM IS EXPLAINABLE MOST SIMPLY ON THE BASIS OF A MAGNETIC DOMAIN FLIP MODEL.

(Cont'd)

CONCLUSIONS AND GUIDELINES (CONT'D)

- A DESIGN GUIDE FOR MINIMIZING IM FROM MAGNETIC PARTICLES IS TO USE LARGE DIAMETER CONDUCTORS, PARTICULARLY WHEREVER HIGH CURRENTS ARE INVOLVED. THIS REDUCES THE B-FIELDS WHICH DRIVE THE PARTICLES AND ALSO REDUCES THE IM COUPLED FROM THE PARTICLES INTO THE SYSTEM. LARGE REDUCTIONS ARE POSSIBLE WITH SMALL INCREASES IN DIAMETER. (FOR THE $I_1^2 I_2$ TYPE OF SCALING, THE IM POWER IS INVERSELY PROPORTIONAL TO THE EIGHTH POWER OF THE CONDUCTOR RADIUS.)

- STEEL TOOLS FOR CUTTING OR PREPARING SEMI-RIGID COAXIAL CABLE SHOULD NOT BE USED. THEIR USE CAN DEPOSIT MAGNETIC PARTICLES INSIDE THE CABLE AND CAN ALSO CONTAMINATE THE DIELECTRIC. WE DO NOT KNOW THE SOURCE OF THE MAGNETIC INCLUSIONS FOUND INSIDE THE COPPER COAX WALLS BUT IT IS LIKELY THAT IT RESULTS FROM WEAR OF THE DRAWING DIE. STEEL WOOL SHOULD NEVER BE USED FOR DEBURRING OR POLISHING.

- IT IS DESIRABLE TO "SWEEP" MACHINING, ASSEMBLY AND TESTING AREAS WITH A POWERFUL MAGNET BEFORE SETTING DOWN ANY WORK SURFACE THAT WE USE, WILL BE EXPOSED TO HIGH UHF FLUX DENSITIES. POSSIBLY AN IM SNIFFER SHOULD BE SCANNED OVER SUCH AREAS. USE OF NON-MAGNETIC, BUT HARD WORKING SURFACES WOULD BE DESIRABLE.

- THE POLISHING OF MATING SURFACES REDUCES THE IM LEVEL PRODUCED BY A COMPONENT. THERE ARE TWO POSSIBLE REASONS FOR THE UTILITY OF POLISHING.

(Cont'd)

CONCLUSIONS AND GUIDELINES (CONT'D)

1. REMOVAL OF CONTAMINANT PARTICLES ADHERING TO THE SURFACES OR REMOVING INCLUSIONS IN THE SURFACE.

2. BURIAL OF CONTAMINANT PARTICLES AND INCLUSIONS WITHIN THE PURE BULK, METAL (COLD FLOW).

- USE A DC MAGNETIC FIELD (PERMANENT MAGNET) TO DETERMINE WHETHER GIVEN IM LEVELS IN SYSTEM HARDWARE CONTAIN SIGNIFICANT CONTRIBUTIONS FROM INADVERTENT MAGNETIC MATERIALS.

- MAGNETIC MATERIALS SUCH AS KOVAR SHOULD NOT BE USED UNLESS THEY CAN BE COMPLETELY COVERED BY AN ADEQUATE THICKNESS OF HIGH-CONDUCTIVITY NON-MAGNETIC PLATING.

- ELECTROLESS NICKEL PLATE CAN BE USED IF IT IS COMPLETELY COVERED BY COPPER PLATE AT LEAST 0.0002" THICK. ALTHOUGH THIS THICKNESS IS ONLY A LITTLE GREATER THAN THE SKIN DEPTH IN COPPER AT 250 MHz, THE MEASUREMENTS INDICATE THAT IT IS ENOUGH TO GREATLY REDUCE IM GENERATION. FOR SMALLER DIAMETER CONDUCTORS, A SLIGHTLY GREATER THICKNESS MAY BE NECESSARY.

- BRAIDED WIRE SHIELDS ARE COPIOUS SOURCES OF INTERMODULATION AND SHOULD BE AVOIDED.

(Cont'd)

CONCLUSIONS AND GUIDELINES (CONT'D)

- PRESSURE-CONTACT RF CONNECTORS REPRESENT A RISK, SINCE THE QUALITY OF THE CONTACT CAN DEGRADE WITH TIME.

- METAL JUNCTIONS SHOULD BE SOLDERED, WHERE POSSIBLE, AVOIDING RELIANCE ON PRESSURE CONTACTS.

As a result of experimentation on thin graphite fibers we conclude that the translational forces exerted on induced dipole moments by a spatially nonuniform electric field can be significant. It is reasonable to conclude that small particles (dielectric or metallic) that may reside inside UHF components (multicoupler, filters, antenna feeds, and baluns) will be likewise drawn into high field regions and there become IM sources as did the graphite fibers.

There is a disparity between conclusions on the IM behavior of soft solder joints obtained here and those reached in the hardware development program. Soft solder joints have been benign insofar as IM generation is concerned in this phenomenology investigation. It is possible that magnetic impurities float to the surface of the solder where the UHF currents then produce IMs. Thus the improvement obtained in the hardware where the solder fillets were trimmed away. We have no evidence to support this conjecture and have not resolved the disparity of behavior for soft soldered joints.

4. INVESTIGATION – REQUIREMENTS FOR FUTURE WORK

4.1 EXPERIMENTAL

More experimental work at UHF – Purpose: To find materials and ways of modifying processes so that they may be used without producing IM's.

Determination of IM producing mechanisms in: stripline elements, thermal wrap materials, and other component and structure related items as can be foreseen in projected system.

Experimental programs to firm up the knowledge base in selected frequency ranges. This requires coordination with frequency planning activities so that work is not performed unnecessarily.

Generation of data to allow prediction of power dependence of selected IM sources.

More thorough investigation of pressure contacts, placing emphasis on "good" contacts that may be sources of low level IM.

Develop more complete signature data for different types of IM sources, as a means of identifying the source of IM problems in systems.

Investigate the relative strengths of different IM orders generated by known sources.

Characterize IM sources on the basis of the effect of additional transmitters (two-state IM generators produce a fixed total power in all frequencies generated. The third transmitter depression effect is a consequence of this law. In contrast, non-saturating nonlinearities, e.g., thermal IM's, show no third-transmitter depression effect).

Characterize IM sources according to the erratic versus steady behavior of the IM.

Investigate influence of temperature and mechanical vibration on erratic IM sources.

Build a probe device for discovering and localizing sources of IM in fabricated components and systems, as well as for inspecting stock.

4.2 IM INVESTIGATION – REQUIREMENTS FOR FUTURE WORK

Theoretical

IM production in resonant cavities, resonant in modes other than principal.

*The role of non-propagating source terms in IM production in coaxes.

Determination of Green's function for IM production in coaxes.

Thermal effects in barrier transmission (tunneling).

Effect of magnetic switching time on strength of IM products.

---

*Non-propagating waves array from the nonlinear interaction of the form

$$E = E_0 e^{-i(\Omega t + Kx)}$$

where

$$\Omega = 2\omega_1 - \omega_2$$

and

$$K = \omega/c = \frac{\omega_1 - \omega_2}{c}$$

rather than

$$\frac{2\omega_1 - \omega_2}{c}$$

ADDENDUM 1

THERMAL HEATING CONTRIBUTION TO INTERMODULATION FIELDS IN COAXIAL WAVEGUIDES

ABSTRACT

We investigate intermodulation production due to the thermal heating of the waveguide walls. We consider two impressed signals propagating in a coaxial cable in the TEM mode. We find that the power developed in the I.M. product depends upon the thermal coefficient of the electrical conductivity of the metal squared, and is inversely proportional to the conductivity itself. For FLTSATCOM testing conditions (coax uT 141 filled uniformly with Teflon), the minimum power of I.M. products of third order ($\omega = 2\omega_1 - \omega_2$) varies for short distances as

$$P = 1.8 \times 10^{-23} P_1^2 P_2 z^2 \text{ watts}$$

where P_1 and P_2 are the impressed powers in watts and z is cable length in meters. I.M. power reaches its maximum at a distance $z_{max} = 28$ meters and is attenuated for distances greater than z_{max}. For I.M. frequency $f = 300$ Mc and $P_1 = P_2 = 30$ watts, we find $P_{max} = 8 \times 10^{-17}$ watts. For FLTSATCOM operating conditions (coax uT 250) I.M. power varies for short distances as

$$P = 5.5 \times 10^{-25} P_1^2 P_2 z^2$$

and peaks at $P_{max} = 8 \times 10^{-18}$ watts for 50 meters of cable.

1. INTRODUCTION

The purpose of our investigations is to determine the minimum I.M. power to be expected in a coaxial cable. In this particular report, we study the thermal intermodulation mechanism. A report on I.M. production due to the nonlinear response of the waveguide dielectrics is given by us in a separate paper.

Due to the finite conductivity of a metal, there always exists the RF energy loss in metallic walls of a waveguide, in a volume confined approximately by the thickness of the skin depth. The cyclic variations in energy within this volume can be assumed to be followed instantaneously by temperature. Since the metallic conductivity depends linearly on temperature, it has also harmonic components which will produce wall currents at I.M. frequencies. I.M. currents are calculated in Section 2 of this report. The I.M. currents drive the TEM mode in the coaxial cable, this is discussed in Section 3. In the DISCUSSION section, we give numerical estimates of the minimum (ideal bulk conductivity) I.M. products generated by the thermal heating of the metallic walls appropriate to both testing and FLTSATCOM operating conditions.

2. THERMAL CONDUCTION AND I.M. CURRENTS IN METALLIC WALLS OF A COAXIAL CABLE

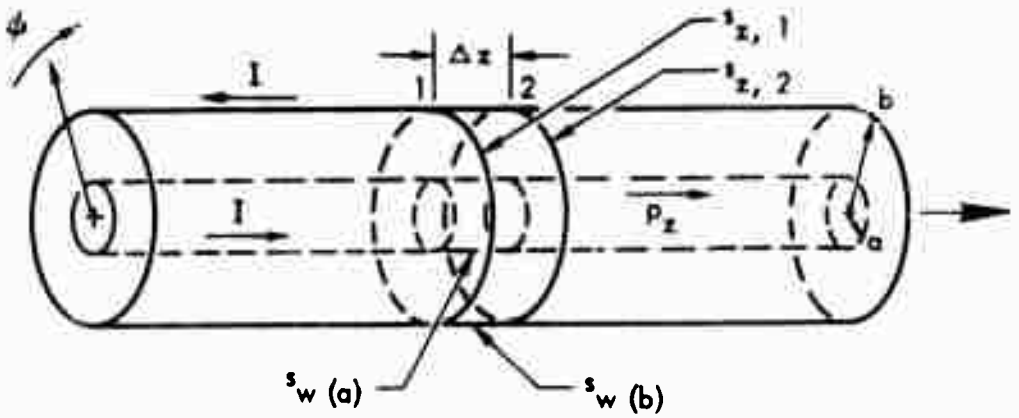

Figure 1. Geometry of Coaxial Cable.

2.1 RF Dissipation

We consider a coaxial cable carrying two signals of frequencies ω_1 and ω_2. The two signals are carried in the TEM mode; the magnetic fields are concentric with walls of the coax. The electric fields are almost radial; however, due to the finite conductivity of metallic surfaces, fields do penetrate into the walls of the coax and the electric fields have small (but finite) tangential components.

Propagation of fields in a coaxial cable is described by Maxwell equations

$$\nabla \times H = \frac{1}{c}\frac{\partial D}{\partial t} + \frac{4\pi}{c}(j_s + \sigma E) \tag{1}$$

$$\nabla \times E = -\frac{1}{c}\frac{\partial B}{\partial t} \tag{2}$$

where j_s is a source current (if any).

For a coax, Equations (1) and (2) yield: Fields in the dielectric ($a \leq r \leq b$):

$$H_y(r) = \sqrt{\epsilon}\, E_r(r) = \frac{2I}{cr}\cos(\omega t - kz) \tag{3}$$

where I is the current in the coax walls. In the metal interior,

$$H_y = H(b)e^{-r/\delta}\cos\left(\omega t - \frac{r}{\delta}\right) \tag{4}$$

$$E_2 = -\left(\frac{\omega}{4\pi\sigma}\right)^{1/2} H(b)\, e^{-r/\delta}\cos\left(\omega t - \frac{r}{\delta} + \frac{\pi}{4}\right), \tag{5}$$

where r is measured from the outer radius b (a similar expression describes fields in the inner wall of radius a). The skin depth δ is given by

$$\delta = \frac{c}{(2\pi\sigma\omega)^{1/2}} \tag{6}$$

where σ is the metallic conductivity.

The electromagnetic energy is dissipated at the rate

$$\vec{j} \cdot \vec{E} = \sigma \left(E_{z,1} + E_{z,2} \right)^2 \quad , \tag{7}$$

where $E_{z,1}$ and $E_{z,2}$ are tangential components inside the metal interior (Equation (5)) r signals ω_1 and ω_2 respectively.

2.2 Thermal Conduction

The RF energy loss is confined to a volume given approximately by the skin depth δ. We shall assume that the energy is lost from this volume only by conduction between the inner and outer walls (thickness of the metallic walls is much greater than the skin depth δ). The thermal wave then satisfies the following differential equation

$$\vec{j} \cdot \vec{E}_2 = \sigma \left(E_{z,1} + E_{z,2} \right)^2 = c_p \frac{dT}{dt} - \kappa \nabla^2 T \tag{8}$$

In Equation (8), c_p and κ are respectively the specific heat and thermal conductivity (per unit volume) of the metal and T is temperature. The heat wave is driven by the RF fields penetrating into the metal - left hand side of Equation (8). If we write the driving term as

$$Ae^{-2r/\delta} \cos (\Omega t - 2r/\delta) \tag{9}$$

then, for boundary conditions $(T(r = \infty) = T(\infty))$, $(\partial T/\partial r)_\infty = 0$ and $(\partial T/\partial r)_{r=0} = 0$, Equation (9) has the solution

$$\Delta T = T(r) - T(\infty) = \frac{A}{2\kappa \left(\frac{1}{\delta_{th}^2} - \left(\frac{2}{\delta} \right)^2 \right)} \left\{ e^{-2r/\delta} \sin \left(\Omega t - \frac{2r}{\delta} \right) - \frac{2\delta_{th}}{\delta} e^{-r/\delta_{th}} \sin \left(\Omega t - \frac{2r}{\delta_{th}} \right) \right\} \tag{10}$$

where $T(\infty)$ is the temperature at the outer wall of the metallic sheet and the thermal depth δ_{th} is defined by

$$\delta_{th} = \left(\frac{2\kappa}{\omega c_p} \right)^{1/2} \quad . \tag{11}$$

Equation (10) can be immediately simplified. Using the values $\kappa = 4 \times 10^7$ erg cm^{-1} deg^{-1}, $c_p = 3.2 \times 10^7$ erg cm^{-3} deg^{-1}, $\sigma = 5.8 \times 10^{17}$ sec^{-1} (appropriate for copper), we find that the ratio

$$\frac{\delta_{th}}{\delta} \quad \frac{1}{c}\left(\frac{4\pi\sigma\kappa}{c_p}\right)^{1/2} \approx \frac{1}{10} \quad .$$

The smallness of this ratio reflects the fact that the electrical energy at frequency Ω is dissipated within the region where the driving fields are finite (skin depth) rather than being conducted away from this region. In what follows, we shall neglect both the $\left(\frac{2}{\delta}\right)^2$ term in the denominator of Equation (10) and term proportional to $2\delta_{th}/\delta$ on the right hand side of Equation (10).

2.3 Intermodulation Current

We now calculate I.M. currents generated in the coax walls. The current density j is equal to

$$j = \sigma\left(E_{z,1} + E_{z,2}\right)$$

where the metallic conductivity σ varies linearly with temperature,

$$\sigma = \sigma_o\ (1 - \gamma\Delta T) \quad .$$

Using Equations (5) - (10) we find that j has I.M. components of frequency $\omega = 2\omega_1 - \omega_2$,

$$j_s = A\, e^{-3r/\delta} \sin\left(\omega t - \frac{r}{\delta} + \frac{\pi}{4}\right) \tag{12}$$

where

$$A_b(r) = \frac{\gamma\sigma^2}{8c_p}\ \frac{5\omega_1 - \omega_2}{\omega_1(\omega_2 - \omega_1)}\ E^2_{1,z}(b)E_{2,z}(b)e^{-3r/\delta} \sin\left(\omega t - \frac{r}{\delta} + \frac{\pi}{4}\right) \tag{13}$$

and where we have assumed that the two skin depths $\delta_1 \approx \delta_2 \approx \delta$. Equations (12) and (13) give the I.M. current density generated in the outer wall of

the coax; similar expressions give current density in the inner wall (radius a). Notice, that the I.M. currents are generated within one third of the skin depth, $\delta/3$.

3. I.M. FIELDS SUPPORTED BY WALL SOURCE CURRENTS

3.1 Boundary Conditions for the TEM Mode

We now calculate fields supported by the source currents j_s. First of all we notice that the ratio of the current densities

$$\frac{j_s(b)}{j_s(a)} = \frac{\Lambda_b(b)}{\Lambda_a(a)} = \frac{a^3}{b^3} \tag{14}$$

also determines the ratio of the corresponding fields and currents,

$$\frac{H_s(b)}{H_s(a)} = \frac{a^3}{b^3} \quad ; \quad \frac{I_s(b)}{I_s(a)} = \frac{a^2}{b^2} \quad . \tag{15}$$

On the other hand, TEM fields in a coax must satisfy $H = \frac{2I}{cr}$, where $I = I(b) = I(a)$. Clearly, fields generated directly by j_s cannot constitute the total of the I.M. fields. Additional currents must be set up in the coax walls such that the sum of the driving and induced fields propagates in the TEM mode.

These considerations are put into the mathematical form by requiring that the I.M. signal satisfies boundary conditions appropriate to the TEM mode:

$$I = I_{ind}(b) + I_s(b) = I_{ind}(a) + I_s(a) \tag{16}$$

$$H_m(a) = H_d(a) = \frac{b}{a} H_m(b) = \frac{b}{a} H_d(b) \quad ,$$

where subscript ind means induced and I is the total current, and subscripts m and d designate fields in metal and dielectric respectively.

Combining Maxwell Equations (1) and (2) we find that H-field in the coax wall satisfies the following equation,

$$\frac{\partial^2 H_m}{\partial r^2} - \frac{2}{\omega\delta^2}\frac{\partial H_m}{\partial t} = \frac{4\pi}{c}\frac{\partial j_s}{\partial r} \tag{17}$$

where δ and ω ($\omega = 2\omega_1 - \omega_2$) are respectively I.M. skin depth and frequency and j_s is the source current (Equation (12)).

Making the approximation that all skin depths are of approximately the same order of magnitude, Equation (17) yields

$$H_m(b) = -\frac{\pi\Lambda_b\delta}{5c} e^{-3r/\delta}\left(7\sin\left(\omega t - \frac{r}{\delta} + \frac{\pi}{4}\right) - \cos\left(\omega t - \frac{r}{\delta} + \frac{\pi}{4}\right)\right) \tag{18}$$

$$+ H_h(b)\, e^{-r/\delta}\cos\left(\omega t - \frac{r}{\delta} + \frac{\pi}{4} + \phi_b\right)$$

where $H_h(b)$ are ϕ_b respectively the amplitude and phase angle of the homogeneous solution of Equation (18) in the outside wall. (Again, a similar expression gives field $H_m(a)$). Using the boundary conditions, Equation (16), we find that the phase angles $\phi_b = \phi_a = \phi = \tan^{-1} 7$. Relating $H_h(b)$ and $H_h(a)$ to amplitudes of H-field in dielectric, we finally have

$$H_m(b) = \left\{\left(H_d(b) - \frac{\pi\Lambda_b\delta}{5c\cos\phi}\right)e^{-r/\delta} + \frac{\pi\Lambda_b\delta}{5c\cos\phi}e^{-3r/\delta}\right\} \tag{19}$$

$$\cos\left(\omega t - \frac{r}{\delta} + \frac{\pi}{4} + \phi\right)$$

where

$$H_d(r) = \sqrt{\epsilon}\, E_r(r) = \frac{2I}{cr}$$

We also calculate the tangential component E_z inside the metallic wall. Using Equation (1), we obtain

$$E_z = \frac{c}{4\pi\sigma}\left(\frac{\partial H_m}{\partial r} - \frac{4\pi}{c} j_s\right) = \tag{20}$$

$$= \frac{c}{4\pi\sigma\delta}\sqrt{2}\left(H_d - \frac{\pi\Lambda\delta}{5c\cos\phi}\right)e^{-r/\delta}\sin\left(\omega t + \phi - \frac{r}{\delta}\right)$$

$$- \frac{\Lambda}{10\sigma}e^{-3r/\delta}\left(\sin\omega t + \phi - \frac{r}{\delta}\right) + 2\cos\left(\omega t + \phi - \frac{r}{\delta}\right) \quad .$$

In Equations (19) and (20), amplitudes $H_d(r)$ and I are as yet undetermined quantities; we shall proceed to calculate their growth.

3.2 Growth of I.M. Fields

Theoretically, it is possible to solve Equations (1) and (2) for I.M. fields directly. However, due to the fact that E-field has a finite component E_z (and varying with r) along the axis of the coax, such a calculation would be too complicated. To calculate the growth of the I.M. fields, we use the energy conservation principles.

The change in power P_z ($P_z = \int \vec{ds}_z \cdot \vec{S}_z$, see Figure 1) crossing the coax cross section per unit length is given by

$$\frac{dP_z}{dz} = \frac{1}{\Delta z}\int_{walls} \vec{ds}_w \cdot \vec{S}_w \qquad (21)$$

where $\vec{S}_z$ and $\vec{S}_w$ are respectively components of Poynting vector $\vec{S}$ parallel and normal to the coax walls and Δz is the length increment along the coax axis. Using Equations (19) and (20), Poynting vector at wall r = b is equal to

$$\vec{S}_w(b) = \frac{c}{4\pi}\left[E_2(b) \times H_\phi(b)\right]_w = \frac{c^2}{2(4\pi)^2\sigma\delta}\left\{-H_d^2(b) + \frac{69}{5}\frac{2\pi\Lambda_b\delta}{c\cos\phi}H_d(b)\right\} \qquad (22)$$

The first term on the right hand side of Equation (22) represents energy dissipated into the coax walls due to the finite conductivity of the metal (Poynting vector is directed into the wall). The second term gives power generated by the I.M. source currents (Poynting vector is directed into the coax). Notice that the phase of j_s (or, equivalent of Λ) determines the phase of H_d.

It is now straight forward to obtain the growth rate of I.M. products: We integrate both Equation (22) and a similar equation for $\vec{S}_w(a)$ over the coax walls and substitute the results into Equation (21). Before doing so, however, we notice that, at this stage, it is convenient to include into our picture also the attenuation rate of the impressed fields (of frequencies ω_1 and ω_2).

The input fields are attenuated as $H \approx E \approx e^{-\beta z}$, where the factor β is given by

$$2\beta = \frac{a + b}{ab \ \ell n \frac{a}{b}} \left(\frac{\varepsilon\omega}{8\pi\sigma}\right)^{1/2} \tag{23}$$

Hence, the source currents vary as $j_s \approx \Lambda \approx e^{-3\beta z}$. Using the result that the propagating power P_z

$$P_z = \frac{c}{4\sqrt{\varepsilon}} b^2 \left(\ell n \frac{b}{a}\right) H^2(b) \quad , \tag{24}$$

we then find that Equation (21) reduces to

$$\frac{dH^2(b)}{dz} = -2\alpha\left(H^2(b) - d \cdot H(b)\ e^{-3\beta z}\right) \quad , \tag{25}$$

which, with the boundary condition that $H(b)/_{z=0} = 0$ yields

$$H(b) = \frac{\alpha d}{\alpha - 3\beta}\left(e^{-3\beta z} - e^{-\alpha z}\right) \quad , \tag{26}$$

where

$$2\alpha = \frac{a + b}{ab\left(\ell n \frac{b}{a}\right)} \left(\frac{\varepsilon\omega}{8\pi\sigma}\right)^{1/2} \tag{27}$$

$$d = 138 \left(\frac{\pi}{\sigma\omega}\right)^{1/2} \cdot \Lambda_b \cdot \left(1 - \frac{b}{a} + \frac{b^2}{a^2}\right) \quad . \tag{28}$$

4. DISCUSSION

Equations (24) + (28) with Λ_b given by Equation (13) are the basic results of this paper. The main conclusions can be summarized as as follows: For small distances z ($z < \alpha^{-1}$), H-field grows linearly,

$$H_{IM}(b) = \frac{69}{128\pi}\left(1 + \frac{b^3}{a^3}\right)\frac{1}{b\ \ell n\ \frac{b}{a}}\ \frac{5\omega_1 - \omega_2}{\omega_2 - \omega_1}\ \frac{\gamma}{c_p}\cdot\left(\frac{\varepsilon\omega_2}{2\pi\sigma}\right)^{1/2} H_1^2(b)H_2(b)z$$

and power quadratically,

$$P_{IM} = \frac{c}{4}\frac{b^2}{\sqrt{\varepsilon}}\ \ell n\ \frac{b}{a}\ H_1^2(b)$$

$$= \left(\frac{69}{128\pi}\right)^{1/2}\frac{c\omega_2}{8\pi\sigma}\frac{\gamma^2}{c_p^2}\left(1 + \frac{b^3}{a^3}\right)^2\ \frac{\sqrt{\varepsilon}}{\left(\ell n\ \frac{b}{a}\right)}\left(\frac{5\omega_1 - \omega_2}{\omega_2 - \omega_1}\right)^2 H_1^4(b)H_2^2(b)z^2$$

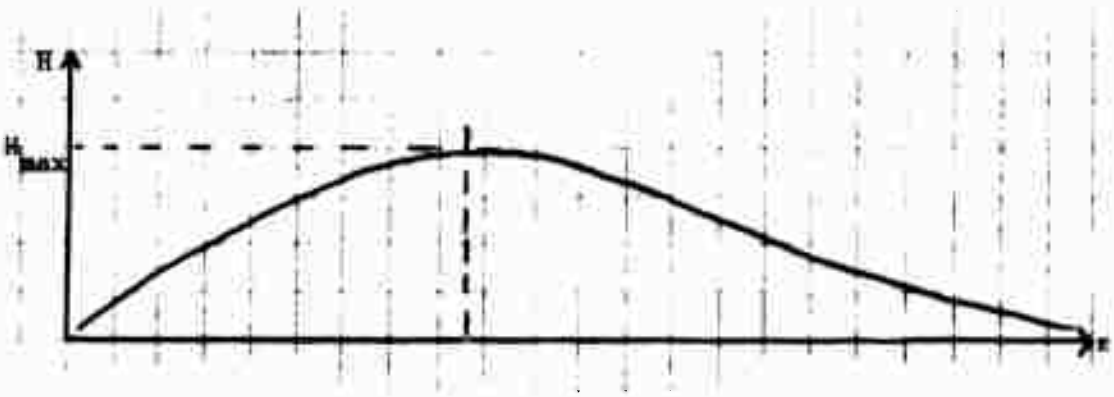

$$z_{max} = \frac{\ell n(3\beta/\alpha)}{3\beta - \alpha}$$

Figure 2. Variation of I.M. Field Strength with Length of Coax.

The I.M. power saturates at the scale length $z = z_{max}$ and for distances greater than z_{max} is attenuated as $e^{-2\alpha z}$. (Notice that the input power is attenuated as $e^{-2\beta z}$, where $\alpha/\beta = \sqrt{\omega/\omega_2}$. Hence, though different, the two rates are of approximately the same magnitude).

The I.M. products can be related to the two impressed powers P_1 and P_2. We provide some numerical estimates applicable to the testing and FLTSATCOM operating conditions.

For $\omega_1 = 2\pi \times 146 \times 10^6 sec^{-1}$, $\omega_2 = 2\pi \times 266 \times 10^6 sec^{-1}$, the I.M. frequency is 26 Mc. Then, for a (coax uT 141) coax with radii a = (b/3) $\approx 5 \times 10^{-2} cm$, copper conductivity $\sigma = 5.8 \times 10^{17} sec^{-1}$, specific heat $c_p = 3.2 \times 10^7$ erg $cm^{-3} deg^{-1}$, coefficient of the linear dependence of σ on temperature $\gamma = 4.3 \times 10^{-4} deg^{-1}$, Teflon dielectric constant $\varepsilon = 2$, and $P_1 \approx P_2 \approx 30$ W, we find (in cgs units unless specified otherwise)

$$2\mathcal{C} \approx 3.5 \times 10^{-4} cm^{-1} ,$$

$$\alpha \approx 6 \times 10^{-5} cm^{-1} ,$$

$$z_{max} \approx 4 \times 10^3 cm ,$$

$$H_{IM}(b) \approx 8.6 \times 10^{-14} H_1^2(b) H_2(b) z \quad \text{gauss} ,$$

$$\left(\text{or, } \frac{H(b)}{z} \approx 2.1 \times 10^{-13} \text{ gauss } cm^{-1}\right)$$

$$P_{IM} \approx \left(\frac{69}{16\pi}\right)^2 \frac{\varepsilon^2 \gamma^2}{c^2 c_p^2} \cdot \frac{\omega_2}{8\pi\sigma} \cdot \left(\frac{5\omega_1 - \omega_2}{\omega_2 - \omega_1}\right)^2 \left(\frac{1}{b^3} + \frac{1}{a^3}\right)^2 \frac{1}{\left(\ell n \frac{b}{a}\right)^4} P_1^2 P_2 z^2 \frac{\text{erg}}{\text{sec}} ,$$

$$\left(\text{or, } \frac{P_{IM}}{z^2} \approx 5.6 \times 10^{-21} \frac{W}{m^2}\right)$$

$$H_{max}(b) \approx 6.7 \times 10^{-10} \text{ gauss} ,$$

$$P_{max} \approx 6 \times 10^{-18} \text{ watts} .$$

For $\omega_1 = 2\pi \times 270 \times 10^6 sec^{-1}$ and $\omega_2 = 2\pi \times 240 \times 10^6 sec^{-1}$, the I.M. frequency is 300 Mc. Then,

$$\alpha \approx 2.2 \times 10^{-4} cm^{-1}$$

$$z_{max} \approx 2.8 \times 10^3 cm$$

$$H(b) \approx 8.6 \times 10^{-13} H_1^2(b) H_2(b) z^2 \quad \text{gauss},$$

$$\left(\text{or}, \frac{H(b)}{z} \approx 2.1 \times 10^{-12} \frac{\text{gauss}}{\text{cm}}\right)$$

$$P \approx 1.8 \times 10^{-23} P_1^2 P_2 z^2 \quad \text{watt (z is in meters)},$$

$$\left(\text{or}, \frac{P}{z^2} \approx 5.6 \times 10^{-19} \frac{W}{m^2}\right)$$

$$H_{max}(b) \approx 2.8 \times 10^{-9} \text{ gauss}$$

$$P_{max} \approx 8 \times 10^{-17} \text{ watts} \quad .$$

Notice, that for constant impressed powers P_1 and P_2, H(b) and P vary for small distances as a^{-4} and a^{-6} respectively, whereas the peak values H_{max} and P_{max} scale as a^{-3} and a^{-4} respectively. For FLTSATCOM operating conditions, I.M. frequency is 300 Mc and coax radius (coax uT 250) a = (b/3) ≈ 0.08 cm. For $P_1 = P_2 = 30$ W, we then find

$$\alpha \approx 1.2 \times 10^{-4} \text{cm}^{-1},$$

$$z_{max} \approx 5 \times 10^{3} \text{cm},$$

$$H(b) \approx 4.8 \times 10^{13} H_1^2(b) H_2(b) z^2 \quad \text{gauss},$$

$$\left(\text{or}, \frac{H(b)}{z} \approx 2.1 \times 10^{-13} \frac{\text{gauss}}{\text{cm}}\right)$$

$$P \approx 5.5 \times 10^{-25} P_1^2 P_2 z^2 \quad \text{watt (z is in meters)},$$

$$\left(\text{or}, \frac{P}{z^2} \approx 1.7 \times 10^{-20} \frac{W}{m^2}\right),$$

$$H_{max}(b) \approx 5 \times 10^{-10} \text{ gauss},$$

$$P_{max} \approx 8 \times 10^{-18} \text{ watts} \quad .$$

We note finally that the I.M. power depends upon the thermal coefficient of the conductivity squared and is inversely proportional to the conductivity itself. Hence, our estimate (which used bulk copper conductivity) represents the minimum power expected from an ideal metal. Any physical imperfections and surface effects (e.g., oxide layers) only increase the ideal bulk resistivity. We expect that the smaller magnitude of the actual surface conductivity may increase the I.M. power above our estimate.

ADDENDUM 2

INTERMODULATION PRODUCTS DUE TO THE DIELECTRIC MEDIUM OF THE COAXIAL CABLE

ABSTRACT

We investigate intermodulation production due to the nonlinear response of the wave guide dielectric to two impressed signals propagating in a coaxial cable in the TEM mode. We find that the power developed in the I.M. product depends inversely on Bulk modulus of the dielectric squared. For FLTSATCOM testing conditions (coax UT 141), the I.M. power (products of third order with $\omega = 2\omega_1 - \omega_2$) varies for short distances as

$$P = 1.5 \times 10^{-24} P_1^{\,2} P_2 \left(\frac{z}{\lambda}\right)^2 \text{ watts} \quad ,$$

where P_1 and P_2 are the two impressed powers in watts, z is cable length, and λ is I.M. wavelength in vacuum. The I.M. power reaches maximum at a distance $z_{max} = 28$ meters and is attenuated for distances greater than z_{max}. For f = 300 Mc and $P_1 = P_2 = 30$ watts, we find $P = 5 \times 10^{-20} z^2$ watt, where z is in meters, and $P_{max} = 5 \times 10^{-18}$. For FLTSATCOM operating conditions (coax UT 250), the I.M. power varies for short distances as

$$P = 1.5 \times 10^{-25} P_1^{\,2} P_2 \left(\frac{z}{\lambda}\right)^2 \text{ watts}$$

and peaks at $P_{max} = 1.6 \times 10^{-18}$ watts for 50 meters of cable.

I. INTRODUCTION

The purpose of our investigations is to determine the minimum I.M. power produced in a coaxial cable. In this particular report, we study I.M. production due to the nonlinear response of the wave guide dielectric to two impressed frequencies propagating in a TEM mode. We shall report on thermal intermodulation (I.M. production due to Joule heating) in a separate paper.

In Section II of this report, we shall estimate the magnitude of the nonlinear part of the dielectric constant of Teflon. In Section III we derive formulas which describe propagation (and growth) of the I.M. fields in a uniformly filled coaxial cable. In the Discussion Section, we give numerical estimates of the I.M. products generated in the dielectric medium of the coax appropriate to both FLTSATCOM operating and testing conditions.

II. NONLINEAR RESPONSE OF TEFLON DIELECTRIC CONSTANT

In this study, we wish to investigate a mechanism which would allow for the nonlinear effects in the dielectric media of wave guides.

Consider a dielectric in an electric field E. The electric energy density of the dielectric and field is

$$U = \frac{\vec{D}\cdot\vec{E}}{8\pi} = \frac{E^2}{8\pi} + \frac{\vec{P}\cdot\vec{E}}{2} = \frac{E^2}{8\pi} + \frac{\chi E^2}{2} \quad , \tag{1}$$

where the displacement field D is

$$D = E + 4\pi P = \varepsilon E \quad , \tag{2}$$

and the dielectric constant ε is related to the electric susceptibility χ ($\chi = P/E$) by

$$\varepsilon = 1 + 4\pi\chi \quad . \tag{3}$$

Polarization $\vec{P}$ is defined as the electric dipole moment per unit volume,

$$\vec{P} = N\vec{p} = Ne\vec{x} \quad , \tag{4}$$

and hence the change of the electric susceptibility χ due to the change of a volume V is given by

$$\frac{\Delta\chi}{\chi} = \frac{\Delta N}{N} = -\frac{\Delta V}{V} \quad . \tag{5}$$

Now, according to Eq. (4), polarization P is associated with the displacements $\vec{x}$ of charges in the dielectric. Hence, the second term on the right hand side of Eq. (1) (the change in the energy density of a dielectric placed in an electric field E) gives the corresponding change in the pressure, p, of the dielectric. Designating by B the Bulk modulus of the dielectric,

$$\frac{1}{B} \equiv -\frac{1}{V}\frac{\Delta V}{\Delta p} \quad , \tag{6}$$

the corresponding change in the electric susceptibility is then given by

$$\frac{\Delta\chi}{\chi} = -\frac{\Delta V}{V} = \frac{\Delta p}{B} = \frac{1}{B}\,\chi\,\frac{E^2}{2} \quad , \tag{7}$$

or, using Eq. (3),

$$\varepsilon = \varepsilon_o\left(1 + \frac{4\pi\,\chi^2}{2\varepsilon_o B}\,E^2\right) \quad . \tag{8}$$

Eq. (8) describes the nonlinear character of the dielectric constant ε in strong electric fields due to the elastic properties of the dielectric. Using $\varepsilon = 2$ and $B = 3.5 \times 10^9$ dynes/cm^2 for Teflon,* we find

$$\gamma \equiv \frac{4\pi\,\chi^2}{2\varepsilon_o B} = 6 \times 10^{-12}\left(\frac{\text{stat V}}{\text{cm}}\right)^{-2} \quad . \tag{9}$$

Thus, the nonlinear part of the dielectric constant is inversely proportional to the Bulk modulus B. Since Teflon has a particularly low value of B, the resulting dielectric contribution to intermodulation products will be higher for Teflon than for other dielectrics.

---

* As reported by Altshuler and Holstein in "Dielectric Contribution to Intermodulation Fields," 74.1350.SA-017, 20 September 1974. They quote the Young's Modulus as given in Modern Plastic Encyclopedia. However, the Handbook of Plastics, 2nd Ed., 1949, p. 429, reports a 0.1% deformation of Teflon at 1700 psi. This would translate to a bulk modulus of about 1.1×10^{11} dynes/cm^2.

III. PROPAGATION AND GROWTH OF I.M. FIELDS IN A TEFLON-FILLED COAX

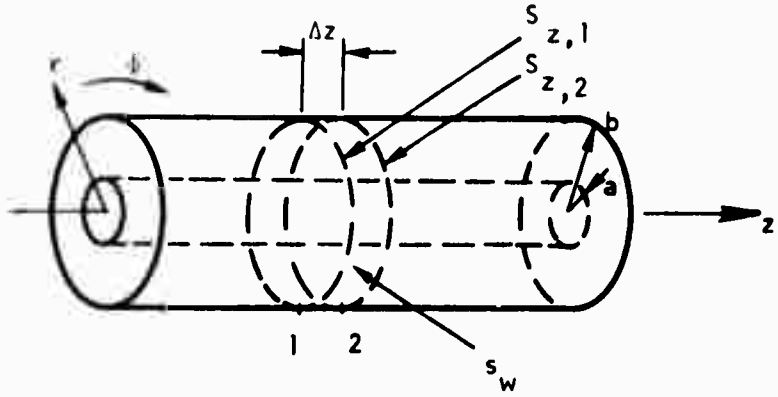

Figure 1. Geometry of coaxial cable.

We consider the propagation problem in a coaxial cable. In a dielectric medium of the coax, fields are described by Maxwell's equations,

$$\nabla \times H = \frac{1}{c}\frac{\partial D}{\partial t} = \frac{1}{c}\left(E\frac{\partial \varepsilon}{\partial t} + \varepsilon\frac{\partial E}{\partial t}\right) \quad ; \tag{10}$$

$$\nabla \times E = -\frac{1}{c}\frac{\partial B}{\partial t} \quad . \tag{11}$$

The input field is a sum of two fields with frequencies ω_1 and ω_2:

$$E = \left(E_1 \cos(\omega_1 t - kz) + E_2 \cos(\omega_2 t - k_2 z)\right) e^{-\beta z} \quad . \tag{12}$$

In Eq. (12), we have explicitly included the attenuation constant, β, for the coax,

$$2\beta = \frac{a+b}{ab}\,\frac{\left(\frac{\varepsilon\omega}{8\pi\sigma}\right)^{1/2}}{\ell n\,\frac{b}{a}} \quad , \tag{13}$$

where a, b are the inner and outer radii of the coax, ω is the frequency, σ the conductivity of the walls of the coax, and ε the dielectric constant.

We calculate I.M. fields generated by the input field. The nonlinear constant ε is given by

$$\varepsilon = \varepsilon_o(1 + \gamma E^2) \quad . \tag{14}$$

Substituting Eq. (14) and (12) into Eq. (10), we find that the right hand side of Eq. (10) has components at the I.M. frequency $\omega = 2\omega_1 - \omega_2$. We shall designate them by A_s. In turn, these I.M. components can be regarded as a source term (specifically, source currents) in Maxwell's Equations describing the propagation of the I.M. fields in the coax. These then become

$$\nabla \times H = \frac{\varepsilon_o}{c}\frac{\partial E}{\partial t} + \frac{4\pi}{c} J_s \quad ; \tag{15}$$

$$\nabla \times E = -\frac{1}{c}\frac{\partial B}{\partial t} \quad , \tag{16}$$

where the source term $(4\pi/c)\, j_s$ is equal to

$$\frac{4\pi}{c} j_s \equiv A_s = -\frac{\gamma\varepsilon_o}{4c}\omega E_1^2 E_2 \cdot e^{-3\beta z} \cdot \sin(\omega t - kz) \quad , \tag{17}$$

where $k = 2k_1 - k_2$, and $j_s = j_s(r)$, $E = E(r)$. Eqs. (15) and (16) can be solved directly, and a growing solution (for small distance z along the axis of the coax) for H and E fields can be obtained. However, if we also wish to account for the attenuation of the I.M. products due to the finite conductivity of the metallic walls of the coax, it is advantageous to adopt a different method for solving Eqs. (15) and (16). This method, based on the energy conservation principle, recovers, of course (for small z), would-be-obtained solutions by the direct integration.

Energy conservation (Poynting's Theorem) yields the relation

$$\frac{c}{4\pi}\int dS[\vec{E} \times \vec{H}]_n = -\int dV\, \vec{E} \cdot \vec{j}_s \quad , \tag{18}$$

where the volume integration is performed over the volume bounded by surfaces S. Choosing the volume element as shown in Fig. (1), we integrate the

Poynting's vectors $\frac{c}{4\pi}\left[\vec{E} \times \vec{H}\right]_n$ over the cross sections 1 and 2 and over the wall surfaces at $r = a$ and b.

Using the relations (valid for a coax),

$$H_\phi(r) = \sqrt{\epsilon}\ E_r(r) = \sqrt{\epsilon}\ \frac{a}{r} E(a) \quad , \quad a \le r \le b \tag{19}$$

and at the conducting walls,

$$H_\phi(b,t) = H_\phi(b)\ \cos(\omega t - kz)$$

$$E_z(b,t) = -\left(\frac{\omega}{4\pi\sigma}\right)^{1/2} H_\phi(b)\ \cos\left(\omega t - kz + \frac{\pi}{4}\right) \quad , \tag{20}$$

Eq. (18) yields

$$\frac{c}{4\sqrt{\epsilon}}\ b^2\ \ell n\ \frac{b}{a}\ \frac{dH^2(b)}{dz} = \frac{-cb}{4}\left(1 + \frac{b}{a}\right)\left(\frac{\omega}{8\pi\sigma}\right)^{1/2} H^2(b) + \frac{cA_o\ H(b)}{8\sqrt{\epsilon}} - b\left(\frac{1}{b^2} - \frac{1}{a^2}\right)e^{-3\beta z} \quad , \tag{21}$$

where we have defined A_o by

$$A_s \equiv \frac{A_o}{r^3}\ e^{-3\beta z}\ \sin(\omega t - kz) \quad , \tag{22}$$

and we have averaged over a period of the I.M. wave. In Eq. (21), the left hand side gives the change of the power flow in the coax per unit length z. The first and second terms on the right hand side of Eq. (21) are, respectively, losses at the walls of the coax, and the driving power generated inside the dielectric of the coax (per unit length). Eq. (21) is finally rewritten as

$$\frac{dH(b)}{dz} = -\alpha\left(H(b) - d \cdot e^{-3\beta z}\right) \quad , \tag{23}$$

which, with the boundary condition that $H(z = 0) = 0$ nas the solution

$$H(b) = \frac{\alpha d}{\alpha - 3\beta}\left(e^{-3\beta z} - e^{-\alpha z}\right) \quad , \tag{24}$$

where

$$\alpha = \frac{1}{2}\left(\frac{\varepsilon\omega}{8\pi\sigma}\right)^{1/2} \frac{a+b}{ab\ \ln\frac{b}{a}} \quad ; \tag{25}$$

$$d = A_o\left(\frac{2\pi\sigma}{\varepsilon\omega}\right)^{1/2} \frac{a}{a+b}\left(\frac{1}{b^2} - \frac{1}{a^2}\right) \quad . \tag{26}$$

IV. DISCUSSION

Eqs. (24) - (26) are the basic results of this paper. We see that for small distances z along the coax ($z < \alpha^{-1}, (3\beta)^{-1}$), H-field grows linearly,

$$H(b) \approx \alpha dz \approx \frac{\epsilon^3}{b}\left(-\frac{1}{b^2}+\frac{1}{a^2}\right)\frac{\gamma\,\epsilon_o\,\pi}{8}\,E_1^{\,2}(a)\,E_2(a)\left(\frac{z}{\lambda}\right) \quad , \qquad (27)$$

and the I.M. power quadratically,

$$P \approx \frac{c}{4\sqrt{\epsilon}}\,b^2\left(\ell n\,\frac{b}{a}\right)H^2(b) \approx \frac{c}{4}\left(\ell n\,\frac{b}{a}\right)a^6\left(\frac{1}{b^2}-\frac{1}{a^2}\right)^2\,\frac{\gamma^2\,\epsilon_o^{\,3/2}\,\pi^2}{64}\,E_1^{\,4}(a)\,E_2^{\,2}(a)\left(\frac{z}{\lambda}\right)^2. \qquad (28)$$

(λ is I.M. wavelength in vacuum.) The I.M. power saturates at the scale length $z = z_{max}$ and for greater distances is attenuated as $e^{-2\alpha z}$. (Notice that the input power is attenuated as $e^{-2\beta z}$, where $(\alpha/\beta) \sim \sqrt{\omega/\omega_1}$. Hence, though different, the two rates are of approximately the same order of magnitude.)

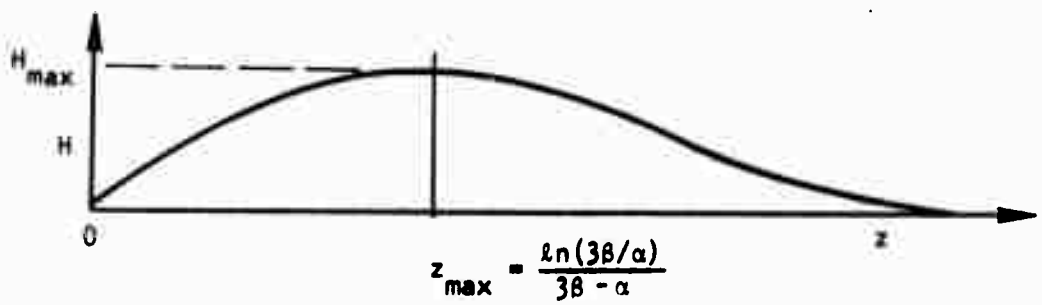

Figure 2. Variation of I.M. field strength with length of coax.

The I.M. products can be related to the two input powers P_1 and P_2. We provide some numerical estimates applicable to FLTSATCOM.

For $\omega_1 = 2\pi \times 146 \times 10^6$ sec^{-1}, $\omega_2 = 2\pi \times 266 \times 10^6$ sec^{-1}, the I.M. frequency is 26 Mc. Then, for a coax with radii a = (b/3) $\approx 5 \times 10^{-2}$ cm

(coax UT 141) copper conductivity $\sigma = 5.8 \times 10^{17}$ sec^{-1}, and $P_1 = P_2 = 30$W, we find (in cgs units unless specified otherwise):

$$2\beta \approx 3.5 \times 10^{-4} \text{ cm}^{-1}$$

$$\alpha \approx 6 \times 10^{-5} \text{ cm}^{-1}$$

$$z_{max} \approx 4 \times 10^{3} \text{ cm}$$

$$\lambda \approx 1.15 \times 10^{3} \text{ cm} \quad \text{(in vacuum)}$$

$$H_{IM}(b) \approx 1.5 \times 10^{-12} E_1^2(a) E_2(a) \left(\frac{z}{\lambda}\right) = 6 \times 10^{-11} \left(\frac{z}{\lambda}\right) \text{ gaus}$$

$$\left(\text{or, } \frac{H(b)}{z} \approx 5 \times 10^{-14} \text{ gauss/cm}\right)$$

$$P_{IM} \approx \frac{\gamma^2 \pi^2}{4c^2} \left(\frac{1}{b^2} - \frac{1}{a^2}\right)^2 P_1^2 P_2 \left(\frac{z}{\lambda}\right)^2 \approx 4 \times 10^{-13} \left(\frac{z}{\lambda}\right)^2 \text{ erg/sec}$$

$$\left(\text{or, } \frac{P_{IM}}{z^2} \approx 3 \times 10^{-22} \frac{W}{m^2}\right)$$

$$H_{max}(b) \approx 1 \times 10^{-10} \text{ gauss}$$

$$P_{max} \approx 1 \times 10^{-19} \text{ watts}$$

Note that for short distances, $H\lambda$ and $P\lambda^2$ are independent of I.M. frequency. The same is not true for the peak field, H_{max} and peak power, P_{max}, however.

For operating conditions such that $\omega_1 = 2\pi \times 270 \times 10^6$ sec^{-1} and $\omega_2 = 2\pi \times 240 \times 10^6$ sec^{-1}, the I.M. frequency is 300 Mc. Then,

$$\alpha \approx 2.2 \times 10^{-4} \text{ cm}^{-1}$$

$$z_{max} \approx 2.8 \times 10^{3} \text{ cm}$$

$$\lambda \approx 10^{2} \text{ cm (in vacuum)}$$

$$H_{max}(b) \approx 6 \times 10^{-10} \text{ gauss}$$

$$P_{max} \approx 5 \times 10^{-18} \text{ watts}$$

Notice, that for constant impressed powers P_1 and P_2, H(b) and P_{IM} vary for small distances as a^{-3} and a^{-4}, respectively, whereas the peak values H_{max} and P_{max} scale as a^{-2}. For FLTSATCOM operating conditions, I.M. frequency is 300 Mc and coax radius (coax UT 250) a = (b/3) ≈ 0.08 cm. For $P_1 = P_2 = 30$ W, we then find

$$\alpha \approx 1.2 \times 10^{-4} \text{ cm}^{-1}$$

$$z_{max} \approx 5 \times 10^{3} \text{ cm}$$

$$H(b) \approx 1 \times 10^{-11} \left(\frac{z}{\lambda}\right) \text{ gauss}$$

$$\left(\text{or, } \frac{H}{z} \approx 1 \times 10^{-13} \ \frac{\text{gauss}}{\text{cm}}\right)$$

$$P \approx 4 \times 10^{-14} \left(\frac{z}{\lambda}\right)^2 \text{ erg/sec}$$

$$\left(\text{or, } \frac{P}{z^2} \approx 4 \times 10^{-21} \ \frac{W}{m^2}\right)$$

$$H_{max} \approx 1.9 \times 10^{-10} \text{ gauss}$$

$$P_{max} \approx 1.6 \times 10^{-18} \text{ watts}$$

In conclusion, we wish to emphasize again that the power developed in the I.M. frequency depends inversely on Bulk modulus squared. It is therefore very important to ascertain what the correct value is. The uncertainty over this quantity has been discussed in the footnote appearing on page 4.

ADDENDUM 3

INTERMODULATION PRODUCTS DUE TO THE NONLINEAR CHARACTER OF THE LORENTZ FORCE

ABSTRACT

We investigate intermodulation production in coaxes due to the nonlinear character of the $[\vec{v} \times \vec{B}]$ term in the Lorentz force driving the conduction electrons in the waveguide walls. We consider two impressed signals propagating in a coaxial cable in the TEM mode. We find that the power developed in the I.M. product depends upon the fourth power of the ratio of the cyclotron and collision frequencies, and is inversely proportional to the conductivity. For FLTSATCOM testing conditions (coax UT 141 with copper walls and filled uniformly with Teflon), the power of I.M. products of third order ($\omega = 2\omega_1 - \omega_2$) varies for short distances as

$$P = 7 \times 10^{-26} P_1^2 P_2 z^2 \text{ watts}$$

where P_1 and P_2 are the impressed powers in watts and z is cable length in meters. I.M. power reaches its maximum at a distance $z_{max} = 28$ meters and is attenuated for distances greater than z_{max}. For I.M. frequency f = 300 Mc and $P_1 = P_2 = 30$ watts, we find $P_{max} = 5 \times 10^{-19}$ watts. For FLTSATCOM operating conditions (coax UT 250) I.M. power varies for short distances as

$$P = 2.2 \times 10^{-27} P_1^2 P_2 z^2$$

and peaks at $P_{max} = 3.5 \times 10^{-20}$ watts for 50 meters of cable.

1. INTRODUCTION

The purpose of our investigations is to determine the minimum I.M. power to be expected in a coaxial cable solely due to the intrinsic properties of its components. In this particular report, we study the intermodulation production due to the nonlinear character of the Lorentz force.

Due to the finite conductivity of a metal, electromagnetic fields propagate into the coax walls and drive the conduction electrons. The electrons have a velocity which has both, harmonic components of the driving fields, and, via the $[\vec{v} \times \vec{H}]$ term of the Lorentz force, also components at I.M. frequencies. The I.M. velocities are calculated in Section 2 of this report. The I.M. currents drive the TEM mode in the coaxial cable, this is discussed in Section 3. In the Discussion section, we give numerical estimates of the I.M. products generated due to the nonlinear character of the Lorentz force and relate them to those generated by the thermal heating of the coax walls.

2. THE NONLINEAR CHARACTER OF THE LORENTZ FORCE

With a finite relaxation time and charge separation, the equation of motion of a conduction electron in an electromagnetic field is

$$\frac{d\vec{v}}{dt} + \nu\vec{v} = \frac{e}{m}\left(\vec{E} - 4\pi\vec{P} + \frac{\vec{v}}{c} \times \vec{H}\right) \tag{1}$$

where $\nu \equiv \tau^{-1}$ is the electron collision frequency (τ is the relaxation time) and the electronic polarization $\vec{P}$ is given by

$$\vec{P} = ne\vec{r} = ne\int dt\, \vec{v} = \frac{nev}{\omega}\hat{r}\,, \tag{2}$$

where $\hat{r}$ is the unit vector in the direction of the polarization $\vec{P}$.

For R. F. fields of our interest, Eq. (1) can be immediately simplified. In good conductors, the electron collision frequency $\nu \approx 10^{13}$ sec^{-1}. The R.F. frequencies in our intermodulation problem are of the order of 10^8 sec^{-1}. Hence, the time derivative $\frac{dv}{dt} = i\omega v << \nu\omega$, and in what follows, we shall neglect the $\frac{dv}{dt}$ term on the left-hand side of Eq. (1). Eq. (1) is then rewritten as

$$\vec{v} = \frac{e}{m\nu}\vec{E} - \frac{\omega_p^2}{\nu\omega} v_r \hat{r} + [\vec{v} \times \frac{\vec{\omega}_H}{\nu}] \tag{3}$$

where the plasma frequency $\omega_p^2 = \frac{4\pi ne^2}{m}$ and the vector of the cyclotron frequency $\vec{\omega}_H = \frac{e\vec{H}}{mc}$. To solve Eq. (3), we form the products

$$[\vec{v} \times \vec{\omega}_H] = \frac{e}{m\nu}[\vec{E} \times \vec{\omega}_H] - \frac{\omega_p^2}{\nu\omega} v_r[\hat{r} \times \vec{\omega}_H] - \frac{1}{\nu}(\vec{\omega}_H(\vec{v} \cdot \vec{\omega}_H) - \vec{v}\,\omega_H^2) \tag{4}$$

and

$$(\vec{v} \cdot \vec{\omega}_H) = \frac{e}{m\nu}(\vec{E} \cdot \vec{\omega}_H) - \frac{\omega_p^2}{\nu\omega} \cdot v_r(\hat{r} \cdot \vec{\omega}_H). \tag{5}$$

Velocity $\vec{v}$ can now be calculated by substituting Eq. (4) and (5) into Eq. (3). Before doing so, however, we simplify Eqs. (4) and (5) for the geometry of the fields in the metallic walls of a coaxial cable. For the TEM mode, the magnetic fields are concentric with the walls of the coax (see Figure (1)) and the electric fields have both tangential and radial components (due to the finite conductivity, the charges inside the metallic walls do not move instantly in response to changes in the fields, and do not produce the correct surface-charge density which would give zero electric field inside a perfect conductor).*

---

* One can show that the magnetic field in a good conductor is $\vec{H}_\phi(r) \simeq \vec{H}_\phi e^{-r/\delta} e^{ir/\delta}$, where δ is the skin depth, and the tangential component of the electric field $\vec{E}_z \simeq \sqrt{\frac{\omega}{8\pi\sigma}}(1-i)[\hat{r} \times \vec{H}_\phi]$. From the continuity of $\vec{H}$ and the equation connecting $\vec{E}$ to $\vec{\nabla} \times \vec{H}$ (Ampere's law) on either side of the surface, one can show that there exists in the conductor a small normal component of electric field, $E_r \simeq \frac{-i\omega}{4\pi\sigma} H_\phi$.

Furthermore, since the polarization vector $\vec{P}$ points in the direction of the radial coordinate $\hat{r}$ only (the direction of the charge displacement in the coax walls), the scalar product $(\vec{v} \cdot \vec{\omega}_H) \equiv 0$. Hence, Eq. (3) becomes

$$\vec{v}\left(1 - \frac{\omega_H^2}{\nu^2}\right) + \frac{\omega_p^2}{\nu\omega} v_r\left(\vec{r} + \left[\vec{r} \times \frac{\vec{\omega}_H}{\nu}\right]\right) = \frac{e}{m\nu}\left(\vec{E} + \left[\vec{E} \times \frac{\vec{\omega}_H}{\nu}\right]\right). \tag{6}$$

First, we solve Eq. (6) for the radial component $\vec{v}_r \equiv (\vec{v} \cdot \hat{r})\,\hat{r}$:

$$\vec{v}_r = \frac{e}{m\nu} \frac{\vec{E}_r + \left[\vec{E}_z \times \frac{\vec{\omega}_H}{\nu}\right]}{1 - \frac{\omega_H^2}{\nu^2} + \frac{\omega_p^2}{\nu\omega}} \quad . \tag{7}$$

In good conductors, the plasma frequency $\omega_p^2 \simeq 10^{31}$ sec^{-1}. For the magnetic fields of interest ($H \simeq 3$ gauss) the cyclotron frequency $\omega_H \simeq 5 \times 10^7$ sec^{-1}. Hence, $\frac{\omega_p^2}{\nu\omega} \gg 1 \gg \frac{\omega_H^2}{\nu^2}$ and Eq. (7) can be approximated by

$$v_r = \frac{e}{m} \frac{\omega}{\omega_p^2}\left(E_r + \frac{\omega_H}{\nu} E_z\right). \tag{8}$$

From Eq. (6), the component $\vec{v}_z (\vec{v}_z \equiv (\vec{v} \cdot \hat{z})\,\hat{z})$ along the axis of the coax is:

$$v_z\left(1 - \frac{\omega_H^2}{\nu^2}\right) + \frac{\omega_p^2}{\nu^2} v_r\left[\hat{r} \times \frac{\vec{\omega}_H}{\omega}\right] = \frac{e}{m\nu}\left(\vec{E}_z + \left[\vec{E}_r \times \frac{\vec{\omega}_H}{\nu}\right]\right) \quad . \tag{9}$$

Substituting Eq. (8) into Eq. (9) yields finally the simple result

$$v_z = \frac{eE_z}{m\nu} \frac{1 + \left(\frac{\omega_H}{\omega}\right)^2}{1 - \left(\frac{\omega_H}{\omega}\right)^2} \simeq \frac{e}{m\nu}\left(1 + \frac{2\omega_H^2}{\nu^2}\right) E_z \quad , \tag{10}$$

which is valid for any harmonic component of the velocity $\vec{v}$, and where $\vec{H}$ and $\vec{E}$ are the total fields acting on the electrons.

3. INTERMODULATION CURRENTS AND FIELDS

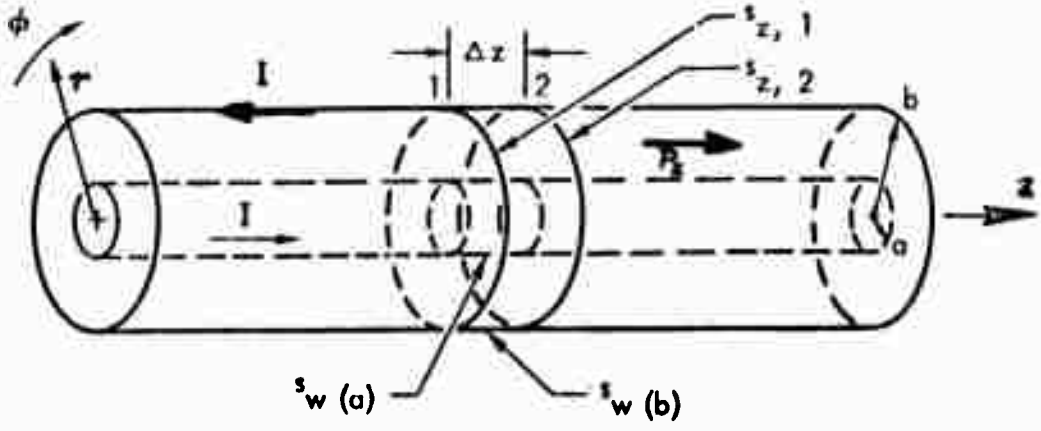

Figure 1. Geometry of Coaxial Cable.

We consider a coaxial cable carrying two signals and frequencies ω_1 and ω_2. The fields are described by Maxwell equations

$$\nabla \times H = \frac{1}{c}\frac{\partial D}{\partial t} + \frac{4\pi}{c}(j_s + \sigma E) \tag{11}$$

$$\nabla \times E = -\frac{1}{c}\frac{\partial B}{\partial t} \tag{12}$$

where j_s is a source current (if any).

Equations (11) and (12) yield, for either frequency, fields in the dielectric ($a \leq r \leq b$):

$$H_\phi(r) = \sqrt{\epsilon}\, E_r(r) = \frac{2I}{cr} \cos(\omega t - kz) \tag{13}$$

where I is the current in the coax walls. In the metal interior,

$$H_\phi = H(b) e^{-r/\delta} \cos\left(\omega t - \frac{r}{\delta}\right) \tag{14}$$

$$E_z = -\left(\frac{\omega}{4\pi\sigma}\right)^{1/2} H(b)\, e^{-r/\delta} \cos\left(\omega t - \frac{r}{\delta} + \frac{\pi}{4}\right), \tag{15}$$

where r is measured from the outer radius b (a similar expression describes fields in the inner wall of radius a). The skin depth δ is given by

$$\delta = \frac{c}{(2\pi\sigma\omega)^{1/2}} \tag{16}$$

where σ is the metallic conductivity.

The vector of the cyclotron frequency $\vec{\omega}_H$ in Eq. (10) is a sum of two vectors,

$$\vec{\omega}_H = \frac{e}{mc}(\vec{H}_1 + \vec{H}_2) \tag{17}$$

where the fields H_1 and H_2 are given by Eq. (14) for either impressed frequency Similarly,

$$\vec{E}_z = \vec{E}_{z,1} + \vec{E}_{z,2}\ , \tag{18}$$

where $E_{z,1}$ and $E_{z,2}$ are given by Eq. (15). Substituting Eqs (14) thru (18) into Eq. (10), we find that the right-hand side of Eq. (10) has components at the I.M. frequency $\omega = 2\omega_1 - \omega_2$. These components, a result of the wave beating of two signals with frequencies ω_1 and ω_2, represent a source term in Maxwell equations for the I.M. fields. We calculate the source currents by using the relation that the current density

$$\vec{j} = ne\vec{v} \tag{19}$$

Using Eqs. (14) - (19), Eq. (10) then yields the I.M. source current (directed along the axis of the coax)*.

$$j_s = - \Lambda \cos(\omega t - \frac{r}{\delta} + \gamma)\ e^{-3r/\delta} \tag{20}$$

where

$$\Lambda_b = \left(\frac{\Omega_H}{\nu}\right)^2 \sqrt{\sigma} \left(\frac{4\omega_1 + \omega_2}{8\pi}\right)^{1/2} H_1^2(b)\ H_2(b), \tag{21}$$

and where we have assumed that the two skin depths $\delta_1 \simeq \delta_2 \simeq \delta$. Ω_H is the cyclotron frequency per gauss, $\Omega_H = \frac{e}{mc}$, σ is the metallic conductivity, $\sigma = (ne^2/\nu m)$, and

$$\gamma = \tan^{-1}\left(\frac{2\sqrt{\omega_1} - \sqrt{\omega_2}}{2\sqrt{\omega_1} + \sqrt{\omega_2}}\right). \tag{22}$$

* The I.M. current density in the radial direction is negligible by virtue of the smallness of the radial component of electric field, E_r (see footnote appearing on p. 4).

Eqs. (20) and (21) give the I.M. current density generated in the outer wall of the coax; similar expressions give current density in the inner wall (radius a). Notice, that the I.M. currents are generated within one-third of the skin depth, $\delta/3$.

We now calculate fields supported by the source currents j_s. Since the calculation proceeds in exactly the same way as our calculation of the I.M. fields generated by the thermal intermodulation mechanism* (we merely substitute j_s as calculated in this report for the thermal currents, Eq. (12) of our report on the thermal intermodulation), below, we shall sketch only the main features of our derivation. For further details, consult our paper on the thermal intermodulation.

Since the ratio of the current densities

$$\frac{j_s(b)}{j_s(a)} = \frac{\Lambda_b(b)}{\Lambda_a(a)} = \frac{a^3}{b^3} \tag{23}$$

also determines the ratio of the corresponding fields and currents,

$$\frac{H_s(b)}{H_s(a)} = \frac{a^3}{b^3} \quad ; \quad \frac{I_s(b)}{I_s(a)} = \frac{a^2}{b^2} \quad , \tag{24}$$

additional currents must be set up on the coax walls such that the sum of the driving and induced fields satisfies boundary conditions appropriate to the TEM mode:

---

* See our report, J. Z. Wilcox and P. Molmud, Thermal Heating Contribution to Intermodulation Fields in Coaxial Waveguides (Addendum 1).

$$I = I(b) + I(a) = I_{ind}(b) + I_s(b) = I_{ind}(a) + I_s(a)$$

$$H_m(a) = H_d(a) = \frac{b}{a} H_m(b) = \frac{b}{a} H_d(b) \tag{25}$$

where subscript, ind, means induced and I is the total I.M. current, and subscripts, m, and, d, designate fields in metal and dielectric respectively. On the other hand, from Maxwell Equations (11) and (12), H-field in the coax wall satisfies

$$\frac{\partial^2 H_m}{\partial r^2} - \frac{2}{\omega\delta^2} \frac{\partial H_m}{\partial t} = \frac{4\pi}{c} \frac{\partial j_s}{\partial r} \quad , \tag{26}$$

where δ and ω ($\omega = 2\omega_1 - \omega_2$) are respectively I.M. skin depth and frequency and j_s is the source current (Equation (20)).

Making the approximation that all skin depths are of approximately the same order of magnitude, and using the boundary conditions, Eq. (25), we find that H-field and the tangential component E_z inside the metallic walls are equal to respectively

$$H_m(b) = \left\{ \left(H_d(b) - \frac{\pi \Lambda_b \delta}{5c \cos\phi} \right) e^{-r/\delta} + \frac{\pi \Lambda_b \delta}{5c \cos\phi} e^{-3r/\delta} \right\} x$$
$$x \sin\left(\omega t - \frac{r}{\delta} + \gamma + \phi \right) \tag{27}$$

and

$$E_z = \frac{c}{4\pi\sigma} \left(\frac{\partial H_m}{\partial r} - \frac{4\pi}{c} j_s \right) = \tag{28}$$
$$= - \frac{c}{4\pi\sigma\delta} \sqrt{2} \left(H_d - \frac{\pi \Lambda \delta}{5c \cos\phi} \right) e^{-r/\delta} \cos\left(\omega t + \phi + \gamma - \frac{\pi}{4} - \frac{r}{\delta} \right)$$
$$+ \frac{\Lambda}{10\sigma} e^{-3r/\delta} \left(\cos\left(\omega t + \phi + \gamma - \frac{\pi}{4} - \frac{r}{\delta} \right) - 2 \sin\left(\omega t + \phi + \gamma - \frac{\pi}{4} - \frac{r}{\delta} \right) \right).$$

where the I.M. amplitude $H_d(r)$ (as yet undetermined) satisfies

$$H_d(r) = \sqrt{\epsilon}\, E_r(r) = \frac{2I}{cr} \tag{29}$$

Eqs. (27 - (29) give I.M. fields in the outer wall; again, similar expressions give also fields inside the inner wall (radius a) of the coax.

To calculate the growth of the amplitude $H_d(r)$ we use the fact that the change in power P_z ($P_z = \int \vec{ds}_z \cdot \vec{S}_z$, see Figure 1) crossing the coax cross section per unit length is given by

$$\frac{dP_z}{dz} = \frac{1}{\Delta z} \int_{walls} \vec{ds}_w \cdot \vec{S}_w \tag{30}$$

where $\vec{S}_z$ and $\vec{S}_w$ are respectively components of Poynting vector $\vec{S}$ parallel and normal to the coax walls and Δz is the length increment along the coax axis.

Including into our picture also the attenuation rate of the impressed fields (impressed fields attenuate as $e^{-\beta z}$),

$$2\beta = \frac{a + b}{ab \ \ell n \frac{a}{b}} \left(\frac{\epsilon\omega}{8\pi\sigma}\right)^{1/2} , \tag{31}$$

where ω stands for ω_1 or ω_2, and using the result that the power

$$P = \frac{c}{4\sqrt{\epsilon}}\, b^2 \left(\ell n \frac{b}{a}\right) H^2(b) , \tag{32}$$

Eq. (30) yields (for further details, see our report on the thermal intermodulation) the I.M. amplitude

$$H(b) = \frac{\alpha d}{\alpha - 3\beta}\left(e^{-3\beta z} - e^{-\alpha z}\right), \tag{33}$$

where

$$2\alpha = \frac{a + b}{ab\left(\ell n \frac{b}{a}\right)}\left(\frac{\varepsilon\omega}{8\pi\sigma}\right)^{1/2} \quad ; \quad \omega = 2\omega_1 - \omega_2 \tag{34}$$

$$d = 138\left(\frac{\pi}{\sigma\omega}\right)^{1/2} \cdot \Lambda_b \cdot \left(1 - \frac{b}{a} + \frac{b^2}{a^2}\right) . \tag{35}$$

4. DISCUSSION

Equations (33) & (35) with Λ_b given by Equation (21) are the basic results of this paper. The main conclusions can be summarized as follows: For small distances z ($z < \alpha^{-1}$), H-field grows linearly,

$$H_{I.M.}(b) = \frac{69\sqrt{\varepsilon}}{8}\left(1 + \frac{b^3}{a^3}\right)\frac{1}{b\ \ell n \frac{b}{a}}\left(\frac{4\omega_1 + \omega_2}{2\pi\sigma}\right)^{1/2}\left(\frac{\Omega_H}{\nu}\right)^2 H_1^2(b)\ H_2(b)\ z \tag{36}$$

and power quadratically,

$$P_{I.M.} = \left(\frac{69}{16}\right)^2\left(\frac{\Omega_H}{\nu}\right)^4 \frac{c\sqrt{\varepsilon}}{\ell n \frac{b}{a}}\left(1 + \frac{b^3}{a^3}\right)^2\left(\frac{4\omega_1 + \omega_2}{2\pi\sigma}\right) H_1^4(b)\ H_2^2(b)\ z^2 \tag{37}$$

$$= \left(\frac{69}{2}\right)^2\left(\frac{\Omega_H}{\nu}\right)^4 \frac{\varepsilon^2}{c^2\left(\ell n \frac{b}{a}\right)^4}\left(\frac{1}{a^3} + \frac{1}{b^3}\right)^2\left(\frac{4\omega_1 + \omega_2}{2\pi\sigma}\right) P_1^2\ P_2\ z^2$$

(P_1 and P_2 are the impressed powers of signals ω_1 and ω_2 respectively.) The I.M. power saturates at the scale length $z = z_{max}$ and for distances greater than z_{max} is attentuated as $e^{-2\alpha z}$. (Notice that the input power is attenuated as $d^{-2\beta z}$, where $\alpha/\beta = \sqrt{\omega/\omega_2}$. Hence, through different, the two rates are of approximately the same magnitude).

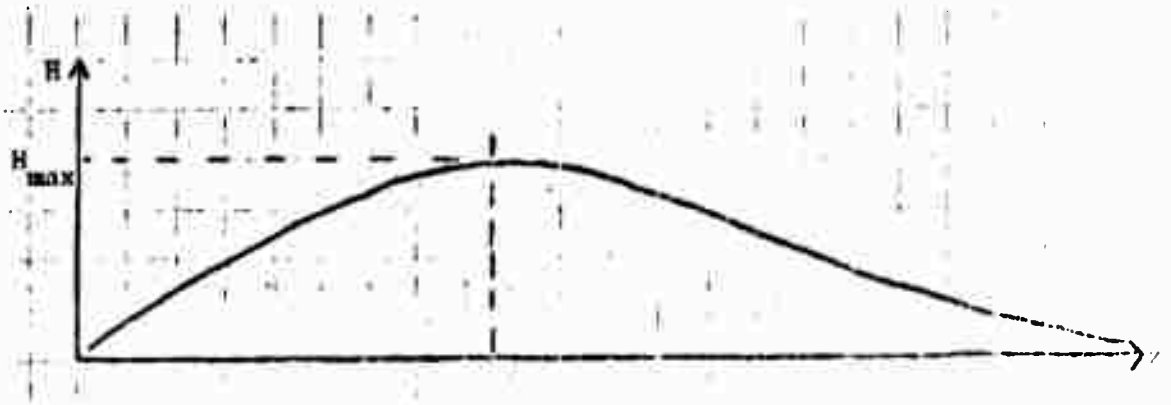

$$z_{max} = \frac{\ell n(3\beta/\alpha)}{3\beta-\alpha}$$

Figure 2. Variation of I.M. Field Strength with Length of Coax.

The magnitude of the I.M. products generated via the nonlinear character of the Lorentz force can be related to magnitudes of the thermal intermodulation products by forming the ratio

$$R = \frac{j_{s,Lorentz}}{j_{s,Thermal}} = \frac{A_{Lorentz}}{A_{Thermal}} = \frac{16\pi c_p}{\gamma} = \left(\frac{\omega H}{\sigma}\right)^2 \frac{\omega_2 - \omega_1}{5\omega_1 - \omega_2}\sqrt{\frac{4\omega_1 + \omega_2}{\omega_2}} \quad , \qquad (38)$$

where c_p is the specific heat and γ is now the thermal coefficient of the conducting of the metal (for derivation, see again our paper on the thermal intermodulation). Notice that R is independent of the coax radius, but rather, is a

function of the physical parameter of the metal as well as of the impressed frequencies.

We provide some numerical estimates of the I.M. products applicable to both FLTSATCOM testing and operating conditions.

For $\omega_1 = 2\pi \times 146 \times 10^6$ sec^{-1}, $\omega_2 = 2\pi \times 266 \times 10^6$ sec^{-1}, the I.M. frequency is 26 Mc. For copper conductivity $\sigma = 5.8 \times 10^{17}$ sec^{-1}, specific heat $c_p = 3.2 \times 10^7$ erg cm^{-3} deg^{-1}, thermal coefficient $\gamma = 4.3 \times 10^{-4}$ deg^{-1}, collision frequency $\nu = 4 \times 10^{13}$ sec^{-1} (corresponding to relaxation times $\tau = 2.7 \times 10^{-14}$ sec, using free electron mass and conduction electron density in copper $n \approx 8 \times 10^{22}$ cm^{-3}) the ratio $\Omega_{H/\nu} = 4.5 \times 10^{-7}$ and $R = 0.42$. Then, for a coax UT 141 ($a = b/3 \approx 5 \times 10^{-2}$ cm), Teflon dielectric constant $\varepsilon = 2$ and $P_1 \approx P_2 \approx 30$ W, we find (in cgs units unless specified otherwise)

$$2\beta \approx 3.5 \times 10^{-4} \text{ cm}^{-1},$$

$$\alpha \approx 6 \times 10^{-5} \text{ cm}^{-1},$$

$$z_{max} \approx 4 \times 10^3 \text{ cm},$$

$$H_{I.M.}(b) \approx 3.5 \times 10^{-14} H_1^2(b) H_2(b) z \text{ gauss},$$

$$\left(\text{or, } \frac{H(b)}{z} \approx 8.7 \times 10^{-14} \text{ gauss cm}^{-1}\right)$$

$$P_{I.M.} \approx 3.4 \times 10^{-26} P_1^2 P_2 z^2 \text{ watt (z is in meters)}$$

$$\left(\text{or, } \frac{P_{I.M.}}{z^2} \approx 9 \times 10^{-22} \frac{W}{m^2}\right)$$

$$H_{max}(b) \approx 2.7 \times 10^{-10} \text{ gauss},$$

$$P_{max} \approx 10^{-18} \text{ watts}.$$

For $\omega_1 = 2\pi \times 270 \times 10^6$ sec^{-1} and $\omega_2 = 2\pi \times 240 \times 10^6$ sec^{-1}, the I.M. frequency is 300 Mc and $R = 6 \times 10^{-2}$. Then,

$$\alpha \approx 2.2 \times 10^{-4} \text{ cm}^{-1},$$

$$z_{max} \approx 2.8 \times 10^{3} \text{ cm},$$

$$H(b) \approx 5 \times 10^{-14} H_1^2(b)\, H_2(b) z \text{ gauss},$$

$$\left(\text{or, } \frac{H(b)}{z} \approx 1.2 \times 10^{-13} \ \frac{\text{gauss}}{\text{cm}}\right)$$

$$P \approx 7 \times 10^{-26} P_1^2 P_2 z^2 \text{ Watt (z is in meters)},$$

$$\left(\text{or, } \frac{P}{z^2} \approx 2 \times 10^{-21} \ \frac{W}{m^2}\right)$$

$$H_{max}(b) \approx 2 \times 10^{-10} \text{ gauss}$$

$$P_{max} \approx 5 \times 10^{-19} \text{ watts}.$$

Notice, that for constant impressed powers P_1 and P_2, H(b) and P vary for small distances as a $^{-4}$ and a $^{-6}$ respectively, whereas the peak values H_{max} and P_{max} scale as a $^{-3}$ and a $^{-4}$ respectively. For FLTSATCOM operating conditions, I.M. frequency is 300 Mc and coax radius (coax UT 250) a = (b/3) = 0.08 cm. For $P_1 = P_2 = 30$ W, we then find

$$\beta \approx 1.1 \times 10^{-4} \text{ cm}^{-1}$$

$$\alpha \approx 1.2 \times 10^{-4} \text{ cm}^{-1},$$

$$z_{max} \approx 5 \times 10^{3} \text{ cm},$$

$$H(b) \approx 3 \times 10^{-14} H_1^2(b)\, H_2(b) z \text{ gauss},$$

$$\left(\text{or, } \frac{H(b)}{z} \approx 1.3 \times 10^{-14} \ \frac{\text{gauss}}{\text{cm}}\right)$$

$$P \approx 2.2 \times 10^{-27} P_1^2 P_2 z^2 \text{ watt (z is in meters)},$$

$$(\text{or, } \frac{P}{z^2} \approx 7 \times 10^{-23} \ \frac{W}{m^2}) \ ,$$

$$H_{max}(b) \approx 3 \times 10^{-11} \ \text{gauss},$$

$$P_{max} \approx 3.5 \times 10^{-20} \ \text{watts}.$$

We note finally that the I.M. power depends upon the fourth order of the ratio $\Omega_{H/\nu} \equiv e/mc\nu$ (or, second order of the parameter R). Hence, in order to determine the correct value of the IM products generated via the nonlinear character of the $[\vec{v} \times \vec{H}]$ force, it is important to determine the exact values of the electron effective mass m and the collision frequency ν. In our estimates, we have used the free electron approximation for the conduction electrons.

ADDENDUM 4

DEVELOPMENT OF A COMPUTER MODEL FOR ELECTROMAGNETIC FIELDS IN TRANSMISSION LINES AND COMPONENTS

INTRODUCTION

A mathematical approach has been formulated which will enable solution of electromagnetic field problems within closed geometries such as cavities, cables and eventually, more complex structures. The components or structural elements may be specified in terms of the dimensions and the electromagnetic parameters of the materials, namely permittivity, permeability and conductivity. The analysis is based upon the use of multiple Laplace transforms for explicit solution of Maxwell's equations in three dimensions. The intermediate results are in the form of algebraic expressions for transforms of field quantities which are manipulated in the same fashion as are the transfer functions in linear system theory. The results are formulated in terms of generalized impedance and admittances. The analogy to the expressions of transmission line theory is complete and, in fact, includes them as a special case. A computer flow diagram is presented for solution of a typical problem. Time has not permitted generation and checkout of a computer program.

The fact that the parameters of the medium, for example finite conductivity, and the size of the component relative to the wavelength presents no mathematical limitation in the development of the equations indicates that the results will be useful for the effects of the size and materials of microwave components upon intermodulation products and similar problems. Since the results are essentially transfer functions for the electromagnetic fields, it has been possible to formulate the equivalent feedback problem for the fields interior to a component and thereby obtain the effects of multiple reflections, or cavity modes, and for multiple section media.

In the following discussion the approach and results will be discussed briefly and illustrated by the computer flow diagram for the computation of the fields within a very small filament or whisker such as may be found inside a UHF coaxial component.*

---

*The method outlined here is not limited to coaxial components, or to the UHF range.

DISCUSSION OF THE APPROACH

The mathematical approach used depends upon a somewhat unfamiliar use of the Laplace transform for solving partial differential equations. The feature which is employed involves taking Laplace transforms of derivatives with respect to spatial coordinates. As a result, the value of the fields at coordinate surfaces are handled in the same way as initial conditions in the usual application of Laplace transforms to differential equations involving only time derivatives. The power of this technique is then coupled with the methods used in transmission line theory to obtain the intrinsic impedance of a medium. It is then possible to treat the free space which surrounds the medium as the termination of the medium inside the component, and therefore the free space intrinsic impedance is the terminal impedance for the component medium. Again using methods analogous to transmission line theory we may write an expression for the input impedance in terms of the intrinsic impedance of the component medium and the terminal impedance. Consequently, it is possible to compute all of the impedances of a connected set of media.

Reflection and transmission coefficients may also be expressed in terms of the terminal and intrinsic impedances. All of these coefficients may be written for the set of media. Finally, the incident field may be summed with the field which is being reflected from the far end of a medium. The result is an equation for the cavity modes which resembles the forward gain equation for a feedback amplifier. Cavity modes, or resonances, correspond to the frequencies of oscillation in such a feedback loop or the poles of the transfer function. In the following section a flow diagram is presented which illustrates the principles which have been discussed and also indicates the flow of information which will occur within a computer program which will implement the equations that have been developed.

DISCUSSION OF THE COMPUTER FLOW DIAGRAM

Figure 1 presents the terminology which will be used in the following discussion and applies to a small filament or whisker. We shall employ the concept of a wave which propagates and is attenuated in a normal medium, the so-called progressive wave, and also the concept of a wave which originates as a reflection and is propagated with attenuation in the opposite

direction, the so-called regressive wave. The incident wave in Figure 1 propagates progressively and penetrates surface 1 according to the transmission coefficient computed as indicated above. A portion is also reflected and becomes part of the wave which is backscattered in the regressive direction. As mentioned above, the total wave within the medium is the sum of the incident wave with the internally reflected waves. The latter may be expressed in terms of the incident field and reflection coefficients for the surfaces involved. Finally, the wave which penetrates the last surface (3 of Figure 1) propagates progressively to infinity.

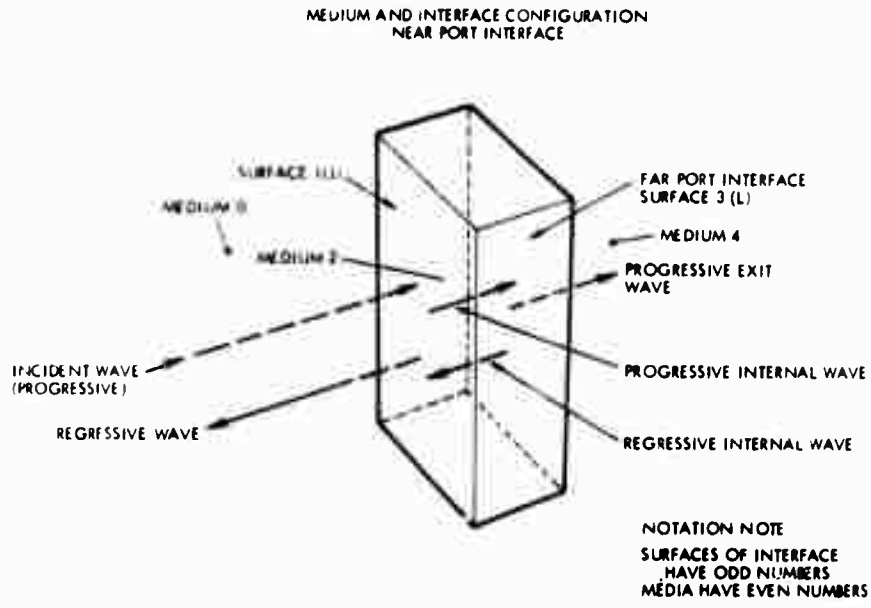

Figure 1. Electromagnetic Fields for a Whisker

The computer flow chart is shown in Figure 2. Two of the six sections which correspond to the propagation equations for certain field components are shown. Briefly it has been found that the linear relation between field quantities which contribute to a field component, as expressed in Maxwell's equations, carry over into the impedance formulations in two ways. As a result, there is a flow scheme for each linear grouping of components. The final field components may easily be solved from these propagation models. In Figure 2 there are indicated three types of operational blocks at each piece of media and its interfaces, namely reflection and transmission coefficients and propagation equations for the medium itself. All four sections of Figure 2 are coupled in the impedance relations which, as mentioned above, resemble those of usual transmission line problems.

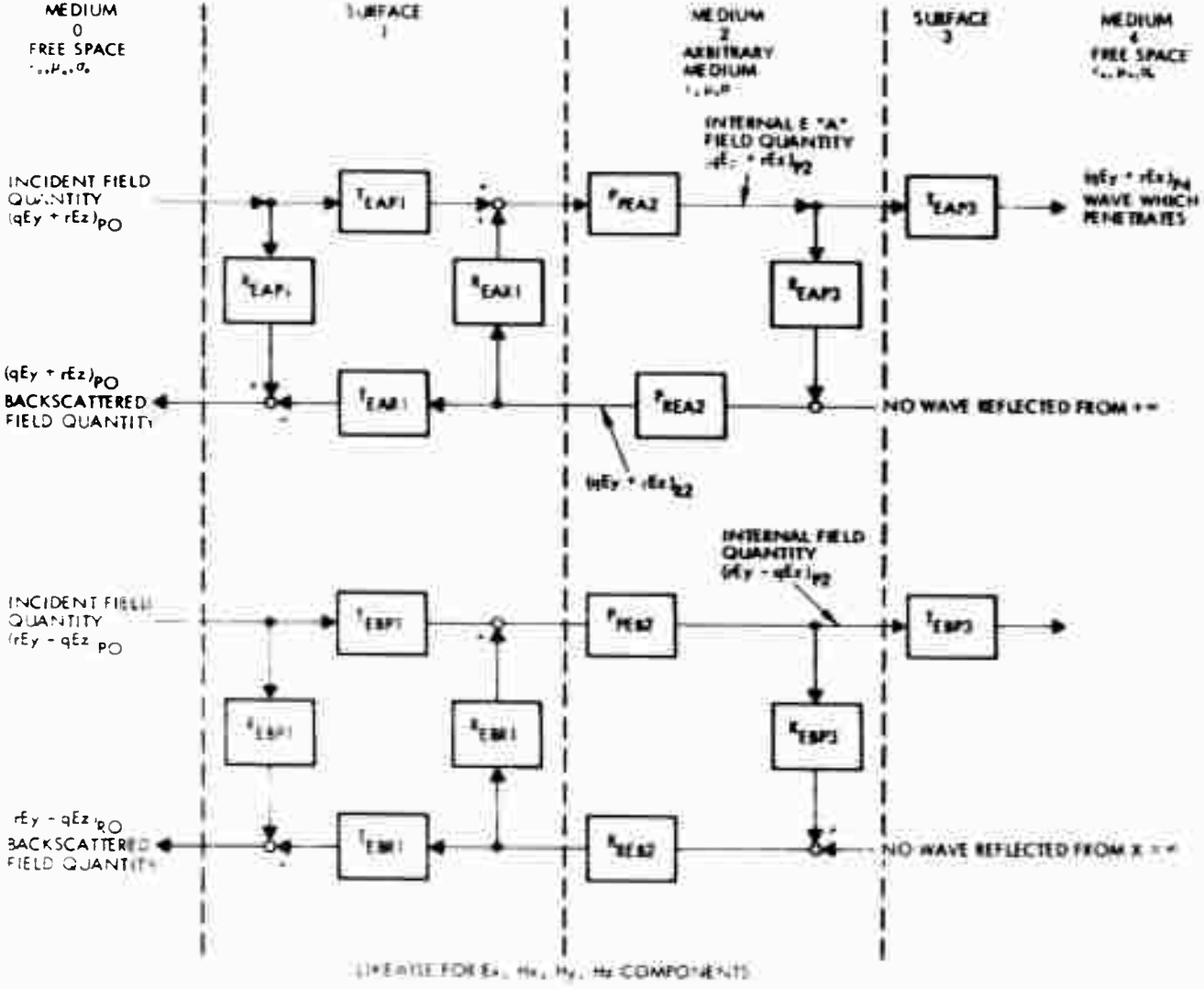

Figure 2. Computer Flow Diagram

DISCUSSION OF RESULTS AND RECOMMENDATIONS

The current status of this work is that the algebraic formulations have been completed and the preliminary architecture of a computer program has been outlined. Some hand computations have also been made of certain quantities. The principal effort to date has involved determination of the methods for obtaining an explicit solution. There were very few guidelines and because the work entailed carrying and evaluating six components at every stage the effort has been tedious and time consuming. The current form of the results will have to be checked out on problems for which solutions are available. After this stage is accomplished, it is expected that the computer program will enable computation of fields and field-dependent data for many types of complex and difficult structures.

ADDENDUM 5

POWER ABSORBED IN SMALL PROJECTIONS FROM COAX WALLS IN TEM FIELD

4351.5.74-022

An attractive conjecture for IM production is that sharp projections, whickers or bosses extend from the walls of the coax and currents are driven within them by the full radial field of the coax. It is reasoned that this is so because the projection is assumed smaller than the skin depth, in thickness. However, to counter this, one must contend with the capacitive limitation of such projections to support currents before depolarizing fields take effect. To resolve this problem, a classical scattering problem – Mie scattering – is considered; the reasoning being that a hemispherical boss on the surface of the metal will, for scattering of the normal component of the field, behave as a sphere (since it and its mirror image form a sphere).

The polarization of a sphere of refractive index N and, where $\frac{2\pi a}{\lambda} << 1$ is given by [1]

$$1) \quad P = \frac{3}{4\pi} \frac{N^2-1}{N^2+2} E_0 e^{i\omega t},$$

The energy deposition per unit volume, $\dot{U}$, is given by

$$2) \quad \dot{U} = \frac{1}{2} R_e (\dot{P} \cdot E^*) = R_e\left(\frac{3i\omega}{8\pi} \frac{N^2-1}{n^2+2} E_0^2\right).$$

Now from Maxwell's equations:

$$3) \quad N^2 = 1 - i \frac{4\pi\sigma}{\omega} .$$

Therefore

$$4) \quad \dot{U} = \frac{9}{32} \frac{\omega 2}{\pi 2\sigma} E_0^2 ,$$

Exactly the same result is obtained from analysis of the absorption cross section of the sphere. To see how important this may be, we compare it with the power absorbed by the tangential component of the field, $10^{-5} E_0$, in the coax

$$5) \quad \dot{U}_{tangential} = 10^{-10} \sigma E_0^2 .$$

---

1. Stratton, Electromagnetic Theory, p. 572.

The ratio is

$$6)\quad \frac{\dot{U}_{tangent}}{\dot{U}} = \frac{9}{32}\frac{\sigma^2}{\pi^2\omega^2} = 75 \times 10^8 .$$

We can gain further understanding of (4) by the following heuristic arguments: The hemisphere being driven by the applied electric field may be considered a circuit with capacitance, $\frac{1}{a}$, and resistance $\frac{a}{\sigma\pi a^2}$. The applied EMF is then, v = 2aE. Writing the equation of motion of the current as

$$7)\quad v = RI + \frac{q}{c} = RI + \frac{I}{i\omega c} = I\left(\frac{1}{\sigma\pi a} + \frac{1}{i\omega a}\right) = 2aE.$$

Solving for I, we obtain,

$$8)\quad I = \frac{2a^2E}{\frac{1}{\sigma\pi} + \frac{1}{i\omega}} ,$$

and current density, $J = \frac{I}{\pi a^2}$.

$$9)\quad J = \frac{2E}{\frac{1}{\sigma} + \frac{1}{i\omega\pi}} .$$

Using $\dot{U} = \frac{1}{2}\,\mathrm{Re}(J \cdot E^*)$ we obtain

$$10)\quad \dot{U} = \frac{E\omega^2}{\pi^2\sigma} ,$$

which aside from the factor of 9/32 agrees with (4).

The remarkably low value of the power being dissipated in the protuberance may now be understood in the light of the immediately preceeding argument; that is, the current in the hemisphere is mainly 90° out of phase with the applied electric field due to the hemisphere's small capacitance. The same arguments should apply to projections of other shapes, such as whiskers and needles.

ADDENDUM 6

INTERMODULATION GENERATION IN RESONANT CAVITIES

5351.4.74-21

We have demonstrated that the power in third order intermodulation products which are generated by the thermal heating of the coax walls, behaves, essentially, as the sixth power of the impressed fields propagating through the coax.[1] Because of this unusual sensitivity to field strength we felt it important to investigate cases where the field strength could exhibit larger values than we had considered, namely, under conditions of resonance. For this purpose we continue our investigation of coaxial waveguides but now employing them as resonant cavities since their analysis, because of their single allowable mode, is so simple.

We consider a length of coax, ℓ, closed at both ends but with sources of E.M. energy at frequencies ω_1 and ω_2 at one end. The E.M. energy propagates in the TEM mode and reflects from each end and, if the length, ℓ, is of the proper magnitude, standing waves are formed. As the E.M. waves propagate and attenuate in the guide, they produce[1] modes at I.M. frequencies which, in turn, propagate, attenuate and reflect from the waveguide ends. For the proper magnitude of the coax length, ℓ, the I.M. can also produce standing waves. In what follows, we shall discuss a case where ℓ is resonant for all three frequencies, however, the analysis need not be restricted to resonance for all or for any of the frequencies.

The field in the waveguide at position, x, may be broken up into right propagating, H_R, and left propagating, H_L, fields. The field H_R may be considered as being made up of waves having encountered respectively, no reflection, two reflections, four reflections, etc. Thus:

---

1. J. Z. Wilcox and P. Molmud, "Thermal Heating Contribution to Intermodulation Fields in Coaxial Waveguides," Oct. 7, 1974, 4351.5.74-19 (Addendum 1).

$$H_R = H_o e^{i\omega t - i\frac{\omega}{c}x - \alpha x}\left[1 + R^2 e^{-i2\frac{\omega}{c}\ell - 2\alpha\ell} + R^4 e^{-i4\frac{\omega}{c}\ell - 4\alpha\ell} + \ldots\right] \quad (1)$$

$$= \frac{H_o e^{i\omega t - i\frac{\omega}{c}x - \alpha x}}{1 - R^2 e^{-i2\frac{\omega}{c}\ell - 2\alpha\ell}}$$

Based upon similar condition,

$$H_L = \frac{H_o R e^{i\omega t + i\frac{\omega}{c}x + \alpha x - i\frac{\omega}{c}2\ell - 2\alpha\ell}}{1 - R^2 e^{-i2\frac{\omega}{c}\ell - 2\alpha\ell}} . \quad (2)$$

In (1) and (2), α is the complex attenuation coefficient ($\alpha = \alpha_o (1 + i)$) for the waveguide and R is the reflection coefficient, assumed equal at each end. The amplitudes of H_L and H_R are maximized when $2\ell\left(\frac{\omega}{c} + \alpha_o\right) = 2n\pi$, where n is an integer. Let us assume this condition applies. Assume also $R = 1$ and $2\alpha_o\ell << 1$. Then

$$H_{total} = \frac{H_o e^{i\omega t - 2\alpha_o\ell + \alpha_o x}}{\alpha_o \ell}\left\{\cos\left(\left(\frac{\omega}{c} + \alpha_o\right)x\right) + \alpha_o(\ell - x)e^{-\frac{i\omega x}{c} - i\alpha_o x}\right\} \quad (3)$$

Equation (3) demonstrates the expected standing wave plus a traveling wave of low amplitude (the result of the attenuation) moving to the right.

At this point, it may be of interest to determine the "Q" of this coax being used as a resonant cavity. "Q" is defined as the energy stored in the cavity divided by the energy dissipated in the walls per half cycle. The stored energy is simply $\frac{H^2_{total}}{4\pi}$ from (3) integrated over the volume between the coax walls. For a coax with the inner and outer radii a and b respectively, the flux of energy into the coax is $\frac{c}{4\pi} H_a^2 \, 2\pi a^2 \ell n \frac{b}{a}$, which in steady state is the dissipation rate. "Q" is therefore:

$$Q = \frac{\ell f}{\alpha_o^2 \ell^2 c} = \frac{n}{2\alpha_o^2 \ell^2} , \qquad (4)$$

where we have used the fact that, for a resonant cavity, $2\frac{\omega}{c}\ell = 2n\pi$. (Here, and in the following, we neglect α in comparison to $\frac{\omega}{c}$). Now, when ℓ = 500 cm, then the coax is resonant simultaneously to f = 270 mHz, f = 240 mHz and their third order I.M. product 300 mHz. Setting ℓ = 500 cm, f = 300 mHz and $\alpha = 2 \times 10^{-4}$ cm^{-1} (coax UT 141, see Ref. 1) in (4), we obtain Q = 500.

We now return to the task of determining the I.M. products. The I.M. field, as are the source fields, will be considered to be composed of right traveling waves and left traveling waves. The sources, being traveling waves also, will feed energy into only those I.M. waves traveling in the same direction. For it is only with those waves which are traveling in the same sense that the sources maintain a constant phase relationship.

The I.M. products are generated in the same fashion as in Reference 1. That is, for $0 < x < \ell$, the right traveling I.M. wave produced by the right traveling source is equal to

$$H_{RIM} = -\frac{\alpha d}{8(\alpha-3\beta)(\beta\ell)^3} (e^{-3\beta x} - e^{-\alpha x}) e^{i\omega t - i\frac{\omega}{c}x} , \qquad (5)$$

using the same notation as in Reference 1.[2] To (5) must be added all the right traveling IM waves which have been reflected 2m times (m = 0, 1, .. ∞)

---

2. Actually, in addition to the propagating I.M. waves of the type as given by Eq. (5), additional I.M. thermal currents (at $\omega=2\omega_1-\omega_2$) will be produced in walls of resonant cavities (this follows upon substituting the total standing fields, Eq. (3), into Eq. (13) of Ref. 1). However, though at I.M. frequencies, these currents have "wrong" k-vector, $k \neq \frac{\omega}{c}$, and do not support therefore propagating I.M. modes.

$$\frac{\alpha d}{(\alpha-3\beta)} \frac{e^{-\alpha\ell}}{(2\beta\ell)^3} (e^{-3\beta\ell}-e^{-\alpha\ell}) \sum_m e^{-2m\alpha\ell} e^{-i\frac{\omega}{c}x - \alpha x} \tag{6}$$

and those (produced by left traveling sources) which have been reflected (2m + 1) times

$$\frac{\alpha d\, e^{-3\beta\ell}}{(\alpha-3\beta)\,(2\beta\ell)^3} (e^{-3\beta\ell} - e^{-\alpha\ell}) \sum_m e^{-2m\alpha\ell} e^{-i\frac{\omega}{c}x - \alpha x} . \tag{7}$$

When this is done, we get (for a coax resonant to all impressed and IM frequencies, and for $\alpha\ell$ and $\beta\ell \ll 1$)

$$H_{RIM,total} = \frac{\alpha d}{(\alpha-3\beta)\,(2\beta\ell)^3} \frac{\alpha e^{-3\beta x} - 3\beta e^{-\alpha x}}{\alpha} e^{-i\frac{\omega}{c}x} . \tag{8}$$

Similarly, to the left-hand running IM wave,

$$\frac{\alpha d}{(\alpha-3\beta)} \frac{e^{-3\beta\ell}}{(2\beta\ell)^3} (e^{-3\beta(\ell-x)} - e^{-\alpha(\ell-x)}) e^{i\frac{\omega}{c}x} , \tag{9}$$

must be added all the left traveling I.M. waves which have been reflected 2m times,

$$\frac{\alpha d}{(\alpha-3\beta)} \frac{e^{-3\beta\ell-\alpha\ell}}{(2\beta\ell)^3} (e^{-3\beta\ell} - e^{-\alpha\ell}) \sum_m e^{-2m\alpha\ell} e^{-\alpha(\ell-x) + i\frac{\omega}{c}x} , \tag{10}$$

and those reflected (2m+1) times,

$$\frac{\alpha d}{(\alpha-3\beta)} \frac{1}{(2\beta\ell)^3} (e^{-3\beta\ell} e^{-\alpha\ell}) \sum_m e^{-2m\alpha\ell} e^{-\alpha(\ell-x) + i\frac{\omega}{c}x} . \tag{11}$$

Summing up, the total left running wave is then

$$H_{LIM,\ total} = \frac{\alpha d}{(\alpha-3\beta)(2\beta\ell)^3}\left(\frac{\alpha e^{-3\beta(\ell-x)} - 3\beta e^{-\alpha(\ell-x)}}{\alpha}\right) e^{+i\frac{\omega}{c}x} . \qquad (12)$$

Making finally the approximation that, for the resonant cavity, βx and $\alpha x \ll 1$ (valid for $0 < x < \ell$), we get the total IM standing wave

$$H_{IM,\ standing} = \frac{2\alpha d}{\alpha(\alpha-3\beta)}\ \frac{(\alpha-3\beta)}{(2\beta\ell)^3}\cos\left(\frac{\omega}{c}x\right) . \qquad (13)$$

The fields propagating in any direction, particularly at $x = \ell$, differ in magnitude from the results of Ref. 1 (Eq. (26)) by the factor

$$\frac{1}{\ell\alpha(2\beta\ell)^3} \approx \frac{10^4}{8} \quad (\text{coaxUT 141})$$

and the power transmitted in any given direction augmented by $\frac{10^8}{64} \approx 1.5 \times 10^6$. [The augmentation factor for power can be written also in terms of the Q's of the cavity for the various frequencies (Eq. (4)) as

$$\frac{1}{4}\ \frac{Q_1^2}{n_1^2}\ \frac{Q_2 Q_3}{n_2 n_3}$$

where the subscript refers to a particular frequency and $n_i = \frac{2\ell}{\lambda_i}$.]
Thus the power propagating to the right at $x = \ell$ is given by

$$P = 2.7 \times 10^{-17}\ P_1^2\ P_2 \ell^2 \text{ watts } (\ell \text{ in meters}) \qquad (14)$$

Taking $P_1 = P_2 = 30$ watts and $\ell = 5$ meters, then $P \approx 2 \times 10^{-11}$ watts.

This is a very large IM signal. Such magnitudes are not expected to happen in practice because waveguides are pretty well matched at the ends and have low reflection coefficients. However, if resonant cavities do exist in

microwave circuits, then, because of the high fields encountered, they should be considered as valid candidates for IM production. Their analysis will be more complicated because of the multimode structures which are usually allowed in such cavities.

ADDENDUM 7

INTERMODULATION OF NOISE LOADED CARRIER DUE TO A POOR METAL-TO-METAL CONTACT

74-7130.28-08

SUMMARY

Intermodulation is analyzed due to a small discontinuous deviation from linearity for the case of n narrow-band Gaussian noise signal sources in combination. It is found that the presence of out-of-band channel signals reduces intermodulation products falling in a narrow-band receiver channel. This reduction was found to be inversely proportional to the number of equally intense (out-of-band) signals with that number raised to a power equal to the order of the intermodulation products that happen to fall in the receive band.

INTRODUCTION

One of the most commonly encountered causes of intermodulation in antenna systems is the very small nonlinearity which occurs at the junction of two pieces of metal that carry current. Intermodulation products due to a small nonlinearity has been observed consistently even where the contacting pieces are made of the same material. Data on the shape of the nonlinearity is unavailable; however, it is well-known that the degree of the nonlinearity is quite small. It is so small that there has seldom been any reason to investigate linearity of clean metallic connections. Where receiving and transmitting antennas are adjacent to one another intermodulation effects smaller than one part in 10 million are of major interest. This situation has caused this paper to be written.

A plausible explanation for the nonlinearity in a metal-to-metal connection is suggested by a micrographic view of two metallic surfaces which are placed in contact. When viewed under sufficient magnification any surface will appear rough. It is then clear that only a fraction of the total overlapping area is in metallic contact. The metallic surfaces not in actual metallic contact are separated by a small gap which acts as an insulator. The insulated regions are formed by gaps of variable thickness that are best characterized as extremely thin. Insulated regions present a potential barrier (to electron flow) which is of the form supporting current flow-by tunnelling. That is, electrons at energy levels well below the height of the potential barrier may tunnel through the barrier because it is sufficiently thin. It is well-known that current flow by tunnelling exhibits nonlinear behavior at voltage and current levels centered around zero. Of course, current flow by tunnelling is presently an hypothesis that remains to be proven.

Current flow by tunnelling is in parallel with the flow of much larger current through regions in good metallic contact. Normally current flow by tunnelling is low enough to be considered negligible relative to current flow by conduction through metal-to-metal paths. However, this has not always been the case in the FLTSATCOM antenna system. In cases such as this, we must consider current by tunnelling since this mechanism may

explain intermodulation which is almost always observable when two current carrying pieces of metal are placed in electrical contact (but not perfectly soldered). We shall consider nonlinear forms suggested by tunnelling.

The work presented here is based on the following model and assumptions. The metal-to-metal contact is considered separated from remaining parts of the structure or circuits. This can be done without affecting the usefulness of the result because the nonlinearity is small. Currents and voltages can be determined using linear analysis since the deviation from linearity is so small. Using the best available information on admittance at the metal-to-metal junction, voltage across the junction may be estimated using linear analysis. The voltage determined in this manner may then be considered to be the excitation which drives the nonlinearity associated with tunnelling. Since the only nonlinear effects of interest are products that are otherwise absent, only terms expressing signals at new frequencies need be considered. These can be considered as signal sources located at the metal-to-metal junction. The effect of the junction itself and the effects of the entire circuit on new signal sources must then be determined in order to calculate intermodulation products that will be observed at the terminals.

The purpose of the present paper is to determine trends and frequencies that may be generated by a metal-to-metal junction. It is hoped that the relations determined here will aid in deducing the nature of nonlinearities introduced when current flows across two pieces of metal in contact. It is also hoped that present analysis will suggest experiments that could be performed to determine the nature and magnitude of the small nonlinearity associated with simple metallic contact.

MODEL ASSUMPTION

Whether due to tunnelling or some unknown effect, a metal-to-metal junction will be represented by two parallel components, one linear and the other nonlinear (see Figure 1). The nonlinear path is taken to conduct a negligible part of the total current, I, that flows into the junction. A voltage, IR_s, is assumed to be impressed on the nonlinear path having a characteristic something like that shown in Figure 2.

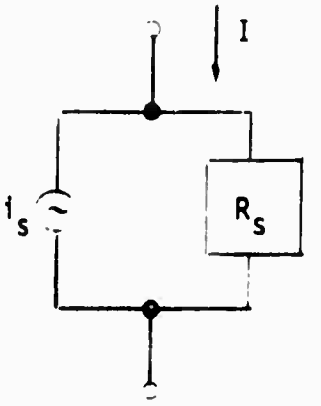

Figure 1. Approximate circuit used to represent a metal-to-metal contact for intermodulation analysis.

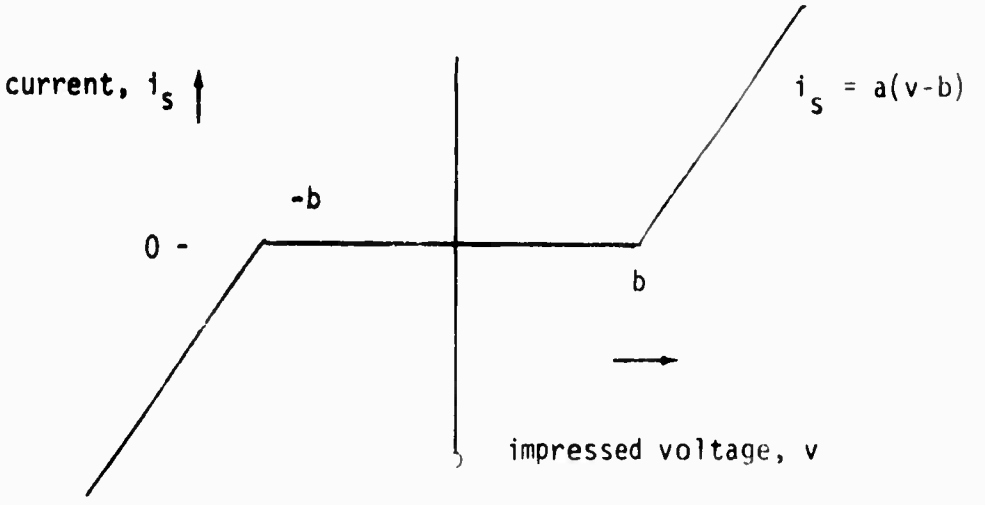

Figure 2. A plausible model for tunnelling current.

The form shown in Figure 2 can be changed without modifying the effects of the nonlinearity significantly by simply adding a small linear term to the branch representing the nonlinearity. In order to keep the circuit unchanged, we add and subtract equal conductances so that the combination effect is zero. The negative conductance is added in parallel with the current generator representing the nonlinearity. The positive conductance is added to the shunt on the right. The combination of the current generator and negative conductance is given by

$$i_t = i_s - vg \tag{1}$$

where

g = the modifying conductance.

ANALYSIS

The negative term in Equation 1 is balanced by an equivalent positive term that is combined with a term representing current flow in R_s. This manipulation is illustrated in Figure 3.

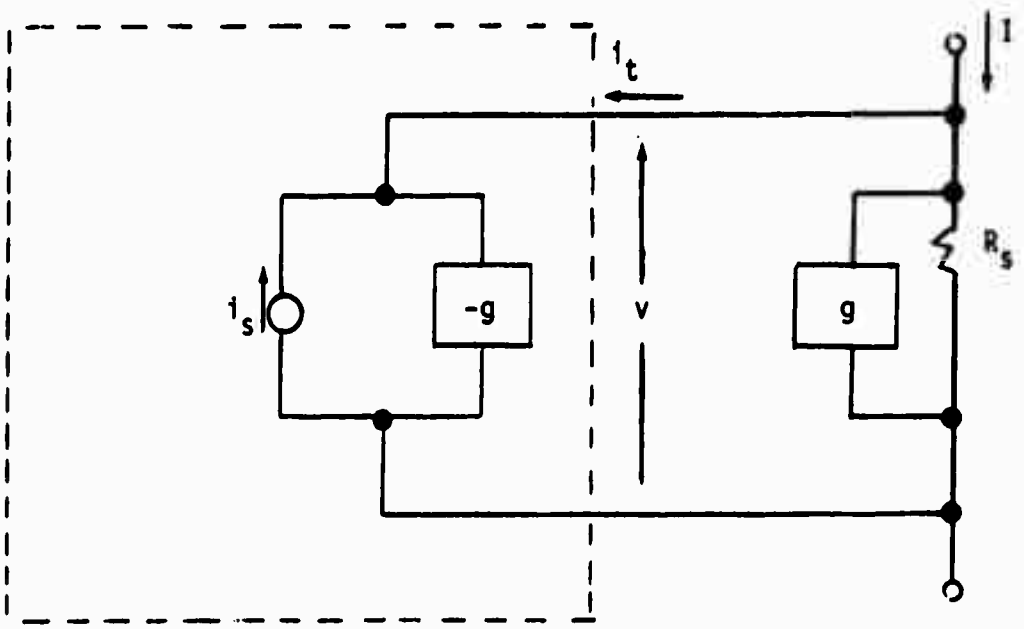

Figure 3. An equivalent form for the circuit in Figure 1.

Using the expression for i_s shown in Figure 2, current flowing into the circuit within the dashed box is given by

$$i_t = \begin{cases} a(v-b)-gv & \text{if } v > b \\ -gv & \text{for } -b \le v \le b \\ a(v+b)-gv & \text{if } v < -b \end{cases} \qquad (2)$$

Setting g equal to a, Equation 2 becomes

$$i_t = \begin{cases} -ab & \text{if } v > b \\ -av & \text{for } -b < v < b \\ +ab & \text{if } v < -b \end{cases} \qquad (3)$$

Equation 3 is close to the form of a hard limiter (see illustration in Figure 4).

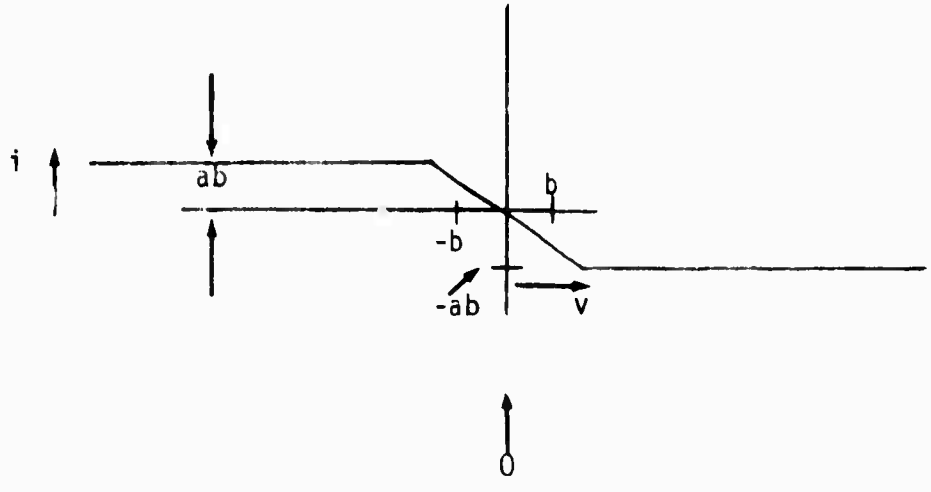

Figure 4. An equivalent form of the nonlinearity shown in Figure 2 (as expressed by Equation 3).

For the purpose of nonlinear effects analysis, the nonlinear forms shown in Figures 1 and 3 are equivalent. This observation is based on the fact that the two forms differ by only an additive linear term. The equivalence is supported further by recalling that the additive linear and negative term (which was combined with the nonlinear term) is exactly cancelled by an equal positive term which, incidentally, tends to lower the resistance of the shunt path (shown as R_s in Figure 1). Since the maximum current due to the nonlinearity is expected to be very small, the positive conductance term (combined with R_s) can be neglected for simplicity. It then follows that intermodulation products due to the nonlinearity in Figure 1 can be determined using analysis for limiters already appearing in the literature.

Note that considerable variation in the shape of the nonlinearity can be accepted without going to something besides a limiter as an analytic model. For example, use of a value for "g" which is greater than the coefficient "a" will convert a nonlinearity like that in Figure 5A into a limiter. Use of a value for "g" less than "a" will convert the nonlinearity in Figure 5B into the limiter in Figure 4. These same general ideas can be applied to nonlinear forms that convert to smooth limiters having the characteristic given in Figure 6. The smooth limiter in Figure 6 is given by

$$i_s = \frac{1}{k}\left[\frac{1}{2} - \frac{1}{\sqrt{2\pi\sigma^2}}\int_0^v e^{-x^2/2\sigma^2}\,dx\right] \qquad (4)$$

Figure 5. Alternative Nonlinear Forms that Reduce to the Limiter Form Shown in Figure 2.

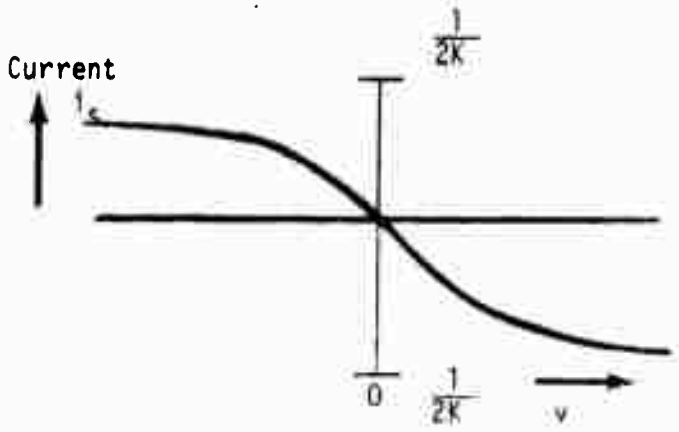

Figure 6. A Smooth Limiter

By simple addition of a linear term this smooth limiter in Figure 6 appears as shown in Figure 7.

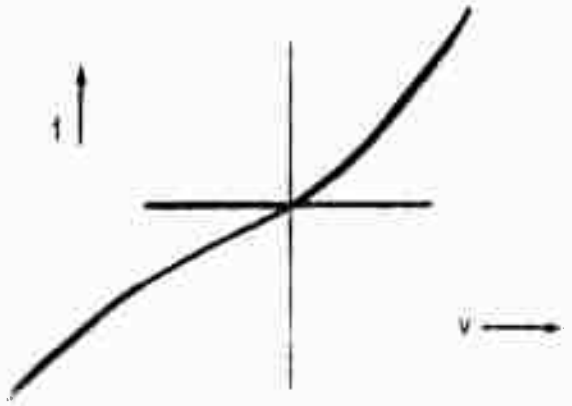

Figure 7. Smooth Limiter of Figure 6 plus an Added Linear Term

It is clear from arguments presented immediately above that intermodulation occurring in a limiter is the same as intermodulation occurring in nonlinearities of the form expected with tunnelling. The essential feature of the nonlinearity allowing reduction to a limiter is that it must be described by parallel lines for large values of the argument. The entire approach presented here is based on the assumption that the nonlinearity does not modify the waveform which drives the nonlinearity. Second order effects of the nonlinearity have been neglected. This approach is limited

to situations where a very small nonlinear effect is combined with a very large linear term. The applicability of the analysis is limited to cases where intermodulation is between frequency components in the driving waveform at the exclusion of interaction with new (small) components introduced by the nonlinearity.

TWELVE NOISE LOADED CHANNELS

The twelve spectral concentrations of power transmitted by the FLTSATCOM satellite are assumed to generate a voltage across one of the small nonlinearities described above. New frequencies due to intermodulation of the applied signal will now be determined by calculating the autocorrelation function of the current generator, i_s, shown in Figure 1. The output power spectral density of this current is then obtained by taking the Fourier transform of the autocorrelation function for i_s. Intermodulation products falling within a receiver band are then revealed by inspection of the spectral density of the current, i_s, at receive band frequencies. Of course, the amplitude or power level of noise due to intermodulation depends on the transfer characteristics of the transmitter and receiver antennas, and in the present context, this would be a rather complex relation beyond the scope of the present paper. However, trends can be determined due to variation in the number of transmitted bands.

The literature contains a considerable quantity of analysis of the passage of noise signals through limiters. This work is directly applicable to the relation between current, i_s, and voltage, v. [The author has given up the pleasure of concealing and reproducing previously published analysis, thinking it would be a vain attempt to amaze the reader.] The smooth limiter illustrated in Figure 6 will develop an output signal having an autocorrelation function given by[1] (for Gaussian noise)

$$R_{i_s}(\tau) = \frac{1}{2\pi K^2} \sin^{-1}\left[\frac{\rho(\tau)}{1+\alpha}\right]$$

where

$$\alpha = \frac{\sigma_i^2}{R_v(0)}$$

$\rho(\tau)$ = the normalized autocorrelation function of voltage, v.

[1] J. B. Thomas, Statistical Communication Theory, John Wiley and Sons, Inc., 1969, p 302.

Note that the smooth limiter defined in Equation 4 converts to the standard hard limiter (except for premultiplication by a negative sign). When $\alpha = 0$ the smooth limiter in Figure 6 converges to the limiter in Figure 4 with $a = 1/(2Kb)$ and $b = 0$. The standard hard limiter is a good approximation to the limiter in Figure 4 when b is much less than the RMS value of v. When the excitation is sufficiently large, coupled with a nonlinearity which is small, the nonlinearity can be approximated by the conventional hard limiter (except for the sign reversal). When the hard limiter is an adequate approximation, the autocorrelation function defining intermodulation products is given by (for Gaussian inputs)

$$R_{1h}(\tau) = \frac{1}{2\pi K^2} \sin^{-1} [\rho(\tau)] \qquad (6)$$

We have seen that the hard limiter in Figure 4 will introduce the same intermodulation products as the assumed nonlinear form suggested by tunnelling (Figure 2). Except for a sign reversal, Figure 4 corresponds to the exact hard limiter that has been treated in the literature. A numerical analysis of the exact hard limiter appears in Reference 2. This analysis relates the correlation function for limiter output to the correlation coefficient for limiter input. The amplitude of the nonlinearity (ab in Figure 4) is expressed in Reference 2, by X where X is the ratio of the magnitude of "ab" to the RMS value of v (with v in the form of gaussian noise). One would expect the exact hard limiter to approach the approximate hard limiter assumed to obtain the result in Equation 6. This is seen to be the case with reference to Table I and Figure 8. Table I presents results taken from Reference 2 for X = .2 together with an evaluation of Equation 6. Figure 8 is simply a plot of results from Reference 2 for X = .2 combined with a plot of

(2) Laning, J. H. and R. H. Battin, Random Processes in Automatic Control, McGraw-Hill, 1956, Appendix B.

Equation 6. Comparisons in Table 1 and Figure 8 were based on the observation that if X = .3 , then

$$\frac{1}{4K^2} = .04\,\sigma^2$$

where

σ^2 is the total power of noise fluctuation of v.

Table 1. Ratio of the Autocorrelation of Limiter Output to Input Noise Power (R_1/σ^2) as a Function of the In Input Autocorrelation Coefficient, ρ.

ρ	R_1/σ^2	
	Exact* Limiter	Equation 6
.05	.00126	.00127
.10	.00252	.00255
.20	.00506	.00513
.40	.0103	.0105
.50	.0131	.0133
.80	.0232	.0236
.90	.0278	.0285
.95	.0308	.0319
1.00	.0358	.0400

* From Reference 2

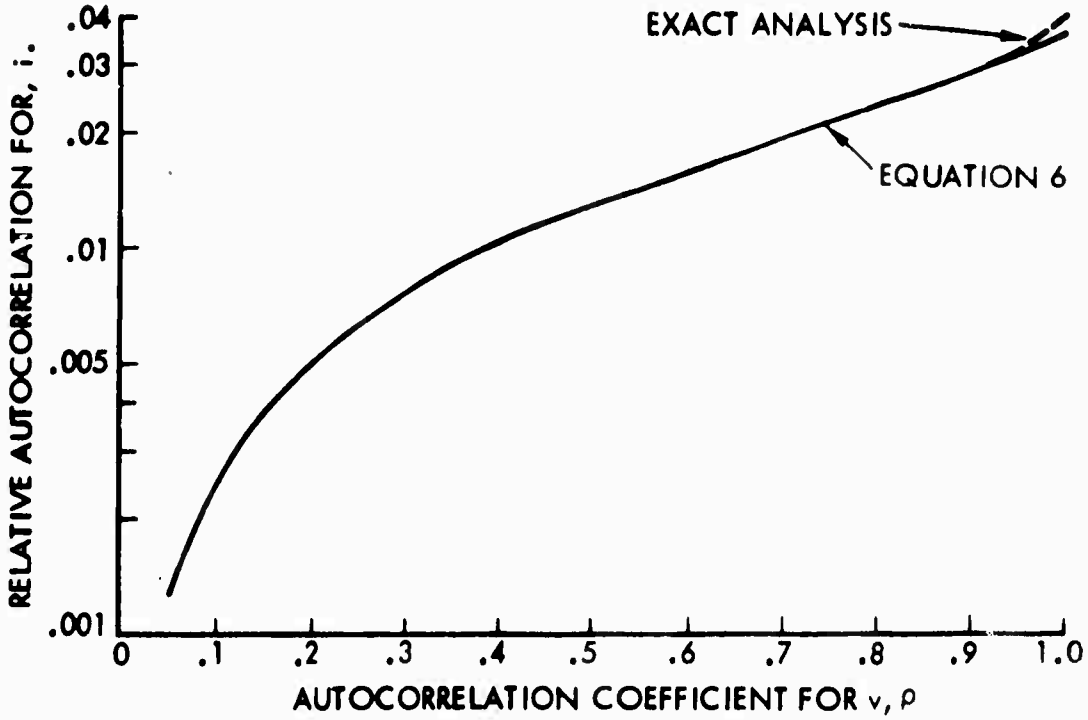

Figure 8. Comparison of Equation 6 with the Exact Hard Limiter. The exact hard limiter appears the same as Equation 6 except for ρ greater than .95.

All of the nonlinear forms described introduce intermodulation products that are described by the inverse sine function if the excitation is large compared to the width of the transition. We have seen that the exact hard limiter and smooth limiter differ in descriptive coefficients but not in form. The output autocorrelation is expressed by the inverse sine of the correlation coefficient for the driving signal. This is a significant observation even though the Fourier transform of the inverse sine function

is not expressible in closed form. The significance of the observation is revealed in the series expansion

$$\arcsin \rho = \rho + \frac{\rho^3}{6} + \frac{3}{40}\rho^5 + \frac{15}{336}\rho^7 + \ldots$$

$$\text{for } \rho < 1$$

$$-\frac{\pi}{2} < \arcsin \rho < \frac{\pi}{2}$$

Intermodulation is determined by terms with ρ raised to odd powers higher than unity.

The autocorrelation function, ρ, is determined by all narrow-band signals which are present in combination. In order to determine, ρ, we consider the autocorrelation function for a single narrow-band channel.

Computations can be simplified by using an approximation for the passband which simplifies the expression for ρ. When expressed in terms of the usual Fourier transform domain (which includes negative frequencies), we approximate a narrow-band noise loaded channel by

$$F_i(\omega) = \left[\frac{\sin(\omega_i+\omega)\frac{1}{B_i}}{(\omega_i+\omega)\frac{1}{B_i}} + \frac{\sin(\omega_i-\omega)\frac{1}{B_i}}{(\omega_i-\omega)\frac{1}{B_i}}\right] N$$

where $\omega_i = 2\pi f_i$ (7)

f_i = center frequency of the channel

B_i = bandwidth of a narrow band channel

The autocorrelation function for this narrow-band noise signal is then given by

$$R_i(\tau) = \int_{-\infty}^{\infty} F_i(\omega) e^{j\omega\tau} \frac{d\omega}{2\pi}$$

or

$$R_i'(\tau) = NB_i \left[u(\tau + \frac{1}{B_i}) - u(\tau - \frac{1}{B_i}) \right] \cos \omega_i \tau \tag{8}$$

where

$u(\tau + \frac{1}{B_i})$ = unit step function at $(\tau = -\frac{1}{B_i})$

We shall assume all twelve of the narrow-band channels are independent so that the autocorrelation function of all twelve channels can be written

$$R(\tau) = \int_{-\infty}^{\infty} \left[F_1(\omega) + F_2(\omega) + \ldots + F_{12}(\omega) \right] e^{j\omega\tau} \frac{d\omega}{2\pi} \tag{9}$$

It is then clear that the autocorrelation function for all twelve noise loaded channels is simply the sum of the autocorrelation functions for each individual channel.

Let us consider the autocorrelation function for n channels with identical bandwidths and well separated center frequencies. The autocorrelation function for this combination is then

$$R_t(\tau) = NB \left[u(\tau + \frac{1}{B}) - u(-\frac{1}{B}) \right] \sum_{i=1}^{n} \cos \omega_i \tau \tag{10}$$

and the related autocorrelation coefficient is given by

$$\rho_t(\tau) = \frac{R_t(\tau)}{R_t(0)} = \frac{1}{n} \left[u(\tau + \frac{1}{B}) - u(\tau - \frac{1}{B}) \right] \sum_{i=1}^{n} \cos \omega_i \tau \tag{11}$$

The autocorrelation function for the output of the assumed limiter is then

$$R_{i_s}(\tau) = \frac{2(ab)^2}{\pi} \sin^{-1}\left\{ \frac{1}{n}\left[u(\tau - \frac{1}{B}) - u(\tau - \frac{1}{B})\right] \sum_{i=1}^{n} \cos \omega_i \tau \right\} \qquad (12)$$

and the power spectral density in the output of the limiter is given by

$$F_o(\omega) = \int_{-\infty}^{\infty} R_{i_s}(\tau) e^{-j\omega\tau} d\tau$$

$$= \int_{-\frac{1}{B}}^{\frac{1}{B}} \frac{2(ab)^2}{\pi} \left[\sin^{-1}\left\{ \frac{1}{n} \sum_{i=1}^{n} \cos \omega_i \tau \right\} \right] e^{-j\omega\tau} d\tau \qquad (13)$$

The limits on the integral allow the unit step functions in the definition of ρ to be dropped.

Since the integral in Equation (13) can not be expressed in closed form, the series just before Equation (7) is substituted for the inverse sine and

$$F_o(\omega) = \int_{-\frac{1}{B}}^{\frac{1}{B}} \frac{2(ab)^2}{\pi} \left[\rho + \frac{\rho^3}{2 \cdot 3} + \frac{1 \cdot 3}{2 \cdot 4 \cdot 5} \rho^5 + \frac{1 \cdot 3 \cdot 6}{2 \cdot 4 \cdot 6 \cdot 7} \rho^7 + .. \right] e^{-j\omega\tau} d\tau$$

where

$$\rho = \frac{1}{n} \sum_{i=1}^{n} \cos \omega_i \tau$$

When our only interest is in new frequencies we consider the term containing ρ^3 and higher power terms after this is complete.

$$\rho^3 = \frac{1}{n^3}\left[\sum_{i=1}^{n} \cos \omega_i \tau\right]^3 \tag{15}$$

Equation (15) can be rewritten as

$$\rho^3 = \frac{1}{n^3}\left\{\sum_{i=1}^{n} \cos^3 \omega_i \tau + 3 \sum_{i=1}^{n} \sum_{\substack{j=1 \\ j \neq i}} \cos^2 \omega_i \tau \cos \omega_j \tau \right.$$

$$\left. + 6 \sum_{i=1}^{n} \sum_{\substack{j=1 \\ j \neq i \\ j \neq k}}^{n} \sum_{\substack{k=1 \\ k \neq i \\ k \neq j}}^{n} \cos \omega_i \tau \cos \omega_j \tau \cos \omega_k \tau \right\} \tag{16}$$

By using trigonometric identities, the powers in Equation (16) can be eliminated and the result is

$$\rho^3 = \frac{1}{n^3} \sum_{i=1}^{n} \frac{1}{4} (\cos 3\omega_i \tau + 3 \cos \omega_i \tau) \tag{17}$$

$$+ \frac{3}{4} \sum_{i=1}^{n} \sum_{\substack{j=1 \\ j \neq i}}^{n} \left[\cos(2\omega_i + \omega_j)\tau + \cos(2\omega_i - \omega_j)\tau + 2\cos\omega_j \tau\right]$$

$$+ 6 \sum_{i=1}^{n} \sum_{\substack{j=1 \\ j \neq i \\ j \neq k}}^{n} \sum_{\substack{k=1 \\ k \neq i \\ k \neq j}}^{n} \left[\cos(\omega_i + \omega_j + \omega_k)\tau + \cos(\omega_i + \omega_j - \omega_k)\tau \right.$$

$$\left. + \cos(\omega_i + \omega_k - \omega_j)\tau + \cos(\omega_j + \omega_k - \omega_i)\tau\right] \Bigg\}$$

To better understand the trend as higher powered terms are considered, observe that

$$\rho^5 = \rho^3 \frac{1}{n^2}\left[\sum_{i=1}^{n} \cos \omega_i \tau\right]^2 = \frac{\rho^3}{n^2}\left[\sum_{i=1}^{n} \cos^2 \omega_i \tau + 2 \sum_{i=1}^{n} \sum_{\substack{j=1 \\ j \neq i}}^{n} \cos \omega_i \tau \cos \omega_j \tau\right]$$

which can also be written

$$\rho^5 = \frac{\rho^3}{n^2}\left\{\sum_{i=1}^{n} \frac{1}{2}\left[\cos(2\omega_i \tau) + 1\right] + \sum_{i=1}^{n} \sum_{\substack{j=1 \\ j \neq i}}^{n}\left[\cos(\omega_i + \omega_j)\tau + \cos(\omega_i - \omega_j)\tau\right]\right\} \quad (18)$$

Substitution of terms in Equation (17) for ρ^3 in Equation (18) will introduce new terms indicating that the following new frequencies will be present in addition to those indicated in Equation (17).

$5\omega_i$, $4\omega_i + \omega_j$, $4\omega_i - \omega_j$,

$3\omega_i + \omega_j + \omega_k$, $3\omega_i + \omega_j - \omega_k$,

$3\omega_i + \omega_k - \omega_j$, $2\omega_i + 2\omega_j + \omega_k$,

$2\omega_i + 2\omega_j - \omega_k$, $2\omega_i + \omega_k - 2\omega_j$

$3\omega_i + 2\omega_j$, $3\omega_i - 2\omega_j$

If the subscripts in the above set are allowed to take on values related to all possible frequencies that are present, we see that new frequencies introduced by the term raised to the fifth power correspond to frequencies that have been defined as fifth-order intermodulation products. Note that ρ^5 also adds terms at frequencies of third-order intermodulation products.

To provide a clear interpretation of these results, select one third order intermodulation product. Any one of them will be due to a term in ρ^3 of the form $A_m \cos \omega_m \tau$, where ω_m is the angular frequency of the intermodulation product of interest. The power spectrum of that term is given by

$$F_{om}(\omega) = \int_{\frac{-1}{B}}^{\frac{1}{B}} A_m \cos \omega_m \tau \; e^{-j\omega\tau} d\tau \qquad (19)$$

Completion of the integral in Equation (19) will result in the original form given in Equation (7). That is, the noise spectrum about each intermodulation product will be the same as the excitation spectrum if each channel is sufficiently different in frequency to prevent significant overlap. Assessment of the degree of overlap will depend upon an investigation of all intermodulation products. However, the frequencies are no different than they are with unmodulated carriers. Note that the shape of the spectrum in the neighborhood of each intermodulation product would be expected to vary from term-to-term in practice. It was the assumption leading to a uniform amplitude on $R_1(\tau)$ which caused the equivalence in shape for input signals and an intermodulation product.

The analysis above emphasized the effect of added noise loaded carriers on intermodulation products appearing in a given receive band. The following portion extends this work by replacing an artificial assumption with a representative form for the shape of a narrow-band spectrum. The spectral shape which was assumed for simplicity of analysis was acceptable for deriving trends with added noise loaded channels that were well separated in frequency. However, a more realistic assumption will now be assumed which does not complicate the analysis very much while revealing the variation in bandspread of intermodulation products.

It is well-known that a number of single tuned narrow-band amplifying stages in tandom can be approximated by a Gaussian shape when all stages are tuned to the same frequency. We then assume that each noise loaded channel has a spectral power density given by

$$P_i(\omega) = \sqrt{\frac{\ell n 2}{\pi}} \left\{ \exp\left[-\left(\frac{\omega+\omega_i}{2\pi B_i} \right)^2 \ell n 16 \right] + \exp\left[-\left(\frac{\omega-\omega_i}{2\pi B_i} \right)^2 \ell n 16 \right] \right\} N \qquad (20)$$

The autocorrelation function is then (from the Fourier transform of $P_i(\omega)$)

$$R_i(\tau) = NB_i \exp\left[-\frac{\pi^2}{\ell n 16} (B_i \tau)^2 \right] \cos \omega_i \tau \qquad (21)$$

The normalized autocorrelation coefficient for n noise loaded carriers of identical bandwidth is then given by

$$\rho_{tg} = \frac{1}{n} \exp\left[-\frac{\pi^2}{\ell n 16} (B_i \tau)^2 \right] \sum_{i=1}^{n} \cos \omega_i \tau \qquad (22)$$

The spectral distribution of intermodulation products is revealed by substituting Equation (22) for ρ in Equation (14) (the limits on the integral in Equation (14) are now taken from $-\infty$ to $+\infty$). The powers on each term in Equation (22) simply multiply the exponent containing B_i. It is then seen by inspection that the spectral density of the νth order intermodulation product is still Gaussian (Equation 20) but of increased bandspread given by

$$B_\nu = \sqrt{\nu} \; B_i \qquad (23)$$

Cross-product terms at the frequency of a given intermodulation product, but arising from higher order terms, have been assumed negligible. This usually is an acceptable assumption since higher order terms are effectively depressed by the coefficient on the respective terms in Equation (14) as well as the $1/_n 2$ proportionality that must be applied to each successively higher order term due to the coefficient $\frac{1}{n}$ in Equation (22).

CONCLUSIONS

Several general conclusions can be drawn from derived results.

1. Note that although the fifth (and higher) powered terms may contribute to third order intermodulation products. The magnitude of the contribution is small because it is suppressed by at least $(1/n^2)$.

2. Intermodulation products appearing at a specific frequency will decrease as new noise loaded narrow band channels are added to the combined signal if the frequency of these channels is such that the resulting intermodulation products do not fall at the observing frequency. A channel with this property will be called an out-of-band channel. It is clear by inspection of Equations (17) and (18) that addition of out-of-band noise loaded channels will decrease an intermodulation product inversely proportional to the number of out-of-band channels raised to the order of the intermodulation product. (All channels were assumed identical.)

3. The nonlinearity assumed (Figure 2 or Figure 4) introduces only odd order intermodulation products.

PART 2

INTERMODULATION CANCELLATION STUDY

CONTENTS

SUMMARY

A 3/8 scale investigation was made of active and passive IM product suppression schemes applicable to the FSC. Three types of IM product sampling antennas were tested. The output of the sample antenna is used in both passive and active cancellation techniques. An array of four 9-turn helices was investigated for usefulness as a receive antenna. The array factor of this design provides an additional means of control of the transfer loss (isolation) with respect to radiation of IM products from the transmit antenna structure. An active suppression system developed by American Nucleonics Corp. for use on another program was tested with the 18-turn receive helix. These tests produced some 20 dB of additional suppression over that provided by the basic transmit antenna to receive helix path loss.

1. INTRODUCTION

This report describes a set of preliminary investigations carried out into active and passive IM product suppression techniques suitable for the FSC application.

2. OBJECTIVE OF CANCELLATION SCHEMES

The objective of the cancellation schemes investigated for the FSC application is to reduce the intermodulation products appearing in the receiver input channels by obtaining a sample of the interference and adding it to the signal-plus-interference in the receiver input with the phase and amplitude of the sample adjusted so as to cancel the interference in the receiver input. Cancellation schemes are identified as either active or passive depending on whether the phase and amplitude of the sample are automatically adjusted by electronic means or whether that adjustment is accomplished manually.

3. IM SOURCES AND POTENTIAL LOCATION

The IM sources can be located in the feed cable to the transmitter antenna, in the feed of that antenna, and in the reflector of that antenna. Their locations and relative magnitude are dependent on the physical characteristics of these component parts. This aspect of the IM product problem is treated at length in Part 1 of this Appendix.

4. IM PRODUCT SPECTRAL AND POLARIZATION CHARACTERISTICS

The frequency level from 292 mHZ through 311 mHZ contains the highest IM level and in this band the level is relatively uniform in spectral density for fully loaded transmitters. IM polarization characteristics depend on the spatial orientation of the surfaces on which they flow. In the region of the receive antennas components both in line with the transmit antenna axis and at right angles to that axis are found to exist.

5. DESIRED AND REQUIRED CANCELLATION PROPERTIES

The transfer function between the transmit antenna and the sample antenna should be the same as the transfer function between the transmit antenna and the main receive antenna for optimum performance of either the active or the passive cancellation scheme.

6. IM SAMPLING ANTENNA CHARACTERISTICS

For use as sample antenna a loop whose axis is in line with the transmit antenna axis, a quarter wave monopole similarly aligned, and a half wave dipole whose axis is at right angles to the transmit antenna axis were tested. They were each located on the ground plane ring of the 18-turn receive helix. The transfer loss and phase of the half wave dipole are shown in Figures 1 and 2. The transfer loss and phase of the one wavelength loop are shown in Figures 3 and 4. The quarter wavelength monopole was used in the ISS suppression, performance tests, and its transfer loss and phase are shown in Section 8 (see Figures 12 and 13).

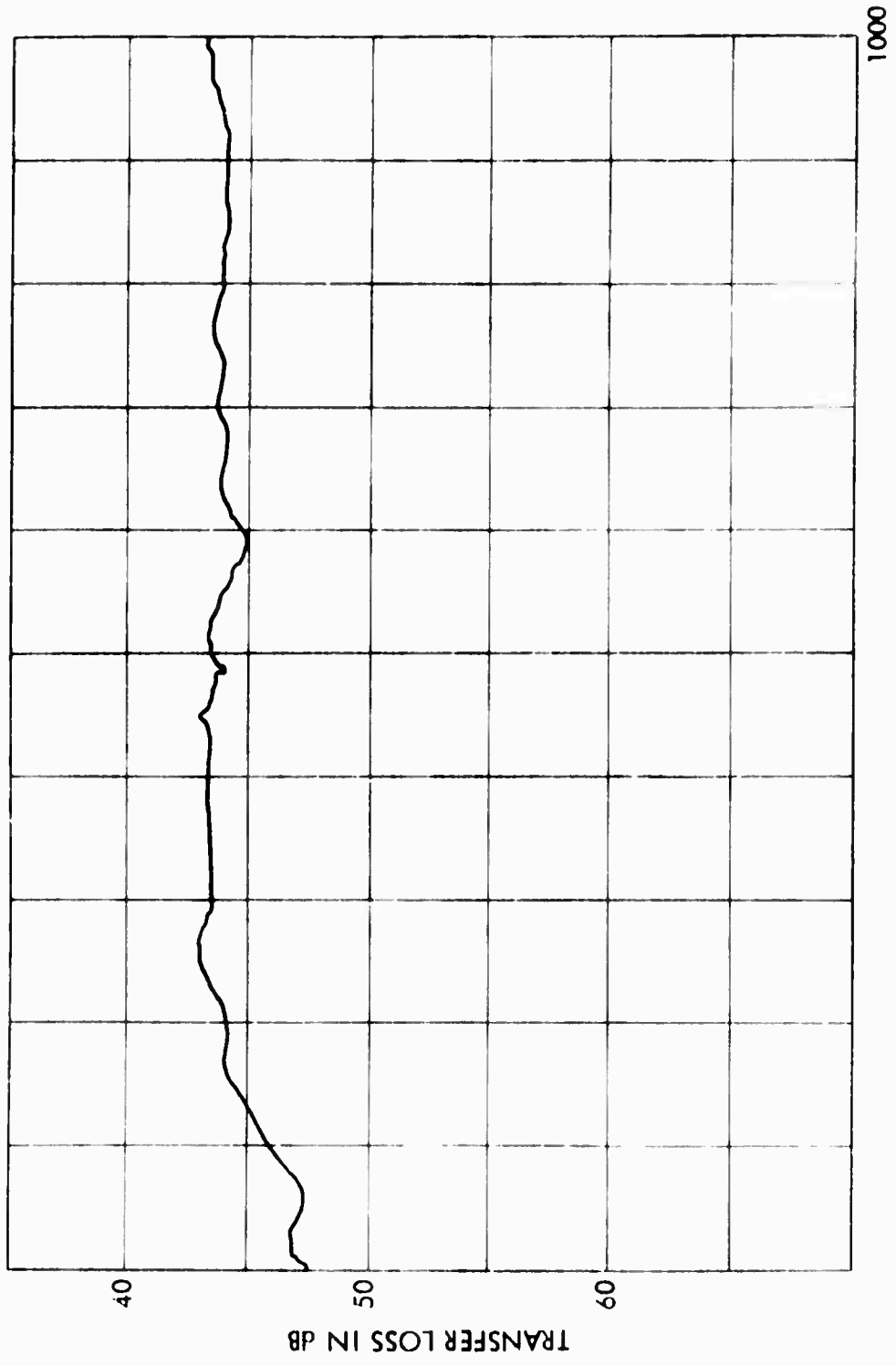

Figure 1. Transfer Loss of Half Wave Dipole

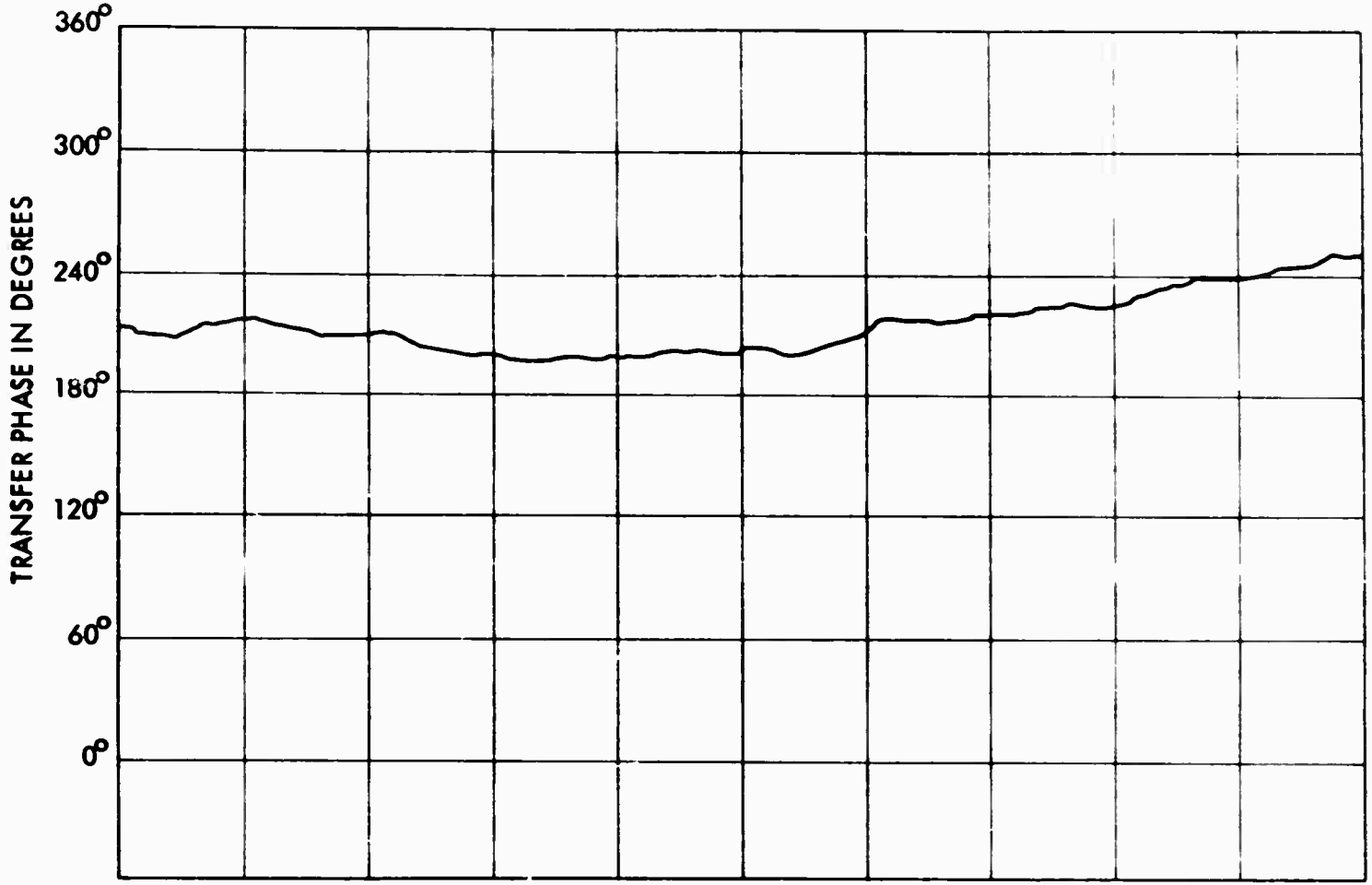

Figure 2. Transfer Phase of Half Wave Dipole

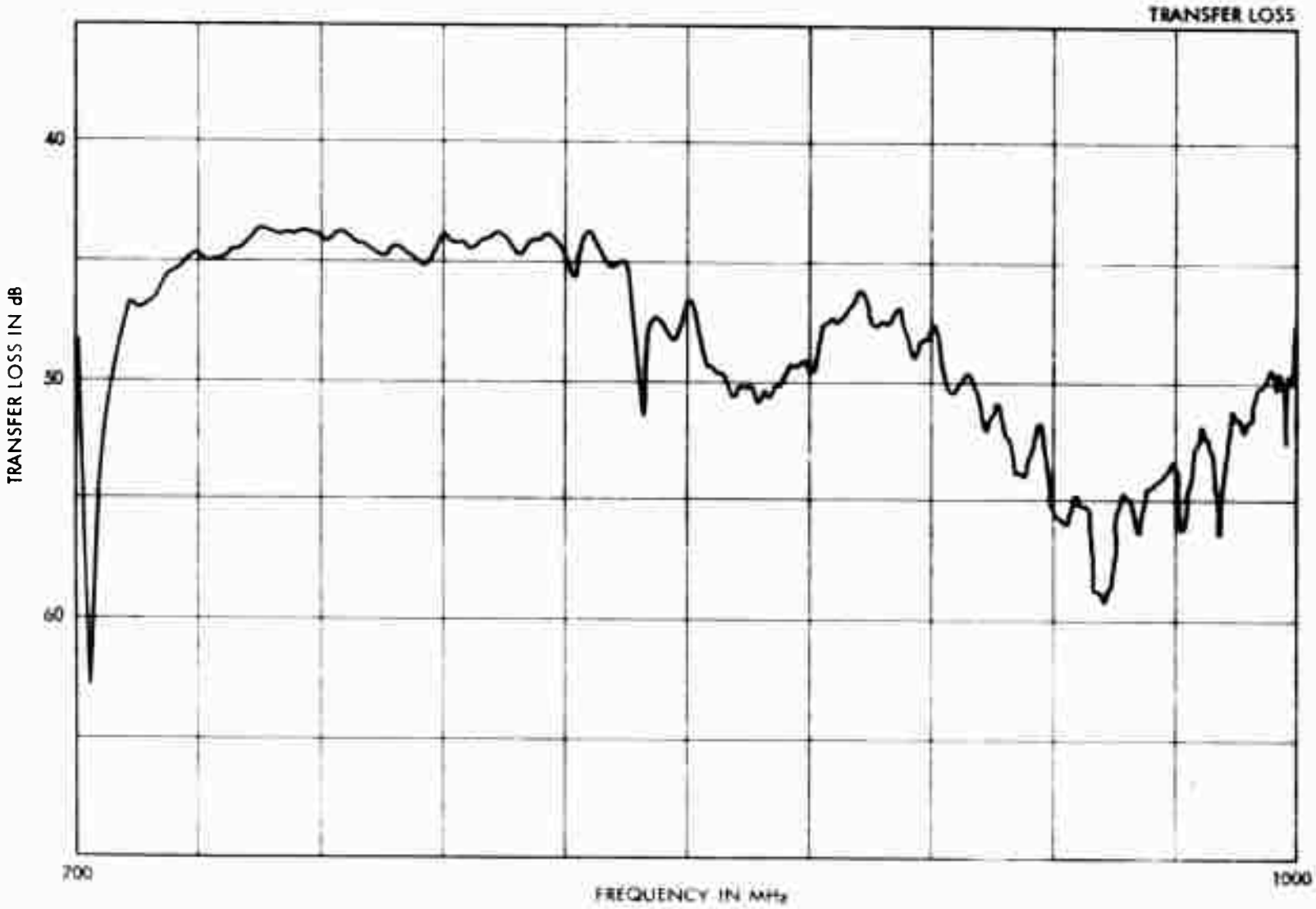

Figure 3. Transfer Loss of One Wavelength Load

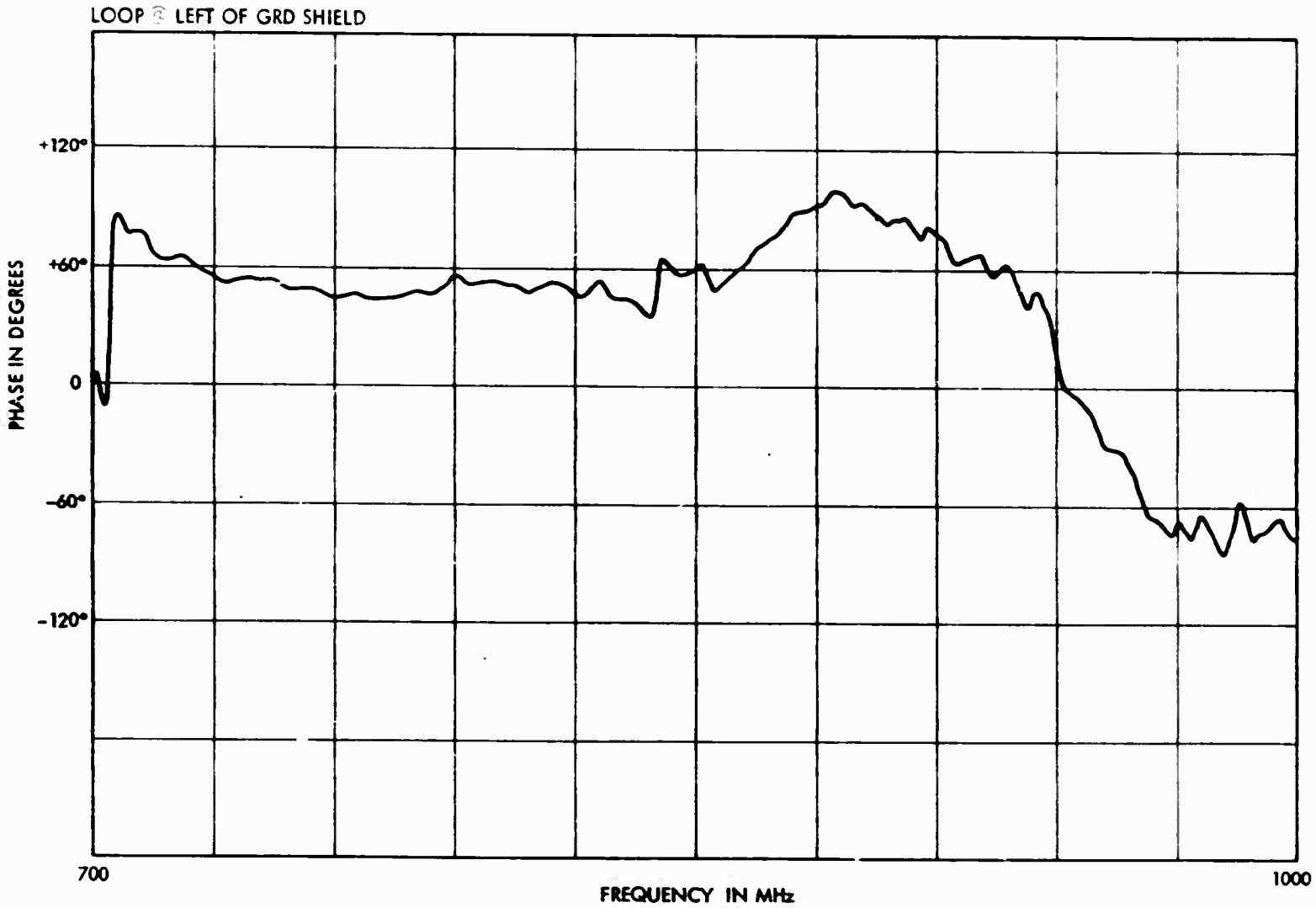

Figure 4. Transfer Phase of One Wavelength Loop

7. ACTIVE CANCELLATION

Active cancellation schemes have the potential of automatically adjusting for changes that may take place in the magnitudes, phases, and locations of IM product sources over a period of time. Their disadvantages include the added hardware weight and volume requirements and the necessity for space qualification of any candidate equipment.

Active cancellation techniques have been investigated in TRW in earlier programs. One such investigation is described in IOC 72-7322.03-17 of 3 October 72. The fundamental technology is closely similar to that used in the Interference Suppression System (ISS) of American Nucleonics Corp. (ANC) whose tests are described in this report. A unit from the Compass Clear program of the Air Force Avionics Laboratory (Contract F33615-72-C-1772) was made available for those tests which were carried out by TRW and ANC personnel on the Building R-2 antenna pattern range.

A block diagram of the ISS tested is shown in Figure 5. Pin diode modulators are used in the A channels and Schottky diode detectors are used in the B channels. The device functions by cross correlating the undesired signal components (the error signal) in the main receive line with corresponding components obtained from the sample antenna circuit. The cross correlation products are used to adjust the magnitude and phase of the injection of the undesired signal components in the main receive line with this injection phased so as to minimize the undesired signal in the main receive line.

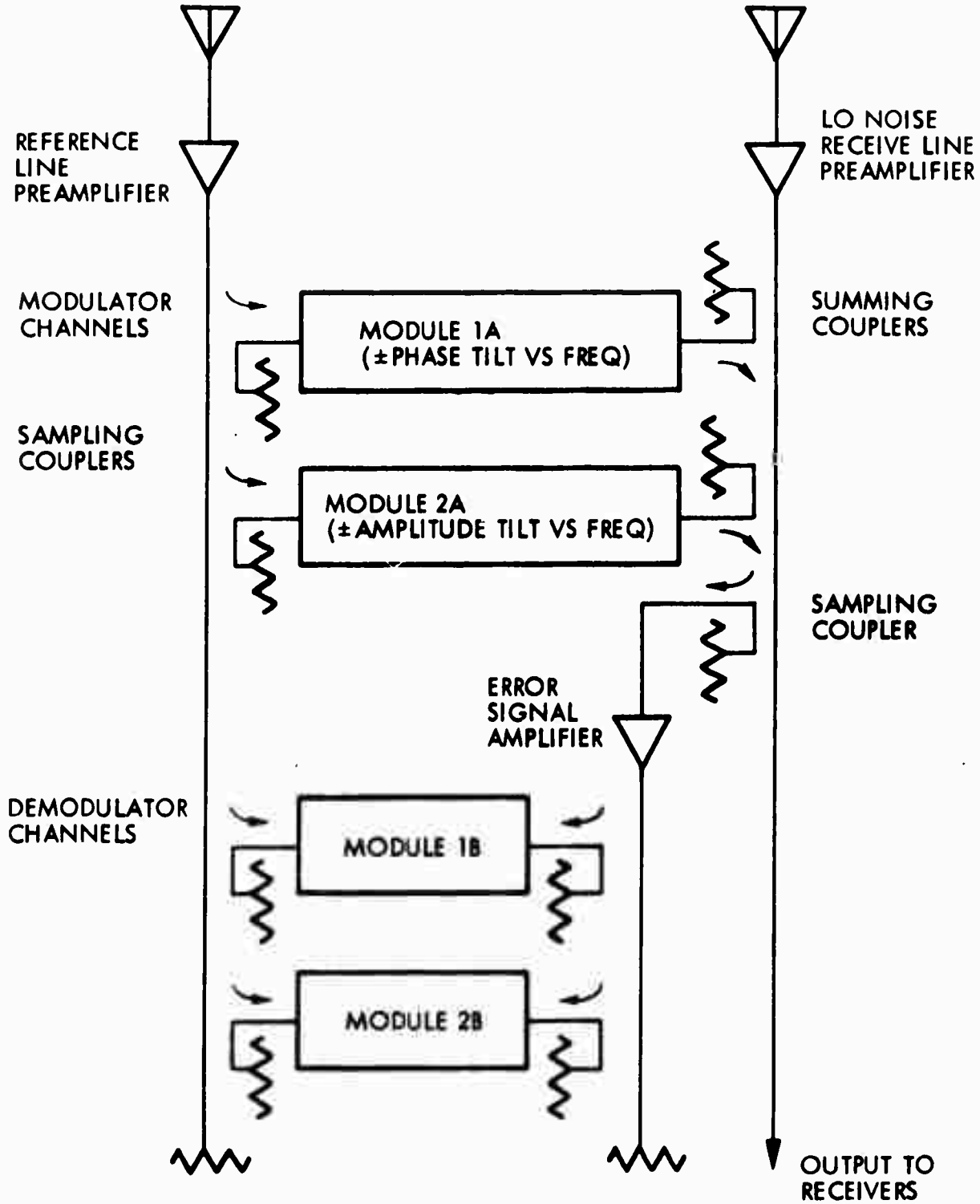

Figure 5. Interference Suppression System with Phase Tilt and Amplitude Tilt versus Frequency

8. PERFORMANCE OF THE ANC ISS AT 3/8 SCALE

Figure 6 shows a photograph of the 3/8 scale transfer loss measurement set-up which was installed on the roof of the antenna range penthouse on Building R2 at Space Park. In the photo two of the three types of sample antennas which were tested are visible at the ring of ground plane of the 18-turn receive helix. The vertical quarter wave monopole is located on the near side of the ring and the half wave horizontal dipole is located on the ring between the receive and transmit antennas. A one wavelength horizontal loop was also tested, and it was located at the ring of the ground plane diametrically opposite the vertical monopole. The location of the test instrumentation is shown immediately below the antenna assembly in Figure 7. Figure 8 shows the antenna assembly with the ANC ISS equipment in place for the active cancellation tests. A close-up of the ANC ISS unit is shown in Figure 9.

Figure 10 shows a block diagram of the test instrumentation used in the transfer characteristics measurements. The outputs of two HP612 signal generators and the HP8690 sweep oscillator are combined with hybrids and connected to an Alford 508 TWT amplifier which drives the transmit antenna. The 18-turn receive antenna is connected into the ANC ISS which then connects into the test channel of the HP8411A connector. The output of the sample antenna was amplified by about 10 dB by an Amplica Model 50 CCTL amplifier of nominally 30 dB gain padded down by 20 dB to prevent its saturation. Both transfer loss and transfer phase measurements were obtained for the several combinations of elements which were tested.

Figure 11 shows the system calibration. It gives the transfer loss measured using a 40 dB pad in place of the unknown. The deviation from 40 dB obtained over the band is due principally to the TWT characteristics. The reference input channel of the HP8411A converter was taken directly from the output of the HP8690 sweep generator to ensure that only the signal from that source appeared in the reference channel. This places the TWT characteristics effectively in series with the unknown impedances under measurements.

Figure 6. Photo of Transfer Characteristics Test Setup

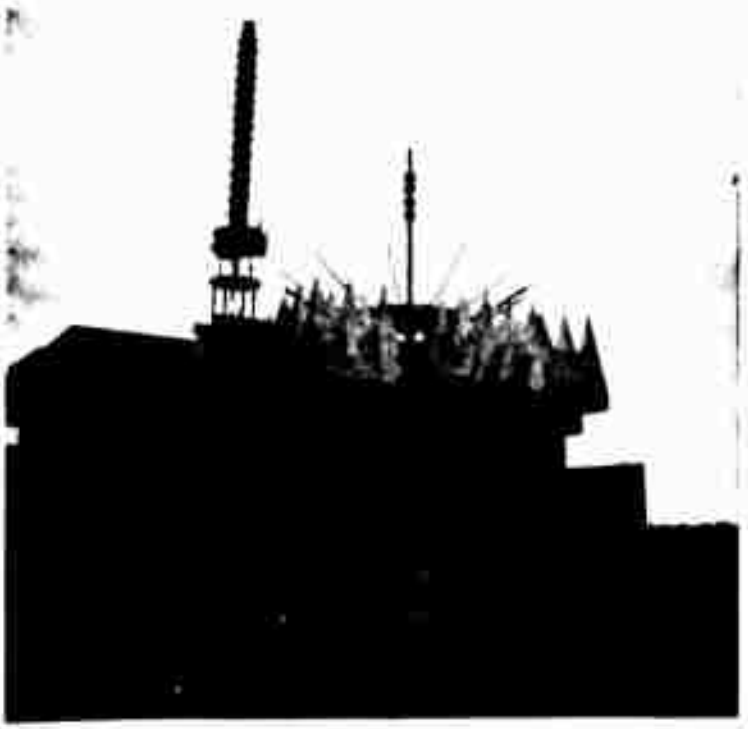

Figure 7. Photo of Transfer Characteristics Test Setup Showing Instrumentation Placement

Figure 8. Photo of Transfer Characteristics Test Setup With ANC ISS In Place

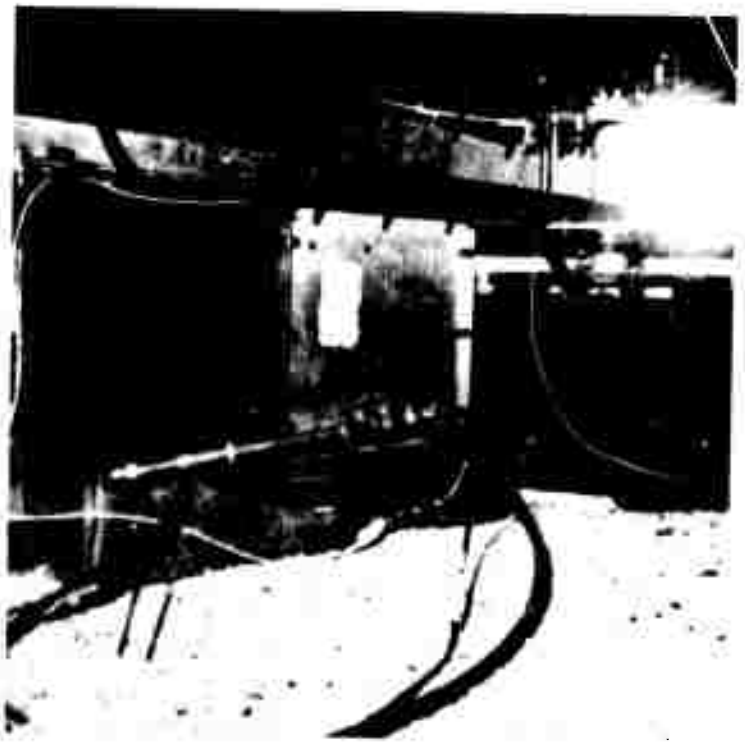

Figure 9. Photo of ANC ISS (Closeup)

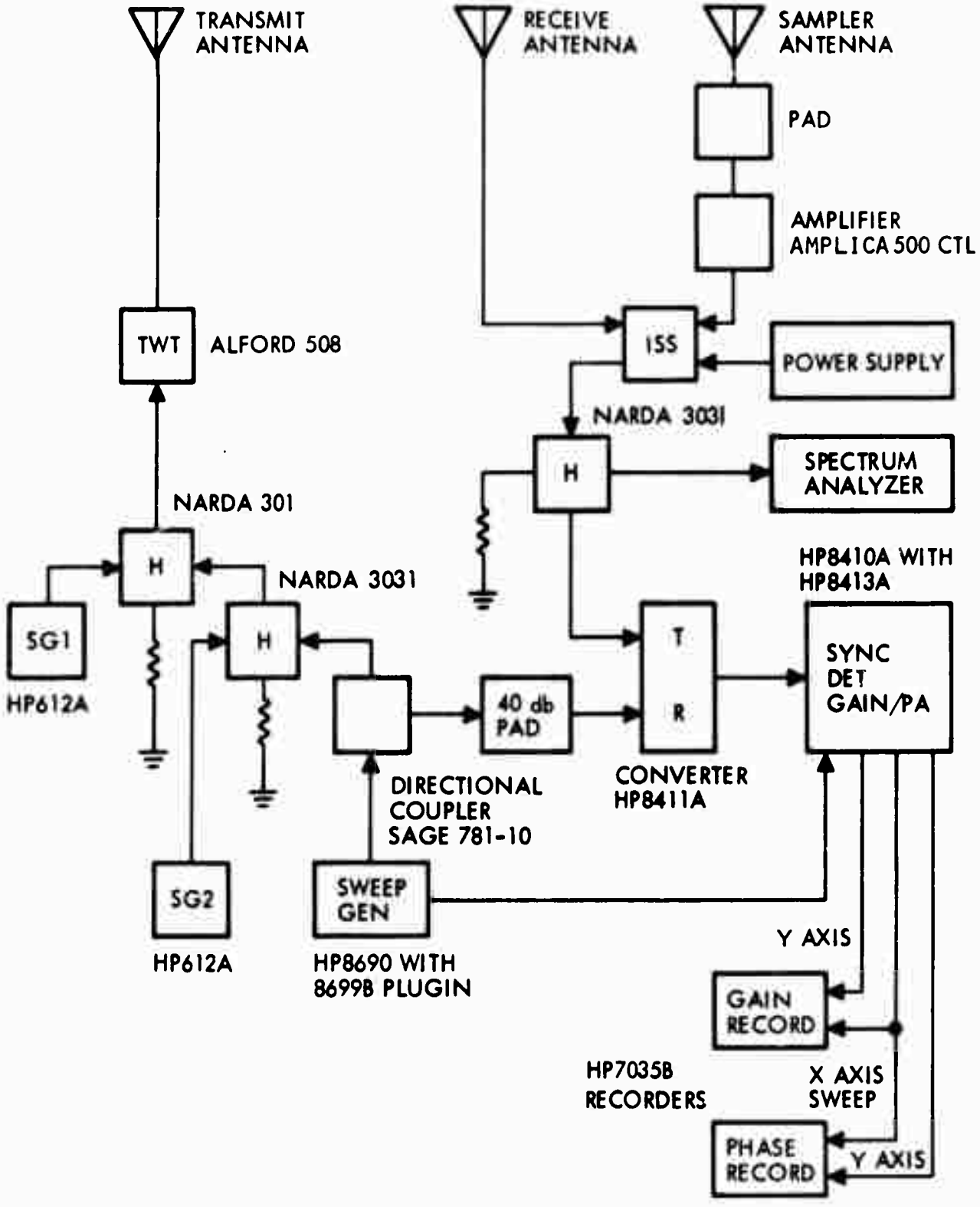

Figure 10. Transfer Loss and Transfer Phase Measurement Instrumentation

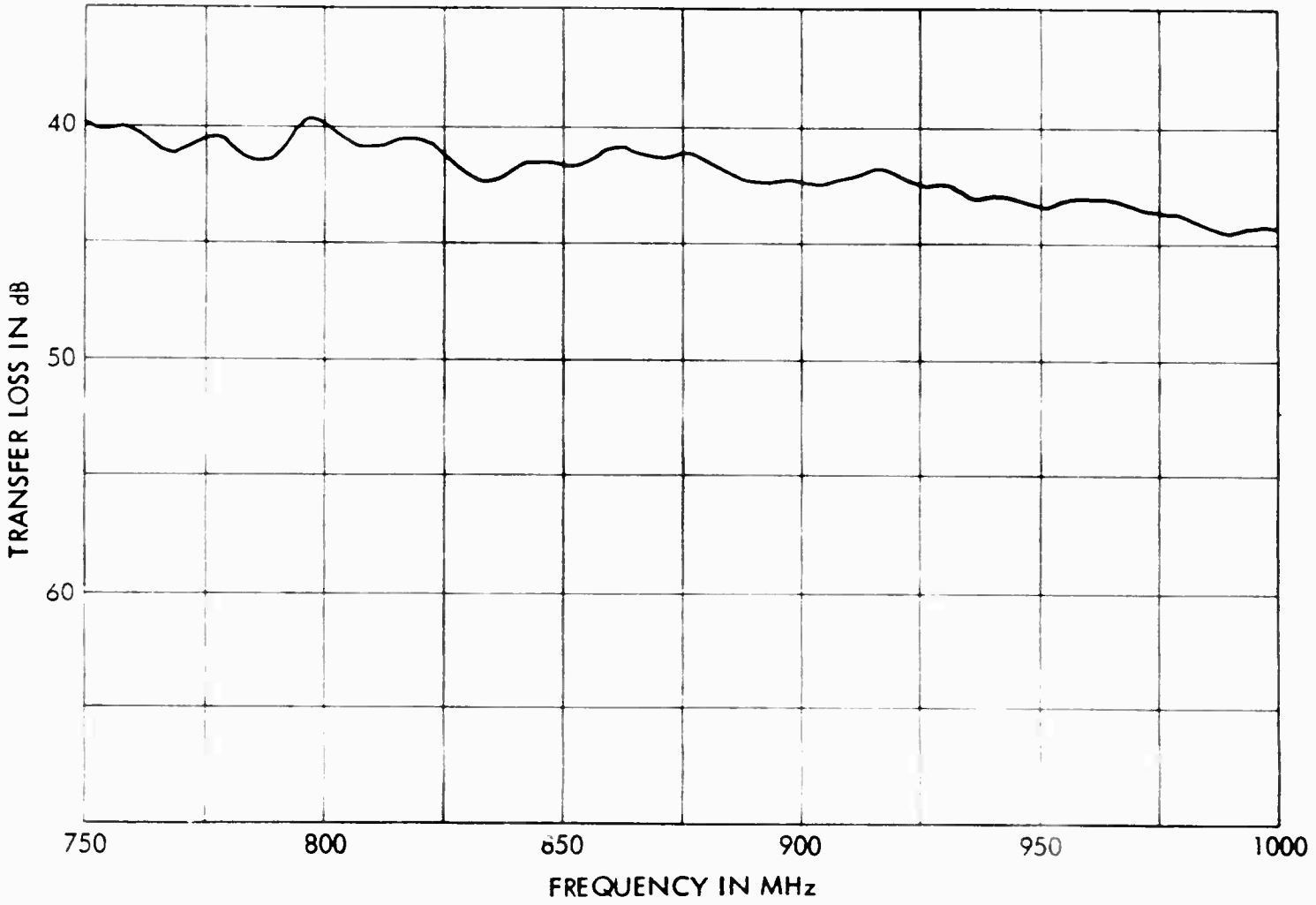

Figure 11. System Calibration Transmit Antenna, Receive Antenna and ISS Replaced by 40 dB Pad

Figures 12 and 13 give, respectively, the transfer loss and transfer phase of the monopole sample antenna and the 18-turn receive helix over the frequency range from 750 mHZ through 1000 mHZ. The two antenna characteristics match one another reasonably well except at the high end of the band.

Figure 14 shows the performance of the ISS over the 750 mHZ through 1000 mHZ band with two IM components simulated. One IM is placed at 780 mHZ with a power level at the signal generator of -10 dBm, and the other is placed at 900 mHZ with a power level of -9 dBm at the signal generator. These two injected signals have captured the synchronous detectors of the ISS. The level of the signal from the sweep oscillator is sufficiently low that it is able to probe the transfer characteristics of the ISS system without affecting the action of its synchronous detectors. This consideration is important to permit observation of system performance without affecting it. For example, if only the probe signal were significant, the ISS would track it as it sweeps, and a maximum of suppression would be achieved throughout the band irresepective of the match of transfer characteristics between sample antenna and the main receive antenna.

Figure 14 shows that over the band where the IM production in the FSC are most significant, 780 mHZ through 830 mHZ, rejection of the order of 20 dB is achieved by the ISS.

Figures 15, 16, and 17 show photos of a set of spectrum analyzer tests which were made. Each figure shows the transfer loss of the system with the ISS shut off and with it turned on. To get these photos, the sweep oscillator was operated at about 100 sweeps/sec, the spectrum analyzer at about 1 sweep/sec, and two one-second exposures were made. The injected signals simulate IM products and their levels were set at -10 dBm in all cases.

In Figure 15 the injected signals are placed at 780 mHZ and 830 mHZ. The photos indicate that both these injected signals are reduced by about 26 dB through operation of the ISS. The third strong line appearing in the photos appears to be an intermodulation product of order $2f_2 - f_1$. Its reduction by the ISS is about 10 dB. If it were produced in the Alford TWT

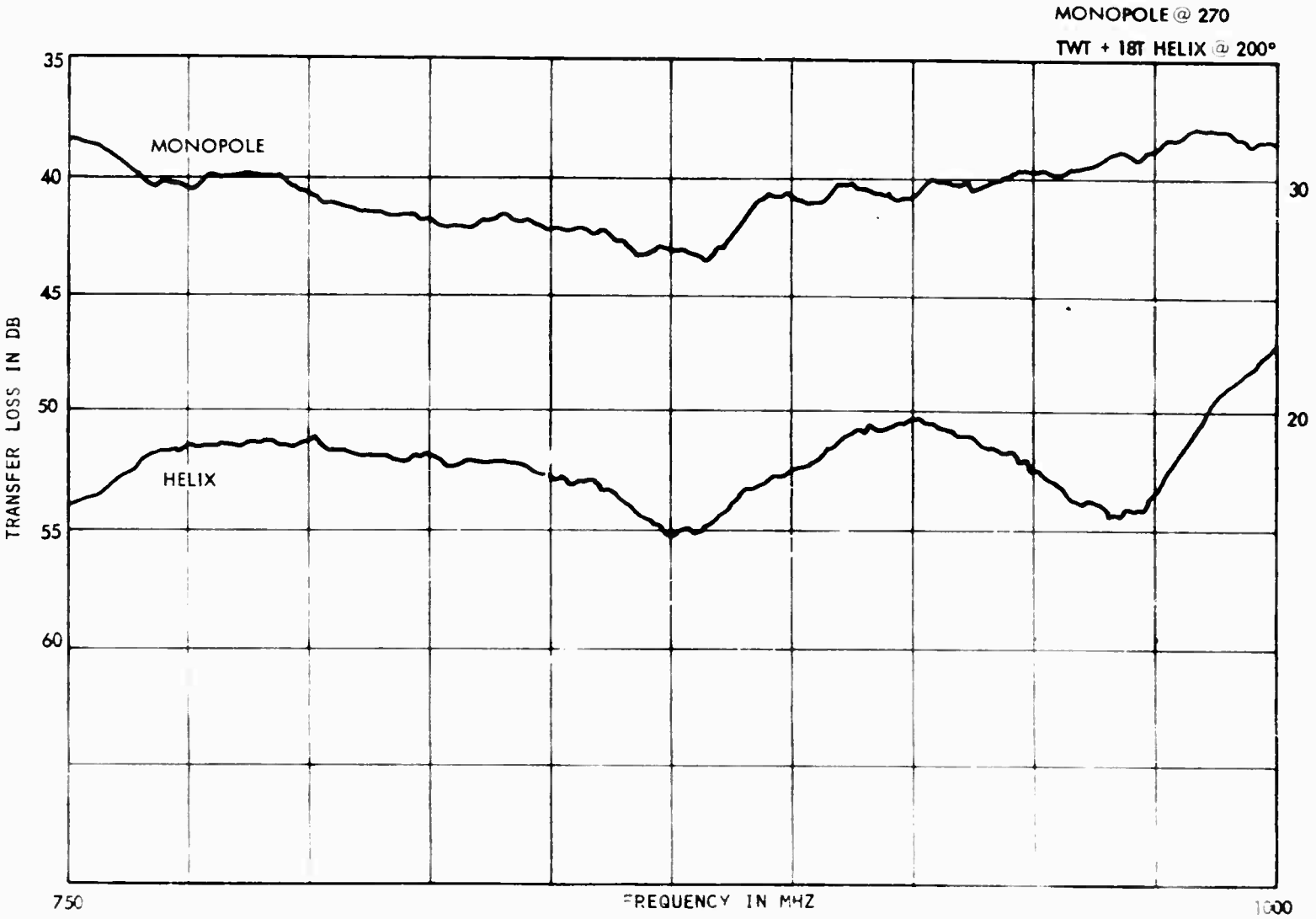

Figure 12. Transfer Loss of Monopole and Helix Antennas

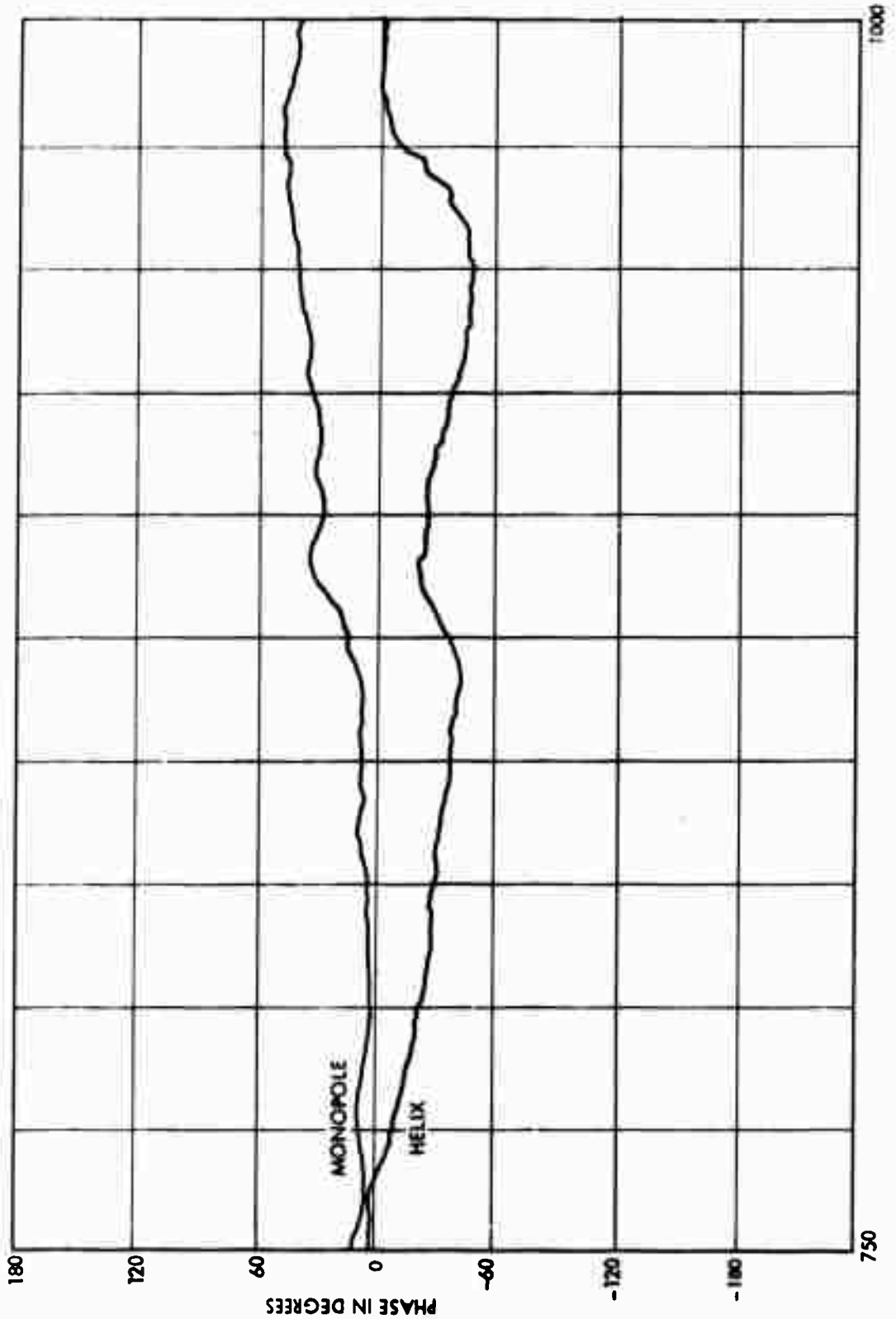

Figure 13. Transfer Phase of Monopole and Helix Antennas

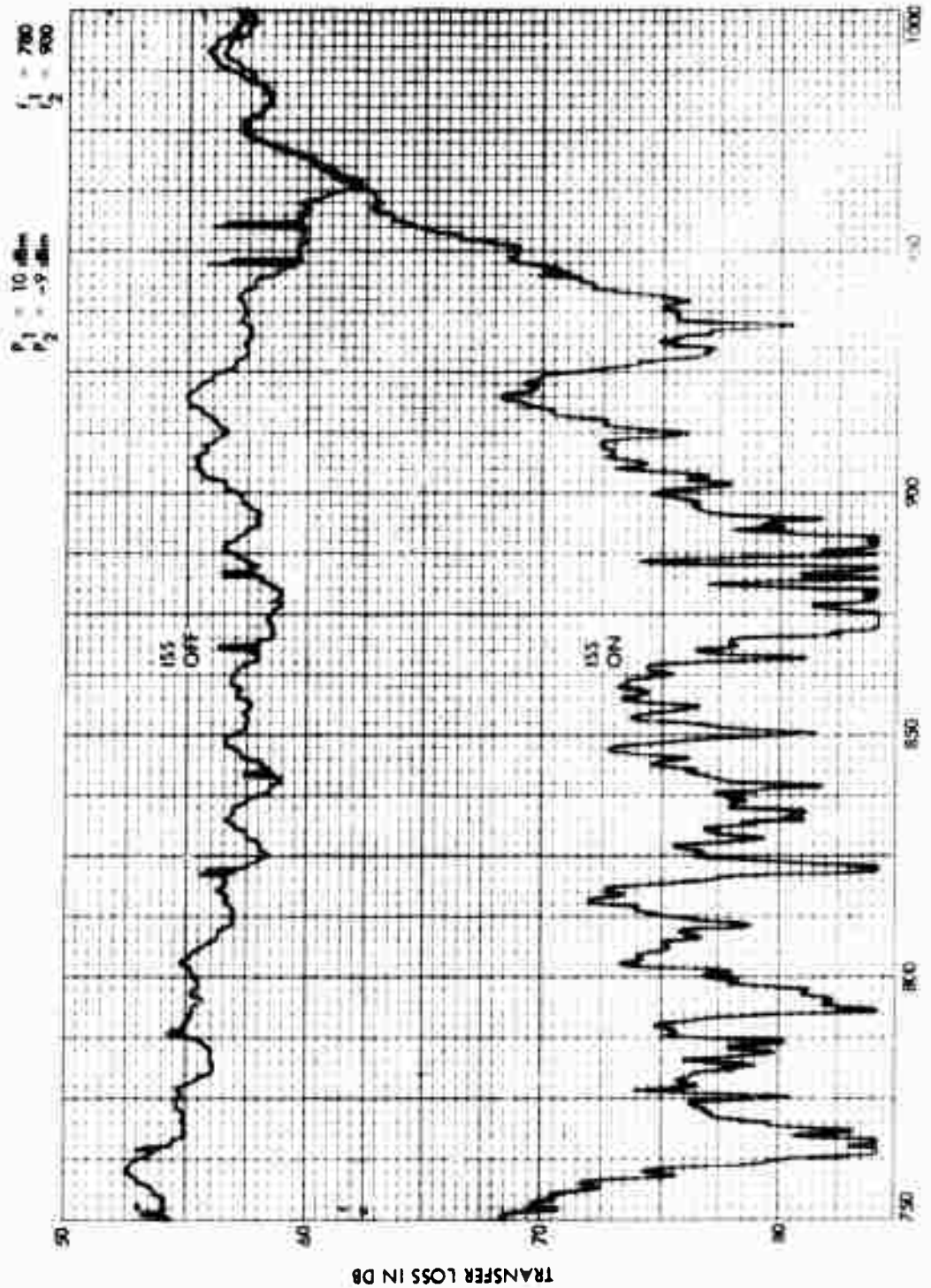

Figure 14. Transfer Loss of Helix with ISS Off and On

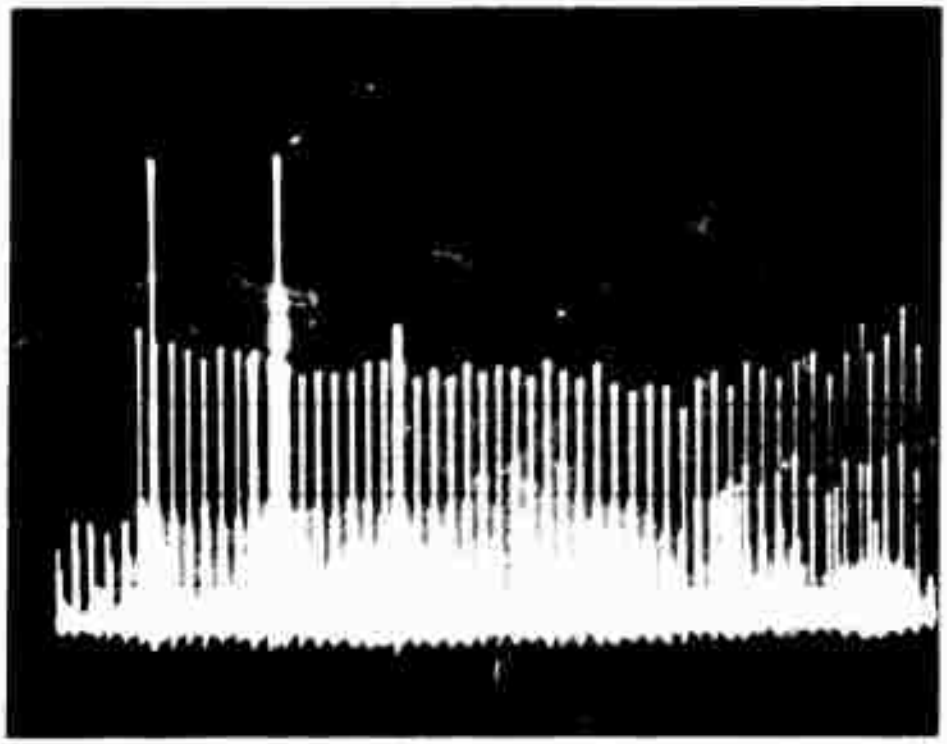

(a) ISS Turned Off

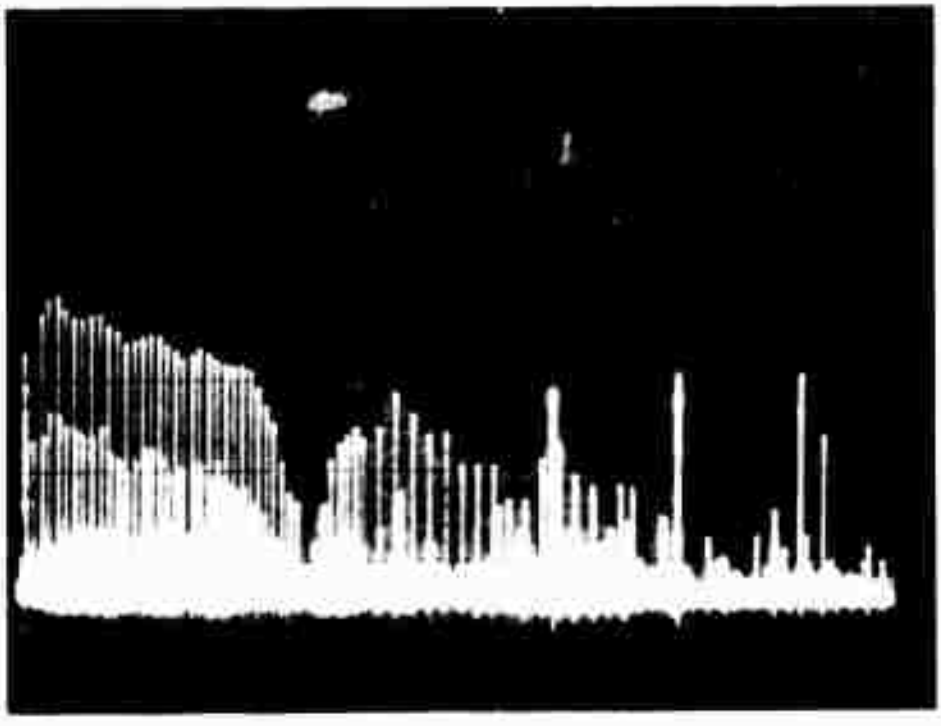

(b) ISS Turned On

Figure 15. Spectrum Analyzer Photos. Simulated IM Products Injected at 780 mHZ and 830 mHZ. Frequency Sweep Range Approximately 750 mHZ-1100 mHZ. 35.5 mHZ/cm.

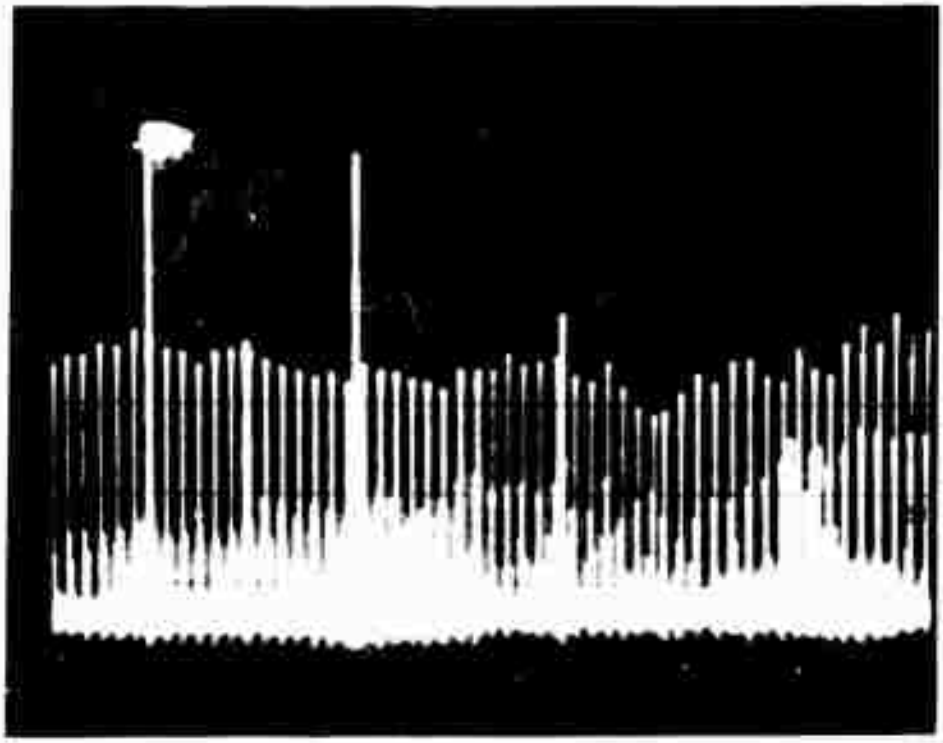

(a) ISS Turned Off

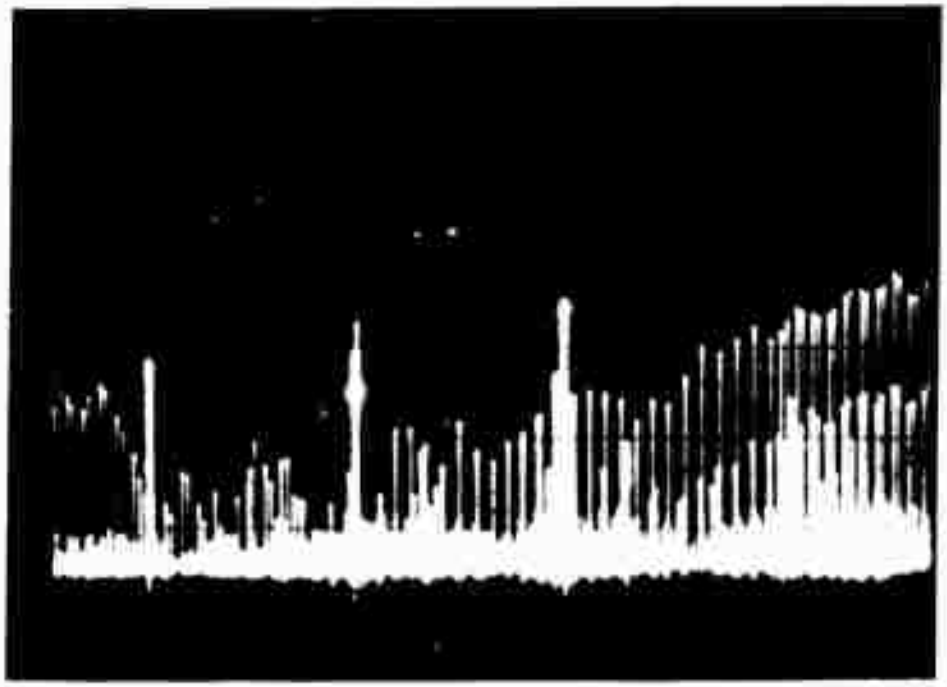

(b) ISS Turned On

Figure 16. Spectrum Analyzer Photos. Simulated IM Products Injected at 780 mHZ and 860 mHZ. Frequency Sweep Range Approximately 750 mHZ-1100 mHZ. 35.5 mHZ/cm.

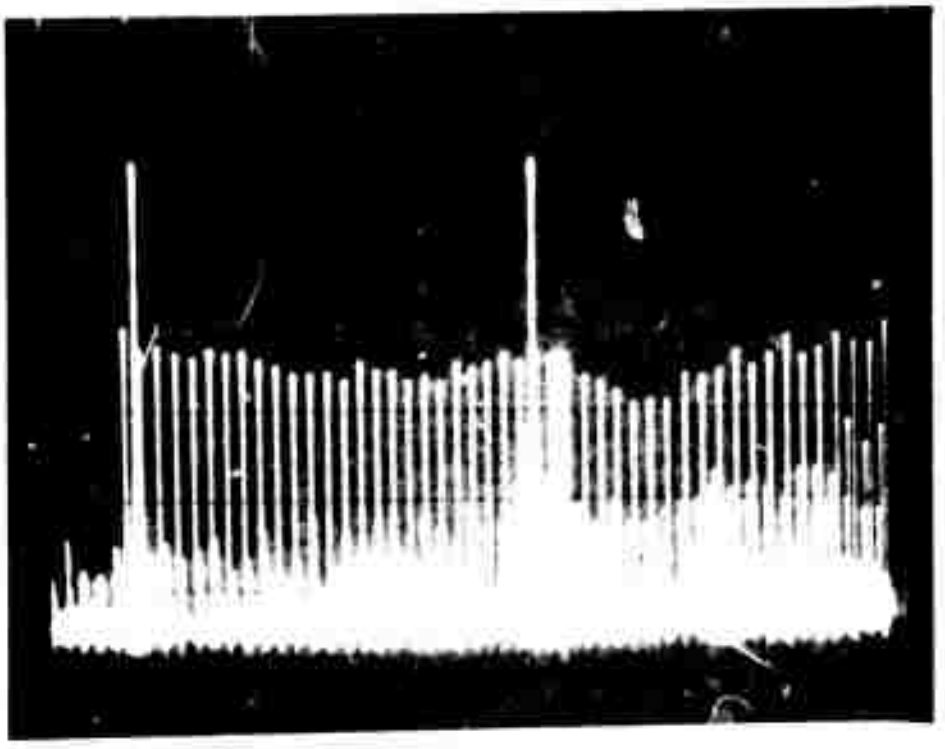

(a) ISS Turned Off

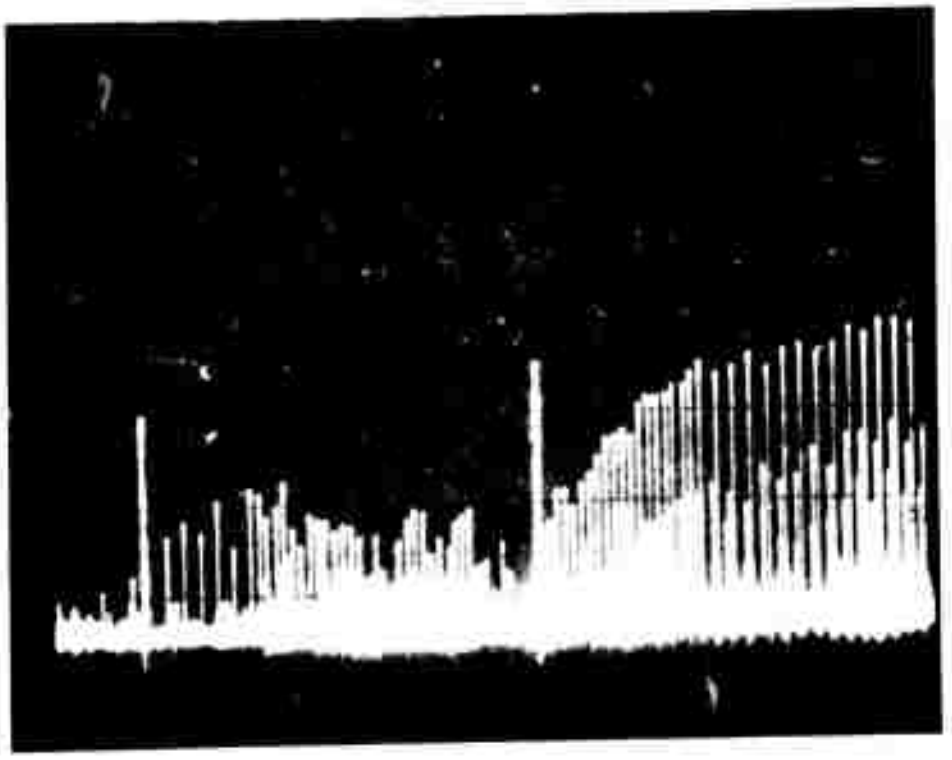

(b) ISS Turned On

Figure 17. Spectrum Analyzer Photos. Simulated IM Products Injected at 780 mHZ and 900 mHZ. Frequency Sweep Range 750 mHZ-1010 mHZ. 25 mHZ/cm.

it would be expected to be reduced approximately as much as the injected signals were, hence it is suspected that it was in part produced in the Amplica amplifier inserted in the reference channel input to the ISS.

In Figure 16 the injected signals are placed at 780 mHZ and 860 mHZ. The signal at 780 mHZ is reduced by 30 dB, and the signal at 860 mHZ is reduced by 24 dB through operation of the ISS. Analogous to the previous case, a third strong line appears on both photos, and it is reduced by about 4 dB by the ISS. Again, this is suspected to be a $2f_2 - f_1$ spur principally produced in the Amplica unit.

In Figure 17 the injected signals are placed at 780 mHZ and 900 mHZ. The signal at 780 mHZ is reduced by 28 dB, and the signal at 900 mHZ is reduced by 21 dB. The spurious strong line seen in the two preceding sets of photos is absent in this set. A $2f_2 - f_1$ spur would be located just off the scale to the right, hence would not appear in this photo.

In operation against two injected signals as was the case in these tests, the ISS achieves a compromise solution in that it tends to minimize the average interference energy of the two signals. From the spectrum analyzer photos, this solution is seen to be a good one also for frequencies lying between those of the two injected signals. The envelopes of the sweep oscillator hits (the spectral lines) in the upper photos of the three sets, Figures 15, 16, and 17, when compared to the envelopes in the lower photos of the sets, show that the transfer loss has been considerably increased by operation of the ISS at frequencies lying between the frequencies of the two injected signals. For example, in Figure 15 where the two injected signals are at the edges of the (scaled) frequency band of primary concern from an IM product standpoint in the FSC, the highest point of the spectrum lying between the two injected signals is seen to be reduced by 20 dB, and the average reduction of the spectrum between the injected signals is some 26 dB.

For frequencies generally removed from the frequencies of the injected signals, the increase in transfer loss caused by the operation of the ISS is comparatively low. This behavior is considered to be due in the main to the imperfect match over an extended frequency range between the transfer

loss and phase characteristics of the transmit antenna-to-18-turn receive helix path and the transmit antenna-to-sample monopole path.

To increase the instantaneous bandwidth of effective suppression enhancement achievable by the ISS, certain steps are indicated. The first is to optimize the match of the above identified antenna-to-antenna paths over the required bandwidth. Equalization networks may be desirable in this approach. In some cases it may be necessary to use more than one sample antenna. The detector and control circuits of the ISS can be cascaded, hence sample antennas responsive to orthogonal polarizations can supply cancellation signals to independent ISS circuits for a more complete cancellation. A third approach is to subdivide the total frequency band over which cancellation is desired into two or more sub-bands by bandpass filters and make use of independent ISS circuits for each of the sub-bands. No degradation of the noise figure of the receive channel should be experienced provided the ISS is connected following a noise figure establishing preamplifier in the receive channel.

9. QUAD HELIX INVESTIGATION

An investigation has been made of an array of four helices to determine its potential as a main receive antenna. The interest in this design lies in the possibility of making use of the array factor of the four elements to minimize its response to IM products emanating from the transmit antenna.

Figure 18 shows a photo of a 3/8 scale model of the array mounted alongside the transmit antenna. The center of the array is at the same distance from the center of the transmit antenna as is the 18-turn receive helix of the FSC. The interconnections of the array are shown in Figure 19. The elements are orientated rotationally in the same position and they are connected with equal length transmission lines for broadside operation. The spacing d is chosen nominally to be a half wavelength at 800 mHZ so that helices Nos. 1 and 2 would have a two-element array null in the direction of the transmit antenna, and similarly for helices Nos. 3 and 4. Consequently, the combinations of the two pairs of helices would have an array null in that direction. Figure 20 shows location of helical elements in the array.

The individual helices have the same diameter, the same coned ends, and are made with the same strip conductor dimensions and spacing as the 18-turn receive helix. Although the circular ground planes have the same diameter as the 18-turn receive helix, they are not provided with the ring structure that is used with that antenna. The feed point of each helix is connected directly to a quarter wave coaxial line transformer made of RG 59U cable to improve the match of the antenna element to a 50 Ω cable. The hybrids used in the array are Anzac Model H-9.

Figure 21 is a Smith chart plot of the impedance of the Quad helix array. At 780 mHZ the VSWR is 1.2:1, and it rises to 1.4:1 at 830 mHZ. Over the band from 700 mHZ through 1000 mHZ it is seen to be at most about 1.45:1.

The gain of the Quad helix array has been investigated and is shown in Figure 22. To make this measurement, the array is placed on the antenna range and is excited by a rotating transmitting antenna. The magnitude of the swing of the sinusoidal oscillations of the gain curve

Figure 18. Photo of 3/8 Scale Model of Quad Helix Array Mounted With Transmit Antenna

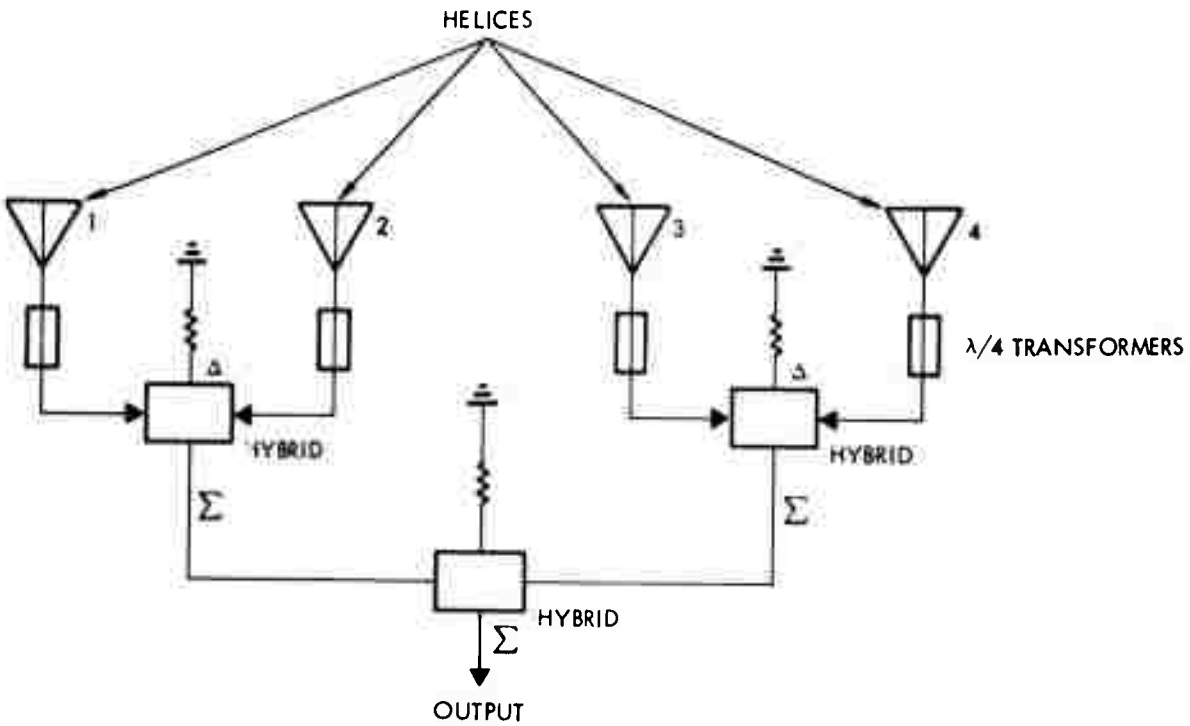

Figure 19. Interconnections of Quad Helix Array

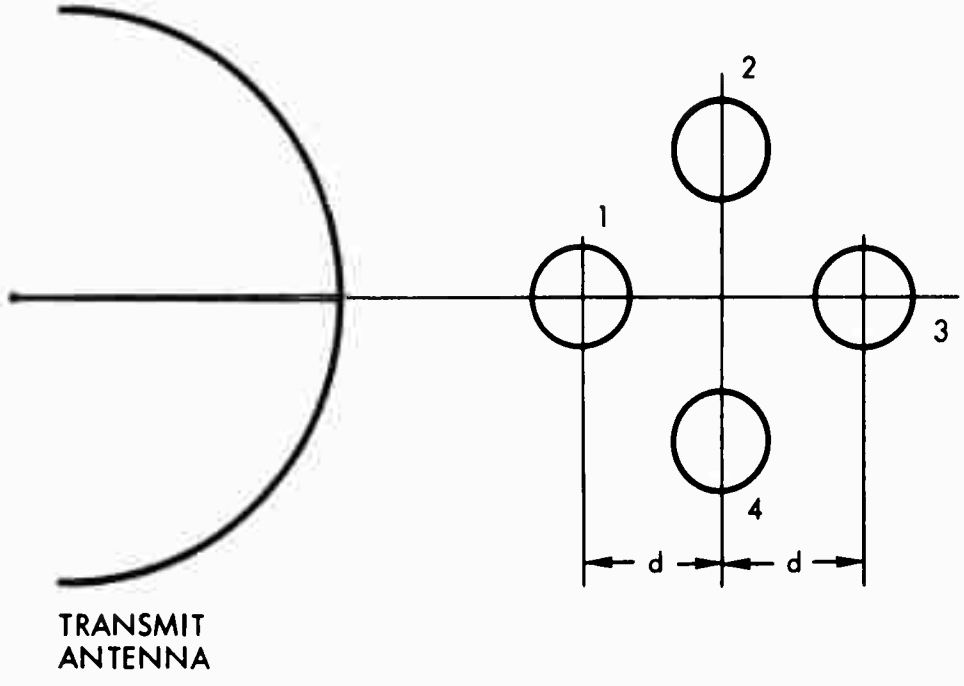

Figure 20. Sketch Showing Location of Helices in Quad Helix Array

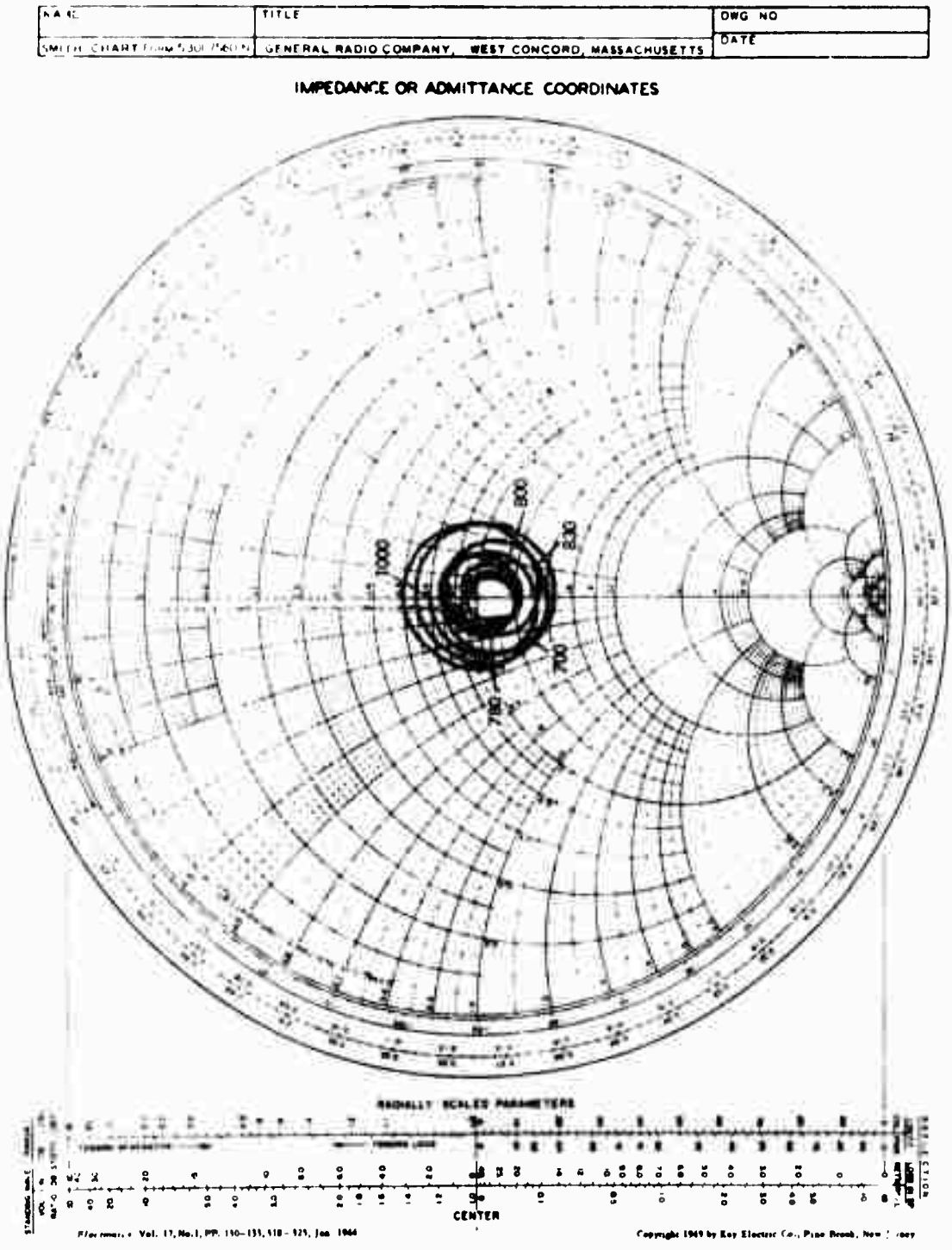

Figure 21. Smith Chart Plot of Quad Helix Array 9-Turn Using Quarter Wave Transformers and Anzac H-9 Hybrids

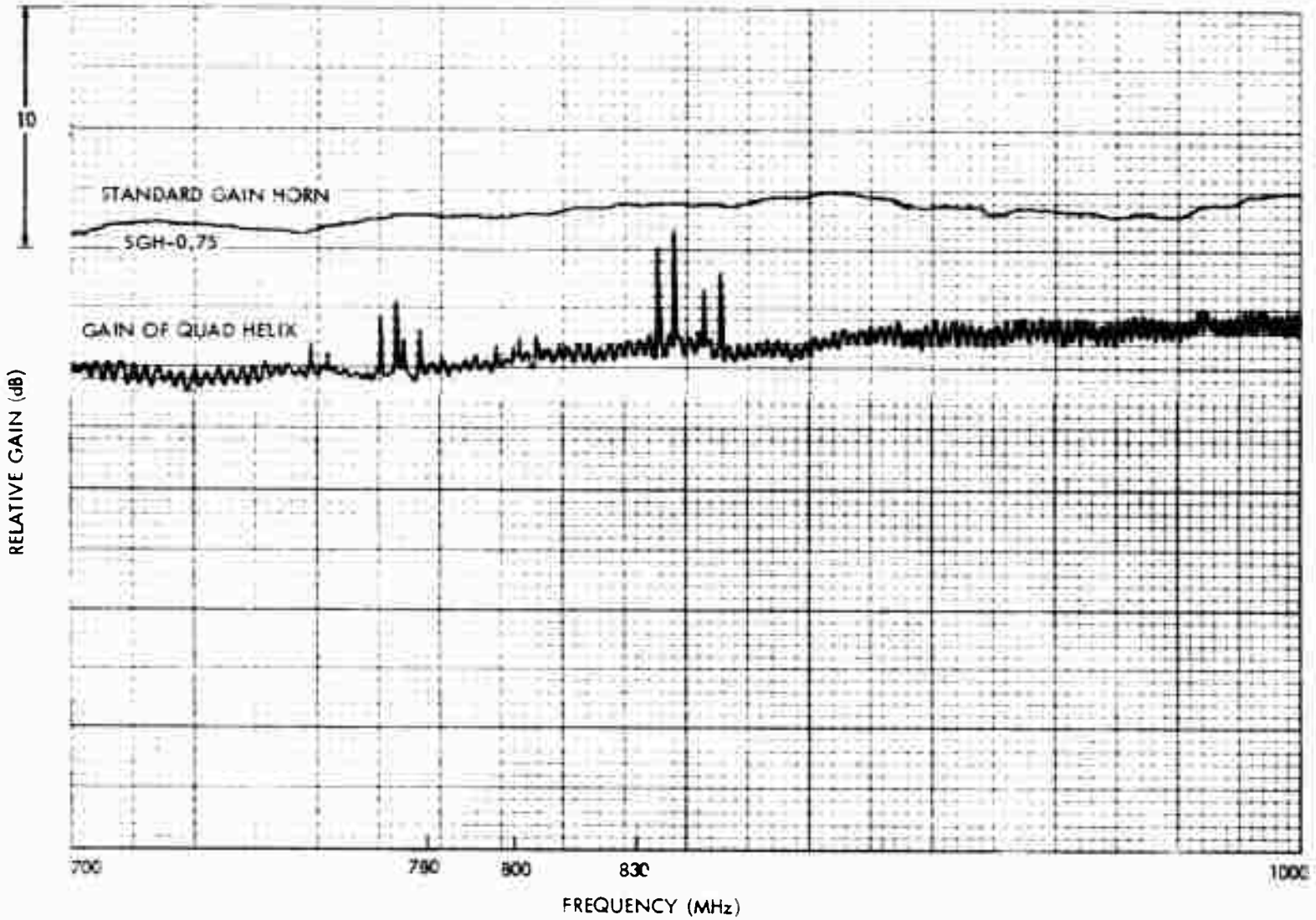

Figure 22. Gain Versus Frequency of Quad Helix Array

measures the ellipticity ratio of the array. Over the band from 780 mHZ through 830 mHZ the ellipticity ratio is 0.75 dB or less, and it increases to 1 dB as the frequency is increased to 1000 mHZ. The vertical spikes on the curve are caused by interfering signals encountered on the pattern range. Also plotted on the same graph is the gain of a Scientific Atlantic standard gain horn, Model SGH-0.75, which is installed in place of the quad helix array with the test conditions maintained the same for both curves. The gain versus frequency curve of this standard horn is given in Figure 23.

Figures 24 through 31 show the patterns of the quad helix array for the spacing d = 20". The principal pattern plane of interest is that which includes the transmit antenna axis. (These patterns were not taken with the transmit antenna in place.) In this plane the side lobes are lower than in the plane oriented at 45^{o} to it and are some 15 dB or more below the main lobe.

Table 1 gives the Net Antenna Performance of the quad helix as obtained from these data. This parameter drops at the high level of the band principally because of the narrowing of the patterns there. These figures include the losses in the commercial hybrids used and can be expected to improve with improved interconnections designed for the specific applications. Array spacings from d = 14.75" to d = 23.25" were investigated. The patterns vary in beamwidth as would be expected. No particular sensitivity was noted in the gain performance as a function of spacing. The gain of the array should increase with increased element length, however the gain performance does not appear to have been optimized as yet for the 9-turn elements.

Figure 32 shows a transfer loss measurement performed on the quad array. As in the case of the gain, the transfer loss performance is not considered to be optimized and in its present state of development the array appears to be about comparable to the 18-turn helix with regard to transfer loss.

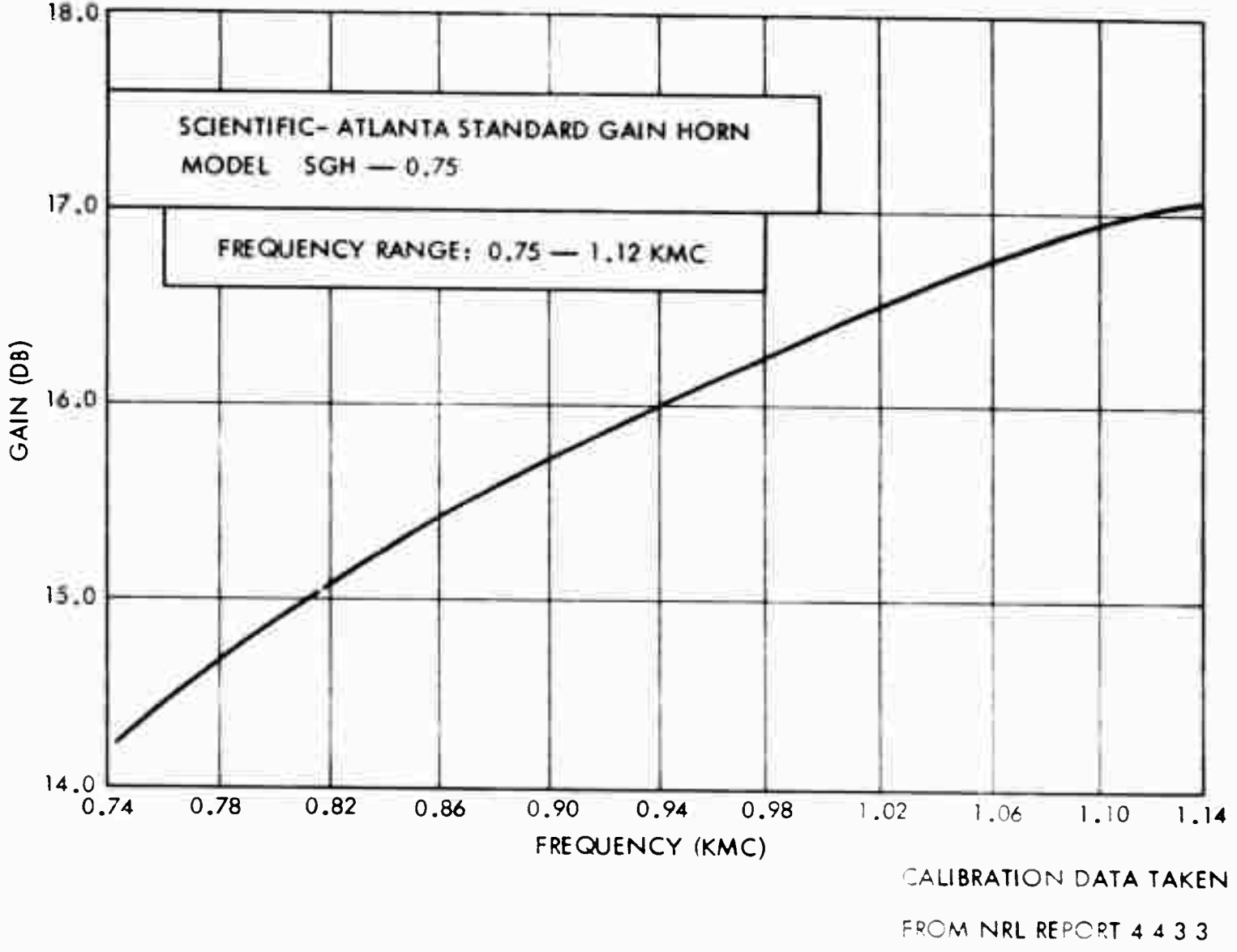

Figure 23. Gain Versus Frequency of Standard Gain Horn Model SGM-0.75

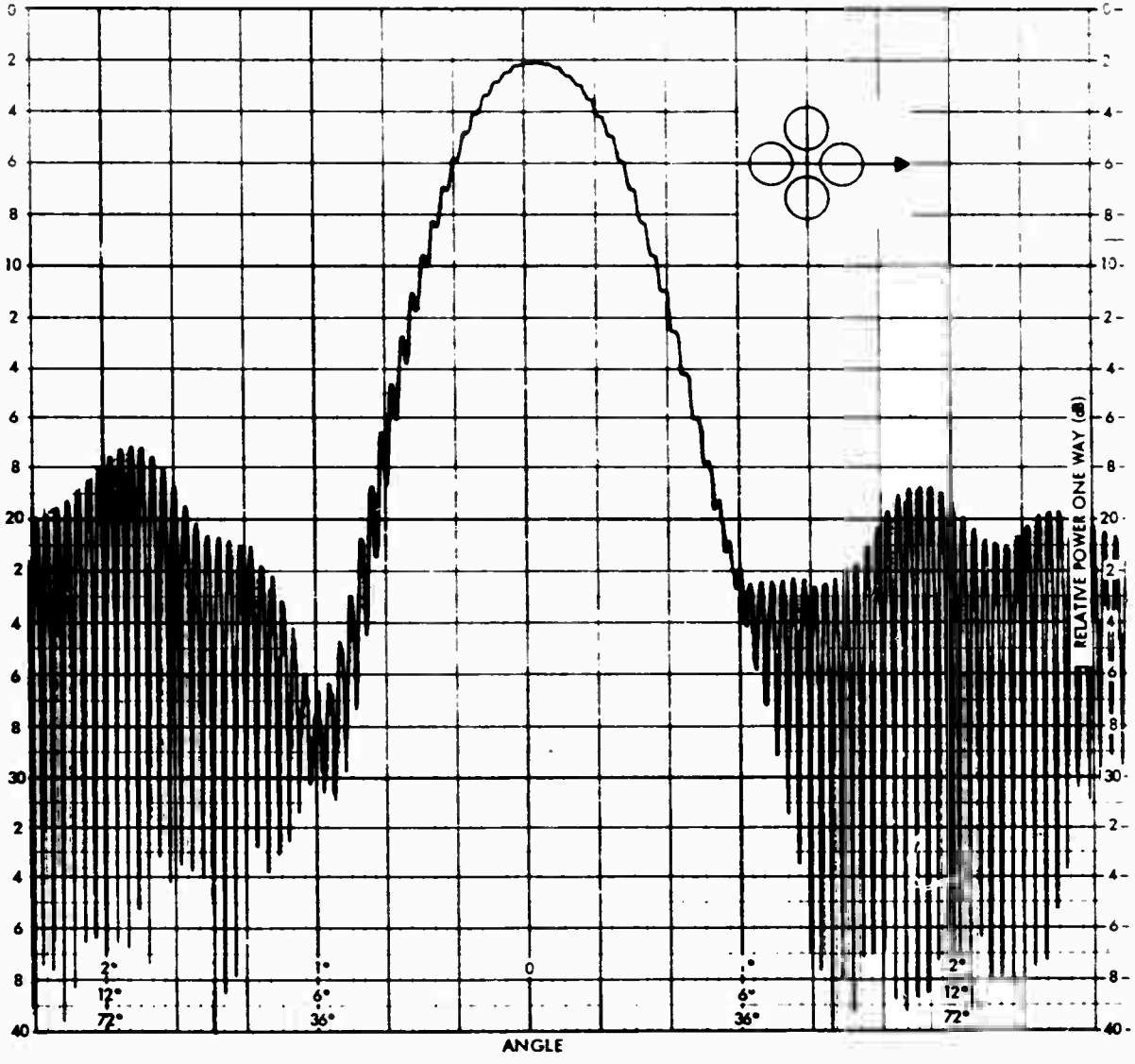

Figure 24. 3/8 Scale Test Quad Helix 9-Turn Frequency 780 MHz Rotating Linear Polarization Spacing d = 20".

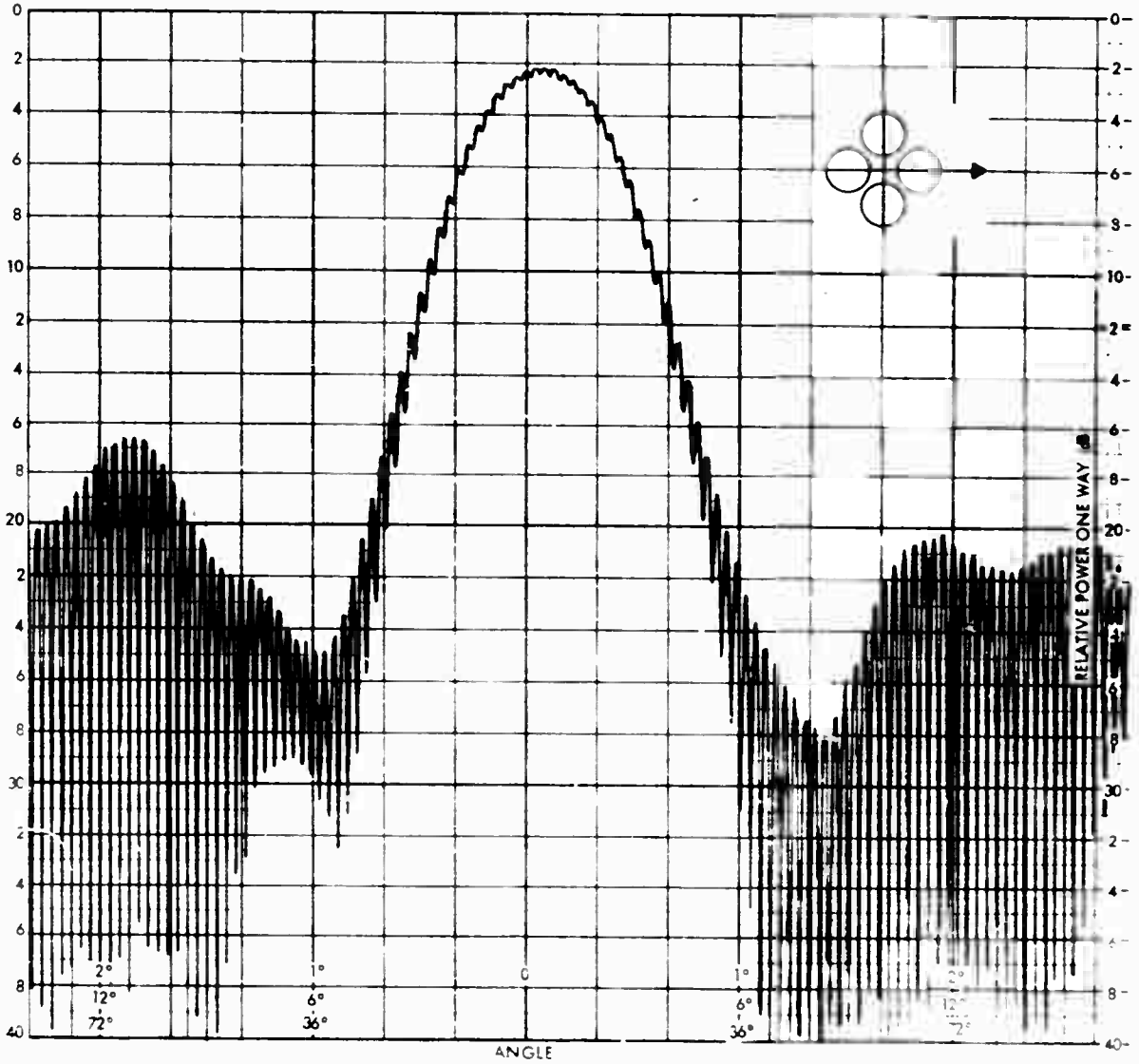

Figure 25. 3/8 Scale Test Quad Helix 9-Turn Frequency 8 [illegible]-z
Rotating Linear Polarization Spacing d = 20 .

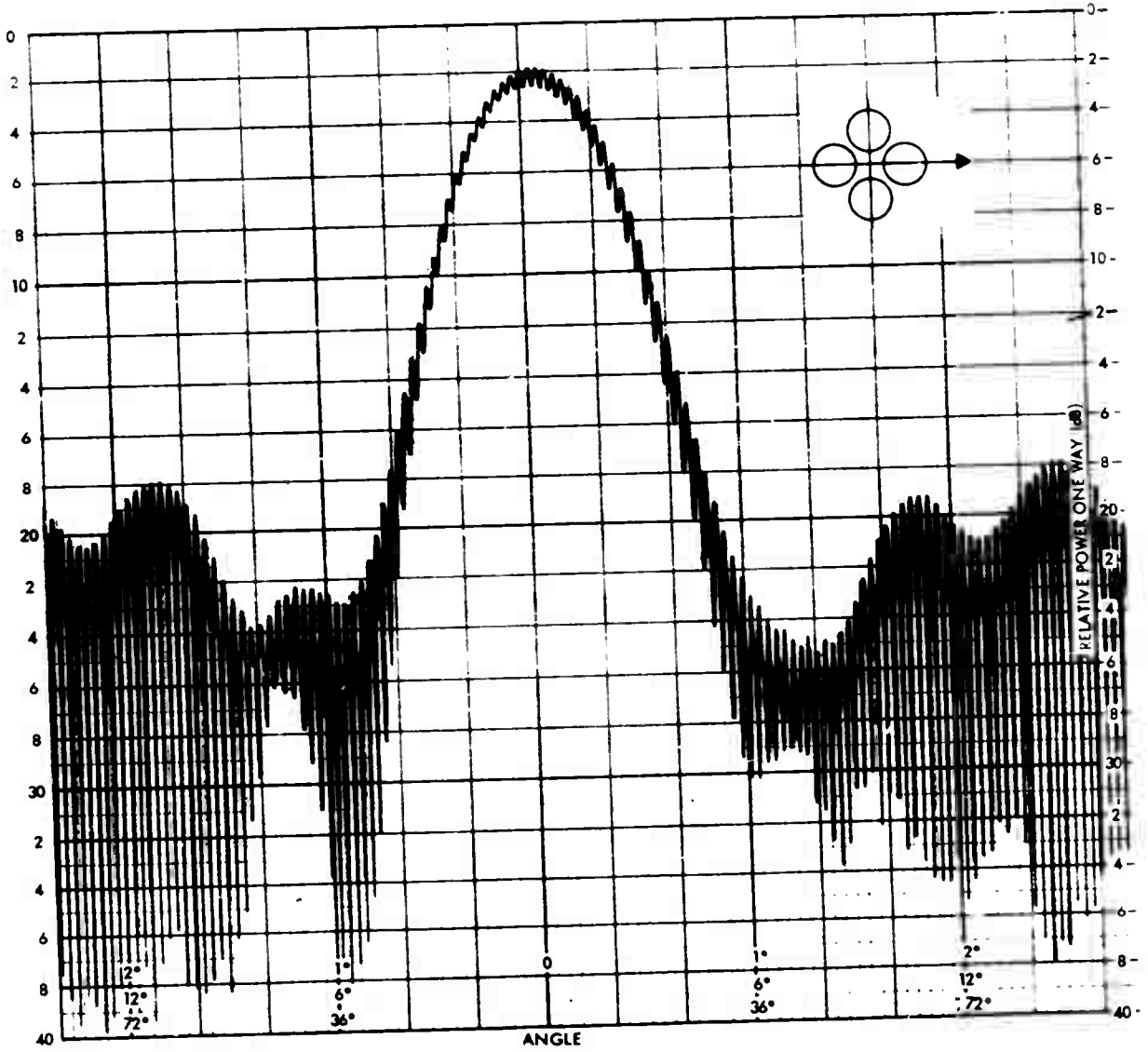

Figure 26. 3/8 Scale Test Quad Helix 9-Turn Frequency 830 MHz Rotating Linear Polarization Spacing d = 20".

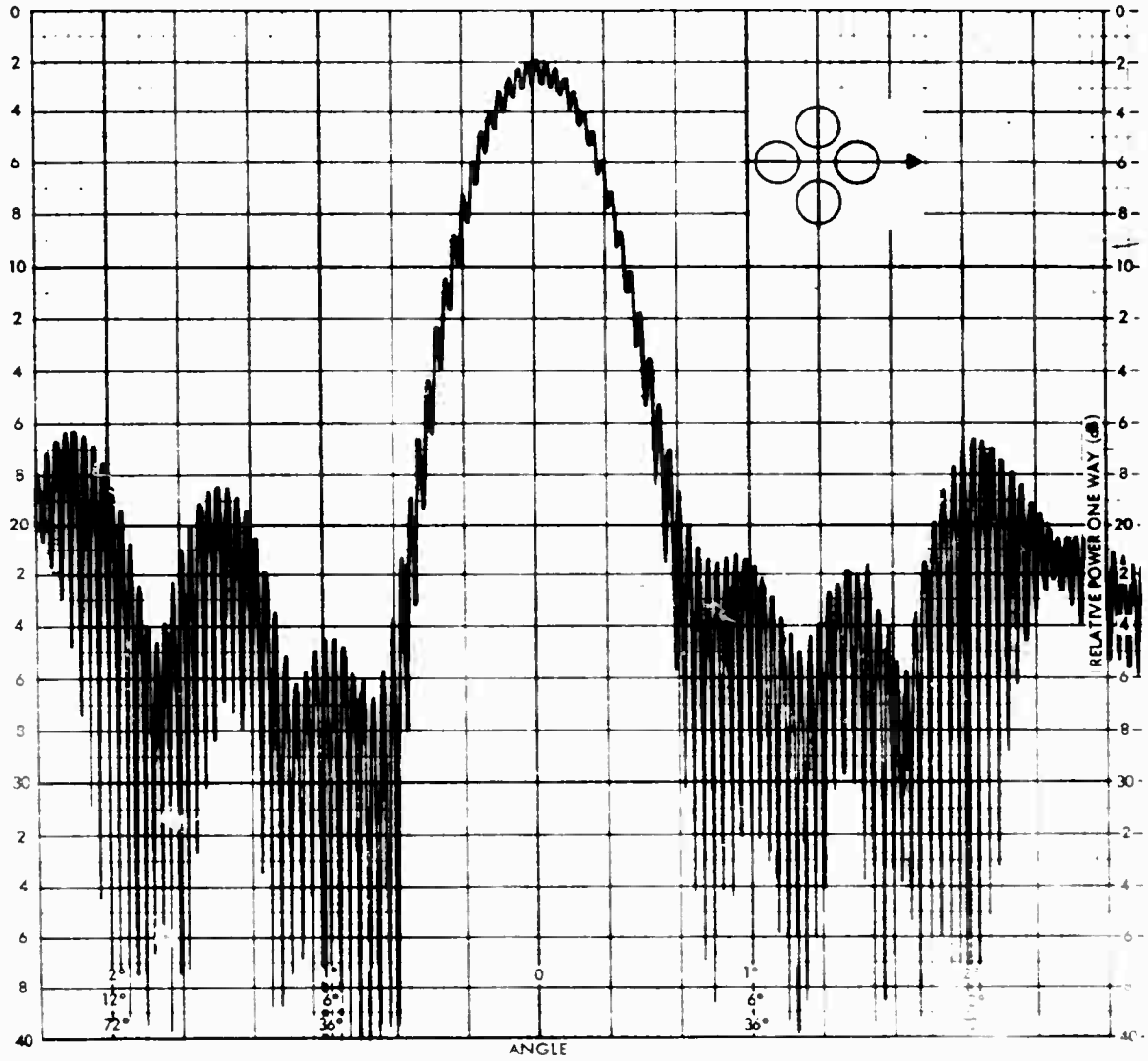

Figure 27. 3/8 Scale Test Quad Helix 9-Turn Frequency [illegible] MHz
Rotating Linear Polarization Spacing d = 20"

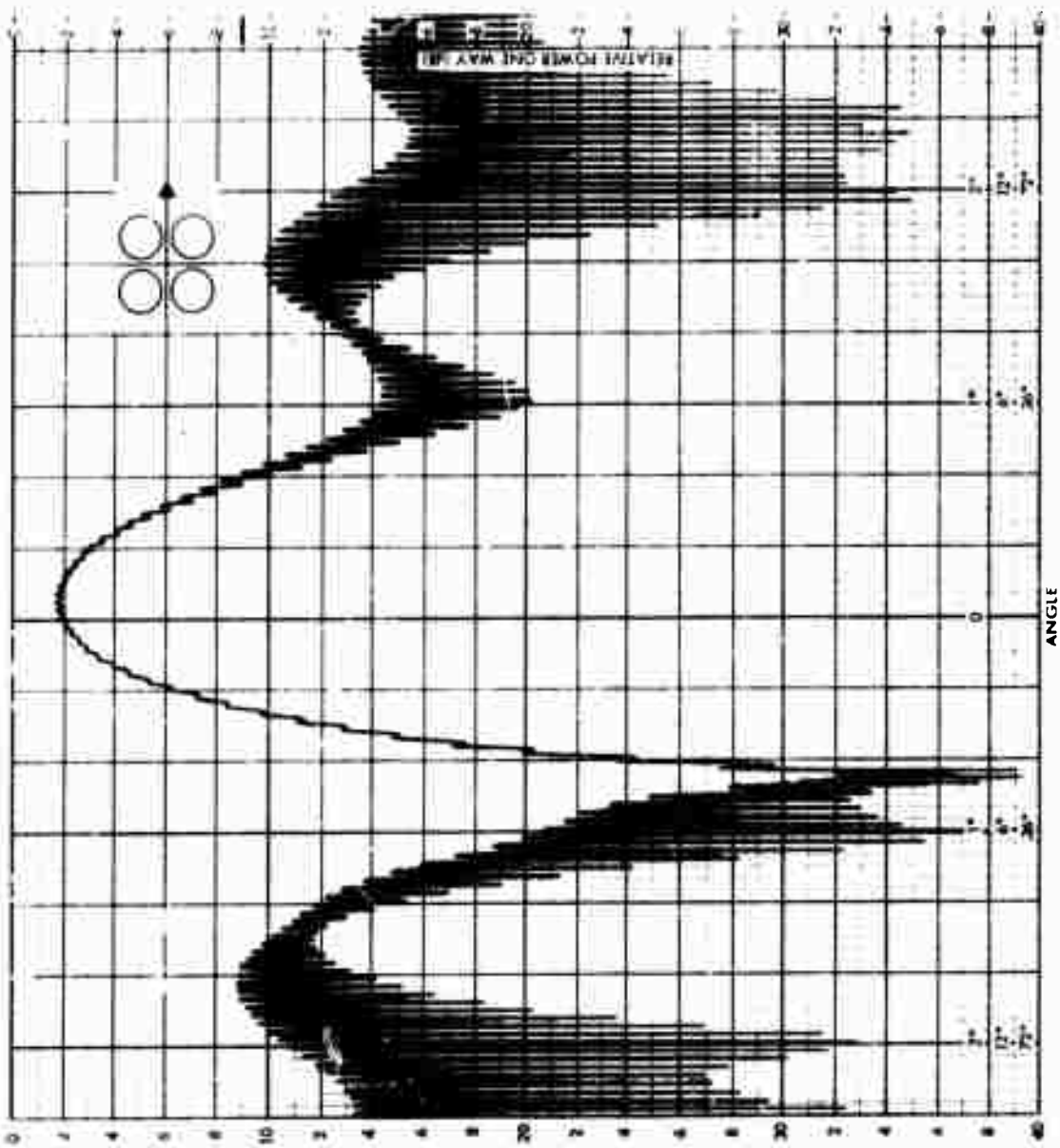

Figure 28. 3/8 Scale Test Quad Helix 9-Turn Frequency 780 MHz
Rotating Linear Polarization Spacing d = 20".

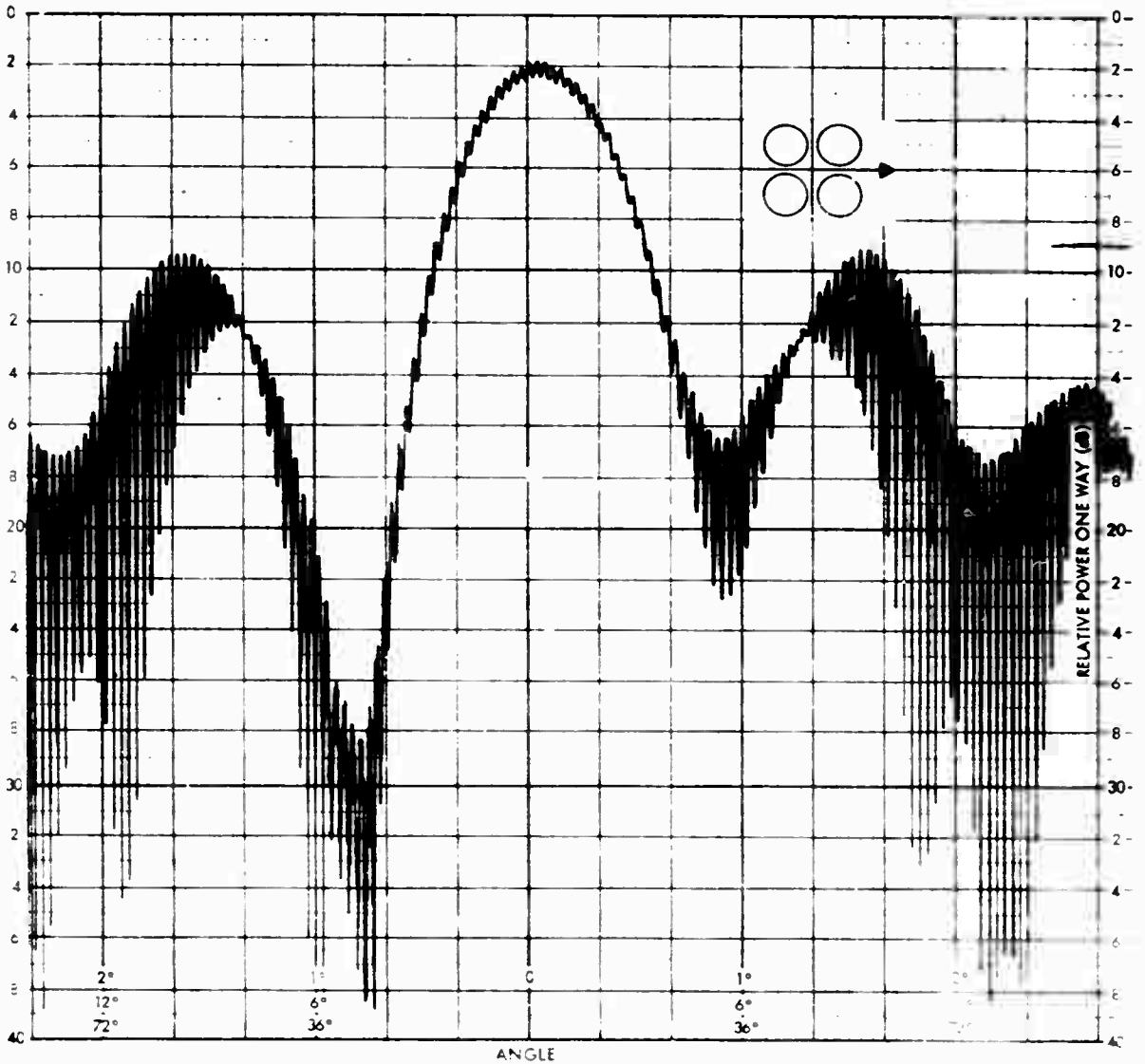

Figure 29. 3/8 Scale Test Quad Helix 9-Turn Frequency 80[illegible] MHz Rotating Linear Polarization Spacing d = 20".

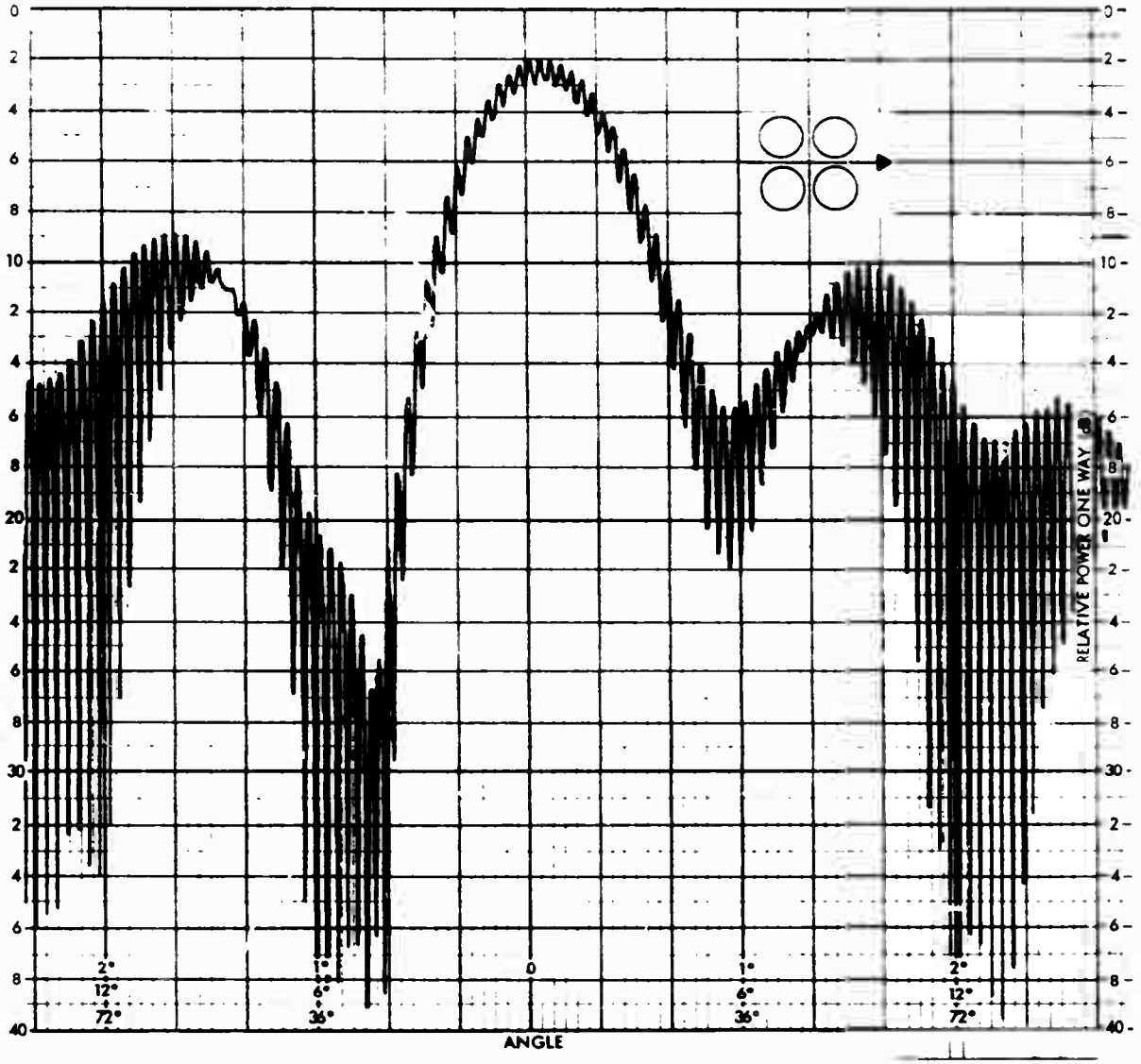

Figure 30. 3/8 Scale Test Quad Helix 9-Turn Frequency 830 MHz Rotating Linear Polarization Spacing d = 20".

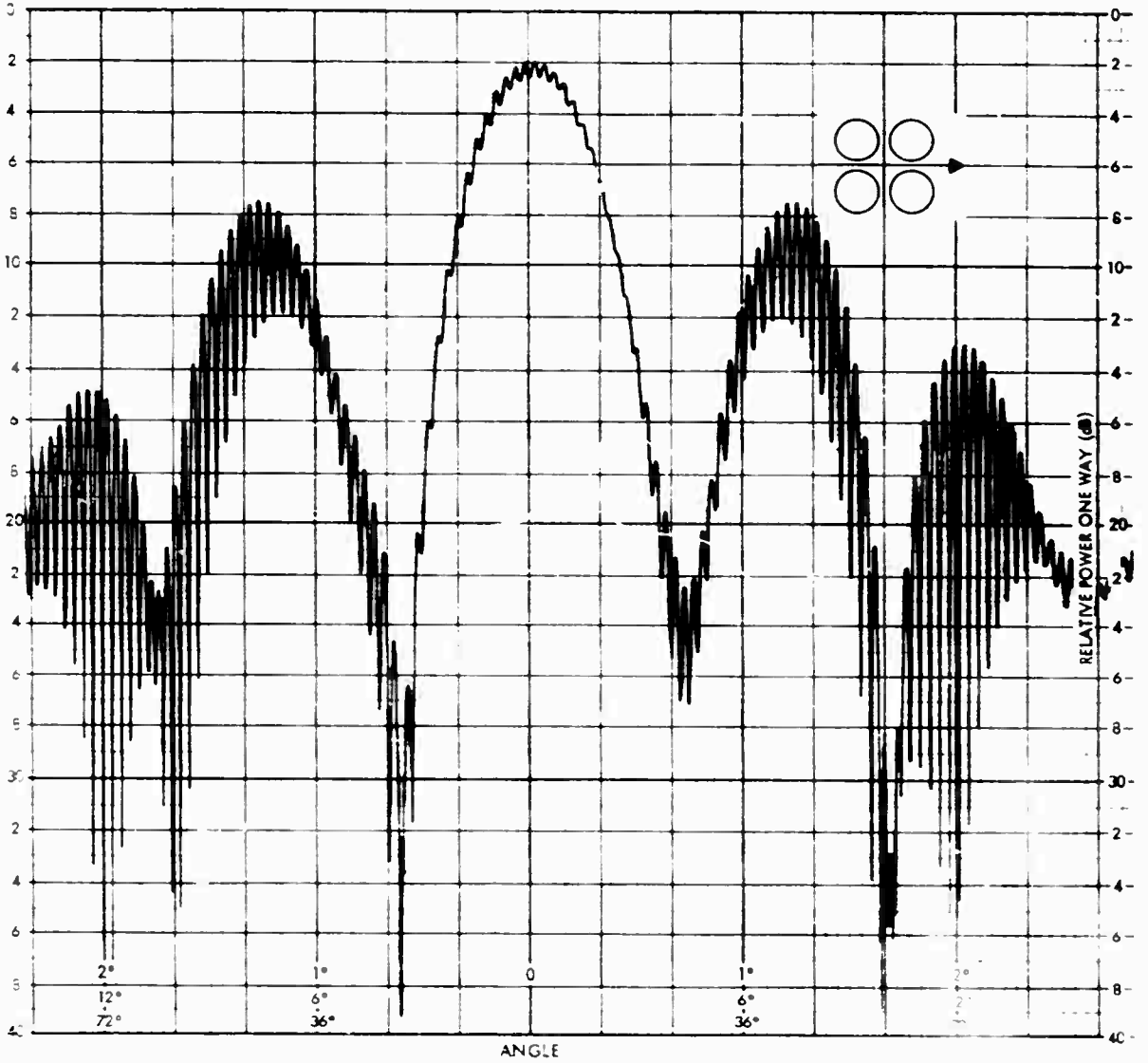

Figure 31. 3/8 Scale Test Quad Helix 9-Turn Frequency 1000 MHz
Rotating Linear Polarization Spacing d = 20'

Table 1. Net Antenna Performance at 10^{o} of 3/8 Scale Model of Quad Helix 9-Turn with $\lambda/4$ Transformers and Anjac Hybrids. Spacing d = 20"

Frequency, mHZ	Gain of Standard Horn, dBi	Quad Gain on Boresight WRT CIRC POL Isotropic Source, dB	Quad Gain Drop 10^{o} From Boresight, dB	Net Antenna Performance, dB
780	14.7	11.2	2	8
800	14.9	11.7	2	10.6
830	15.2	12.4	2	11.3
1000	16.4	13.7	4	10.3

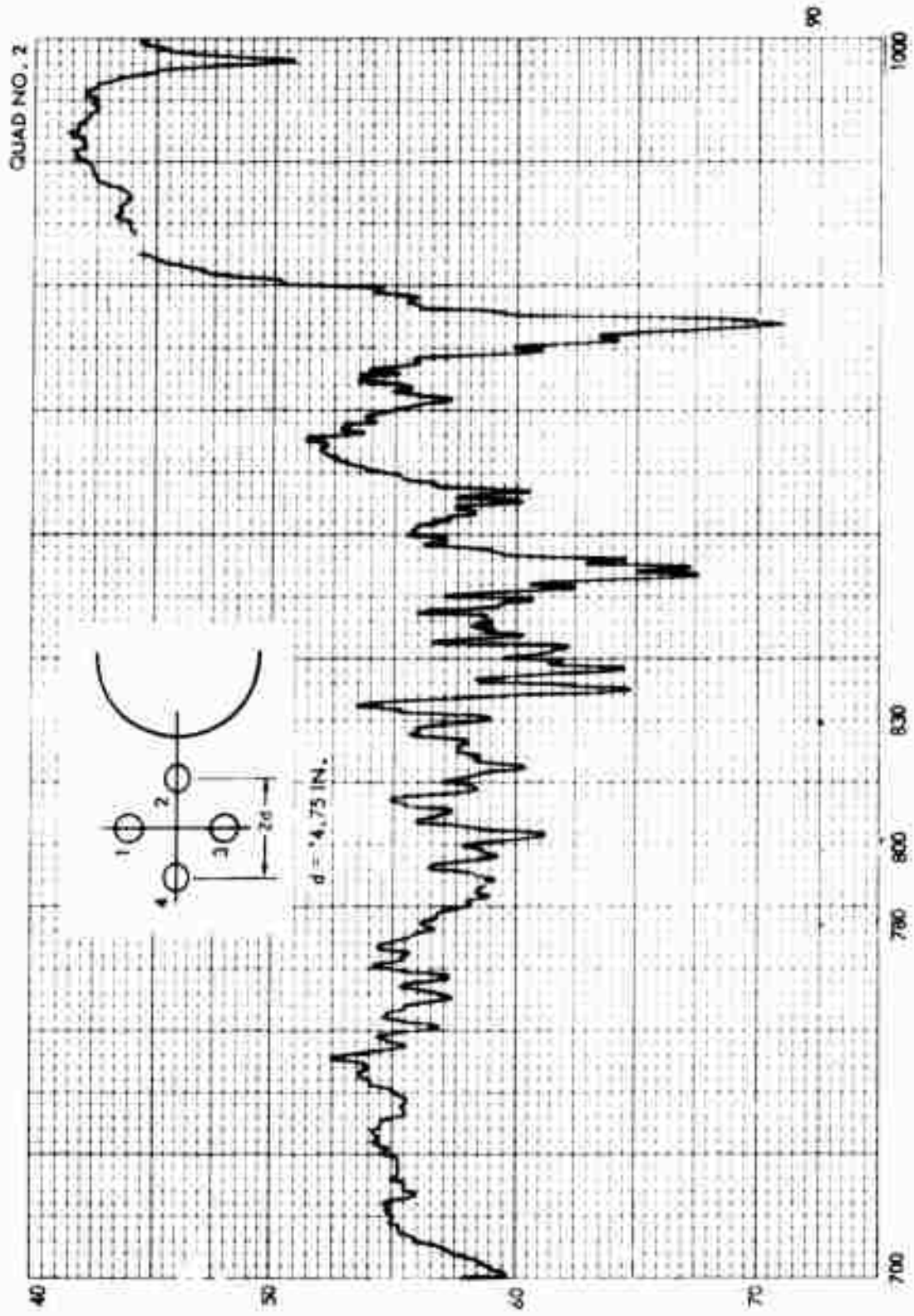

Figure 32. Transfer Loss Between Transmit Antenna and Quad Helix

10. CONCLUSIONS AND RECOMMENDATIONS

With regard to the quad helix investigations, further work is required to increase its gain and increase its transfer loss for the FSC application. It is not considered that the potential inherent in the design has been realized with regard to either of these parameters.

The feasibility of obtaining IM product signals from small unobtrusive sample antennas which are suitable for use in active and passive cancellation schemes was demonstrated.

The ANC ISS tests demonstrated its potential for IM product reduction in the FSC application. Further investigations are required to determine the optimum combination of sample antennas and parameter correction channels which would provide the maximum of suppression. Work is required to configure a design directly appropriate to the FSC.